5-2002

Finite Element and Pullout Test Performance of Welded Wire Mats

Bradley C. Conder
Utah State University

FINITE ELEMENT AND PULLOUT TEST PERFORMANCE OF WELDED WIRE MATS

by

Bradley C. Conder

A thesis submitted in partial fulfillment
of the requirements for the degree

of

MASTER OF SCIENCE

in

Civil Engineering

Approved:

James A. Bay Major Professor	Loren R. Anderson Committee Member
Joseph A. Caliendo Committee Member	Kevin C. Womack Committee Member

Thomas L. Kent
Dean of Graduate Studies

UTAH STATE UNIVERSITY
Logan, Utah

2002

ABSTRACT

Finite Element and Pullout Test Performance of Welded-Wire Mats

by

Bradley C. Conder, Master of Science

Utah State University, 2002

Major Professor: Dr. James A. Bay
Department: Civil and Environmental Engineering

This paper reports on the pullout test performance of welded-wire reinforcing mats. A 126-foot high mechanically stabilized earth wall was constructed at Kennecott Utah Copper. In the lower half of the wall, single lengths of 50-foot long welded-wire mats were used. In the top half of the wall, two lengths of 50-foot mats were overlapped 10 feet to create 90-foot mats. This 10-foot "lap zone" was investigated in this study.

The finite element program Plaxis was used to investigate several pullout test parameters: overburden pressure, gap width, boundary effects, and horizontal spacing of transverse elements from the pullout box face.

Physical pullout tests were performed in a scale pullout box to compare test configurations with single and multiple layers of mats, and test configurations with single and multiple lap zones. Finally, a Plaxis model of the scale pullout box was created to compare the finite element and pullout test results.

(118 pages)

DEDICATION

In memory of my father.

ACKNOWLEDGMENTS

I would like to extend my thanks to Dr. James A. Bay for his long and late hours in helping me to complete my thesis. His guidance and support through the duration of the project are appreciated. I am also grateful for the other members of my thesis committee: Dr. Loren R. Anderson, Dr. Joseph A. Caliendo, and Dr. Kevin Womack.

I would also like to thank Arnfinn Emdal, assistant professor at the Norwegian University of Science and Technology, for his help with the Plaxis program and the finite element models.

Very special thanks go to William Hilfiker of Hilfiker, Inc. for financing and supporting my thesis research. Additionally, I am grateful to Brent Taylor, also of Hilfiker, Inc., for his on-site assistance at Kennecott Utah Copper during the installation of the instrumentation in the reload wall.

Thanks to Brian Barton and Ryan Wilcock for sharing the responsibility of this assignment. Without their hard work this project would not have been completed.

My sincere gratitude goes to Ken Jewkes for his mechanical genius. His help in designing and constructing the pullout box and in performing the pullout tests was invaluable.

Thanks to Brady Cox, Allen Evans, Todd Colocino, Jon Hagen, and Jeff Hodson who provided assistance during the instrumentation of the Kennecott reload wall. Their willingness to work long and late hours during the installation process is gratefully acknowledged.

Thanks to my family for their sincere interest in my education and thesis project. My gratitude to my little girl, Brooke, whose smile and laugh always helped after many a stressful day. Finally, my admiration and love go to my wife, Jill, for her unconditional love and support.

Bradley C. Conder

CONTENTS

LIST OF TABLES

LIST OF FIGURES

CHAPTER 1

INTRODUCTION

Types of earth reinforcing systems

Reinforcing soil is a method of improving the mechanical properties of constructed soil embankments. The French architect and engineer Henri Vidal was the first to formalize a rational design procedure for soil reinforcement with his Reinforced Earth system in the 1960s. This system utilized steel strips as the reinforcement, and required the use of high quality sand or gravel as the backfill (Vidal, 1969). Since the advent of Reinforced Earth, numerous types of reinforcing systems have been introduced. Some of these systems include: metal or polymer strips, welded-wire mats or bar mats, geotextile sheets, polymer grids, and woven wire mesh. The widespread acceptance by the engineering profession of mechanically stabilized earth walls and other reinforced earth systems can be attributed to numerous factors: ease of construction, low cost, performance, ability to accommodate substantial deformations and settlement, and adaptability to varied subsoil conditions (Mitchell and Christopher, 1990).

One type of reinforcing system is the Hilfiker welded-wire wall, developed by William Hilfiker in the mid-1970s. The first instrumented welded-wire wall was constructed in 1977 for the Southern California Edison Power Company to repair roads along a power line in the San Gabriel Mountains of Southern California (Mitchell and Christopher, 1990). This system uses a welded-wire mat configuration, as shown in Figure 1.1. The first mats were constructed of seven- and nine-gage wires with the longitudinal wires spaced at 2 inches and the transverse wires spaced at 6 inches.

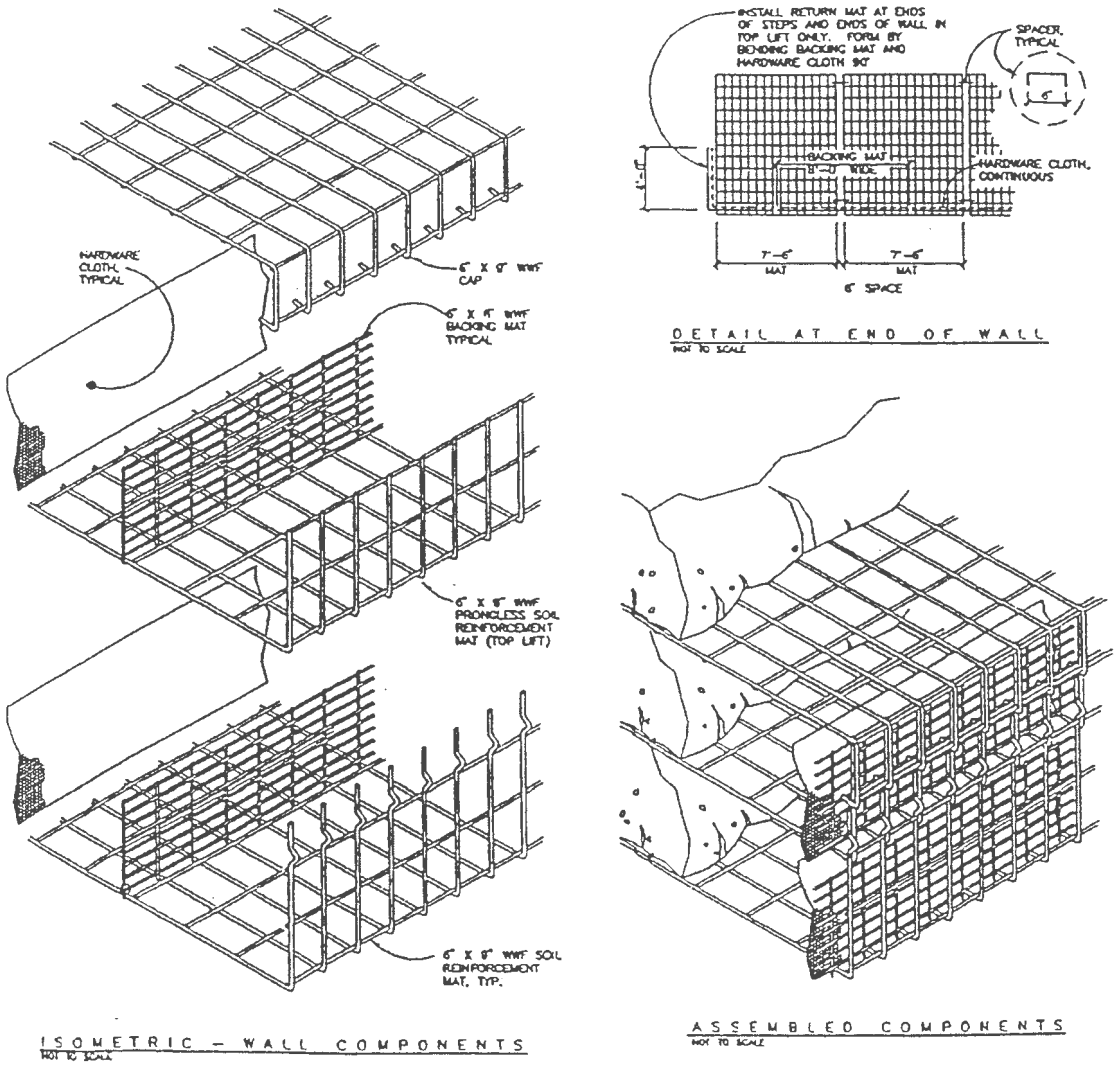

Figure 1.1. Schematic of a welded-wire wall.

Since the first walls, numerous longitudinal and horizontal spacings have been utilized. This includes a recent project at Kennecott Utah Copper where the longitudinal spacing was 6 inches and the transverse spacing was 24 inches. Hilfiker welded-wire mats were the soil reinforcement system modeled in this study.

Kennecott Utah Copper project

In November of 1999, Utah State University became involved with a construction and research project at Kennecott Utah Copper. Jerold Bishop of Geotechnical Design Services of Salt Lake City, Utah, designed two large retaining walls that were built at the mouth of Bingham Canyon, just west of Copperton, Utah. The two identical 126-foot high walls were used as "reload" walls for the transportation of ore. The ore from the open pit at Kennecott was loaded onto large dump trucks, hauled to the reload walls, and dumped off the top of the walls to form stockpiles of material that rested against the base of the walls. Large electric shovels at the base of the walls loaded railroad cars with the stockpiled ore, which was then transported to the concentrator facilities for further processing.

As part of his reload wall design, Jerold Bishop incorporated several unique features. First, he added a rigid concrete face to the mechanically stabilized earth wall. Second, he used two lengths of reinforcement for the entire 126-foot height of the wall. In the lower 62 feet of the wall, the length of the welded-wire reinforcement mats was 50 feet. In the upper 64 feet, the reinforcement length made a dramatic jump from 50 feet to 90 feet. This led to the third design innovation in the wall, a lap zone. In order to create the 90-foot lengths of reinforcement, two 50-foot mats were laid on top of one another.

The mats overlapped a distance of 10 feet, with no mechanical connection made between the two mats. This 10-foot overlapped section is what was referred to as the lap zone.

Utah State University became involved with the project to monitor the performance of one of the reload walls. The wall was instrumented with 150 precision strain gages, 12 vibrating wire total pressure cells, and one horizontal inclinometer. Barton (2001) presented a complete description of the instrumentation scheme, as well as the results and interpretations of the data collected from the instrumentation.

Objectives and scope of research

The purpose of this research is to investigate the performance of the lap zone in the 90-foot Hilfiker welded-wire mats, and whether complete stress transfer occurs between the two lapped mats. Two analysis tools were used to investigate the lap zone. First, a finite element analysis was performed using the computer program Plaxis. Second, physical modeling was completed using a scale model pullout box.

Using Plaxis, two sets of finite element computer models were created. The first set was a parametric study of pullout testing. The models investigated the influence of overburden, gap width, boundary effects, and horizontal spacing of transverse elements on pullout resistance. Following the completion of both the parametric study and the scale pullout tests, the second set of computer models was completed. The final models contained the same dimensions, welded-wire mat configurations, and soil parameters as the scale pullout tests. The second set was used to verify that Plaxis could calculate pullout resistance similar to that recorded during the scale pullout testing and to validate

the parametric study completed in the first set of models. Two final Plaxis models were completed whose results were similar to those obtained during the scale pullout testing.

The second area of research utilized physical pullout testing. A scale model pullout box was designed and built on campus at Utah State University to accommodate the pullout testing. Two sets of pullout tests were performed. The first set of tests was performed using a closed pullout box. Four pullout test configurations were used: (one) a single layer of welded-wire mats without a lap zone, (two) three layers of mats without a lap zone, (three) a single layer of mats with one included lap zone, and (four) three layers of mats with three included lap zones. This initial set of pullout tests was performed at varying overburdens of 77, 212, 326, and 581 psf.

The second set of pullout tests was performed using a split pullout box. This set of pullout tests was performed using five pullout test configurations (numbered in sequence from the previous four tests): (five) three levels of mats with three lap zones, free split box; (six) three levels of mats with three lap zones, fixed split box; (seven) three levels of mats with three lap zones, fixed box, pullout forces applied to left side only; (eight) three levels of mats with three lap zones, free box; (nine) three levels of mats with no lap zone, fixed box. All of the pullout tests for the final test configurations were performed at the overburden pressure of 326 psf.

CHAPTER 2

LITERATURE REVIEW

Introduction

This chapter discusses some of the design parameters dealing with mechanically stabilized earth walls. Since the introduction of the Reinforced Earth system by Henri Vidal, numerous soil reinforcement systems have been introduced. Regardless of the proprietary system used, all mechanically stabilized earth walls need to meet the same basic design requirements.

Principal components of mechanically stabilized earth walls

All earth reinforcement systems are composite structures built using alternating horizontal layers of reinforcing elements and compacted soil. These alternating layers of soil and reinforcement are typically spaced 12 to 30 inches, depending on the wall design. The reinforcing elements add tensile strength to the soil mass and reduce both vertical and lateral wall deformations. Although different reinforcement materials and design configurations are used for each mechanically stabilized earth wall system, all contain three major components: (1) the reinforcing elements, (2) the backfill soils, and (3) the facing elements (Anderson, Nelson, and Sampaco, 1995). Figure 2.1 shows the principal components of a mechanically stabilized soil mass.

As stated previously, numerous types of reinforcing systems and materials are available for design purposes. As each system has its unique advantages and possible

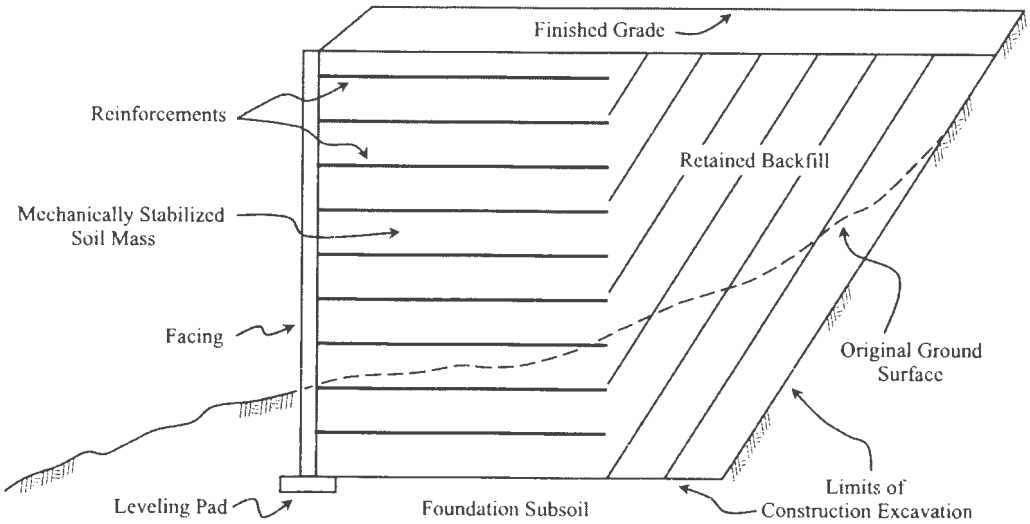

Figure 2.1. Principal components of a mechanically stabilized soil mass (after Anderson, Nelson, and Sampaco, 1995).

disadvantages, careful consideration should be made of the project requirements before selection of a reinforcement system. An important requirement is the selection of the backfill material used in the wall. The type of backfill chosen depends upon the design requirements of the structure and upon the economics of the available soil. For most soil structures, well-graded cohesionless fills (granular material) are used due to their free drainage and stability. Cohesive backfills can also be used, though they are usually undesirable due to their poor drainage, low strength, compressibility, and creep properties (Mitchell and Christopher, 1990).

Another important requirement is the selection of the facing elements used in the wall. The type of facing element chosen depends upon the amount of settlement the wall can tolerate. A flexible wall face, such as the welded-wire facing mat used in the Hilfiker system, can tolerate large amounts of settlement. A stiff wall face, such as the cruciform

facing panel used with the Reinforced Earth system, can tolerate little, if any settlement. Of course, a stiff-faced system can still be used on projects where large settlements are projected if the primary settlement is allowed to occur before placing the facing panels.

Stability requirements

Irrelevant of the basic components used, all mechanically stabilized earth walls must meet the important design criteria of external and internal stability. The external stability is generally evaluated by considering the entire reinforced soil structure as a reinforced concrete or gravity wall system with active pressure acting behind it. The wall can then be analyzed using the conventional stability criteria of sliding, overturning, bearing capacity, and deep stability. Figure 2.2 shows the four mechanisms of external failure in reinforced soil walls.

The internal stability of any reinforced wall is evaluated against: (1) tensile failure of the reinforcements and (2) pullout failure if the reinforcing elements. The strength of the reinforcing elements is critical because tensile failure can lead to progressive collapse of the reinforced structure as the load is transmitted to the remaining elements. The pullout resistance is vital because any slippage between the reinforcing elements and the soil can lead to progressive deformation of the wall due to a redistribution of stresses (Budhu, 1999). Additionally, slippage or pullout failure normally occurs for short embedment length to wall height ratios (L/H), when the soil/embedment interaction is not sufficient to prevent pullout (Schlosser, 1990). Figure 2.3 shows the two modes of internal failure.

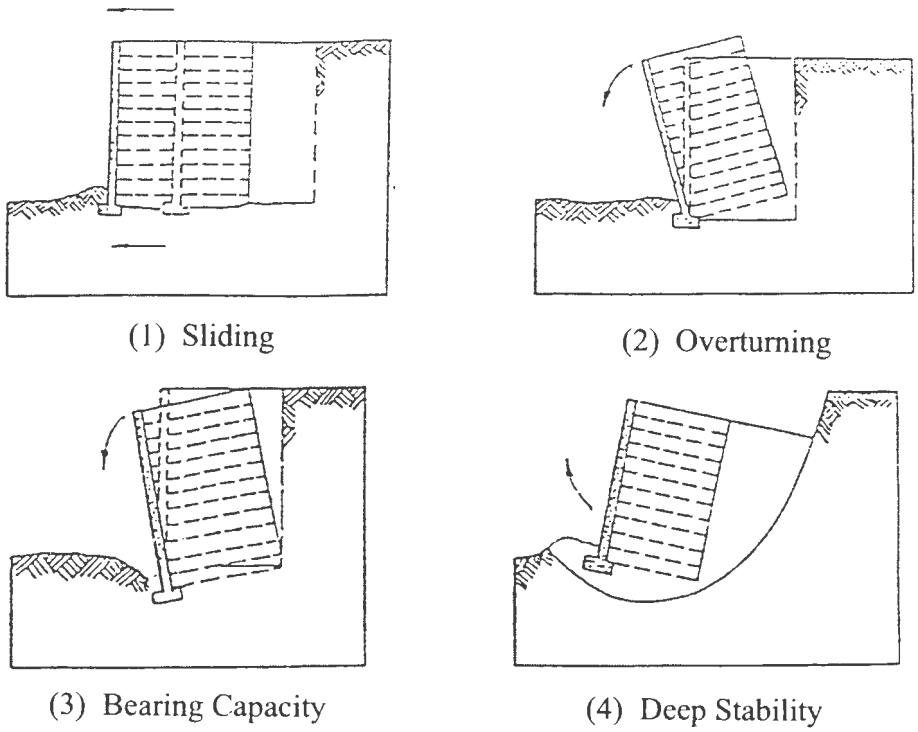

Figure 2.2. Mechanisms of external failure in reinforced soil walls (after Christopher et al., 1989).

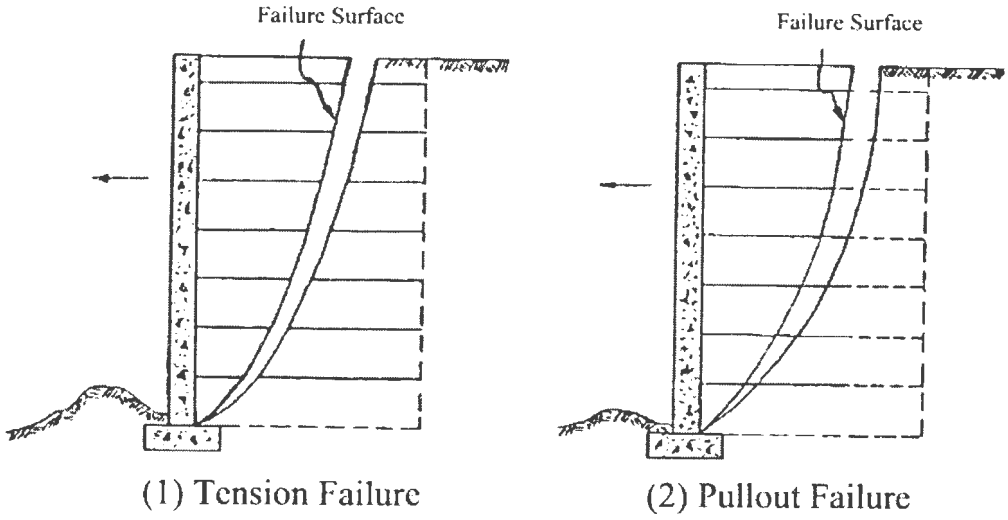

Figure 2.3. Mechanisms of internal failure in reinforced soil walls (after Anderson, Nelson, and Sampaco, 1995).

Lateral earth pressure coefficient

The lateral earth pressure that develops within a mechanically stabilized earth wall can be grouped into three conditions: (1) the active condition, (2) the at-rest condition, and (3) the passive condition. The active condition, K_a, develops if the wall reinforcement is flexible enough to allow substantial movement during or after construction. The at-rest condition, K_o, develops if the wall reinforcement is stiff enough that a minimal amount of lateral movement occurs during or after construction. The passive condition, K_p, develops if compressive forces within the wall force the reinforced mass into the native slope.

When considering the internal stability of the reinforced wall, it is important to understand that stresses are transferred differently from the reinforcement to the soil depending upon the system selected. All systems fall under two basic categories: extensible and inextensible reinforcement. Anderson, Nelson, and Sampaco (1995, p. 7) noted that extensible systems, such as geotextile sheets or polymer grids, "require relatively large strains to mobilize the strength of the reinforcement and thus larger internal deformations generally occur in these types of walls and embankments." On the other hand, inextensible systems, which comprise the majority of the available systems today, derive their name from the fact that the strains "required to mobilize the full strength of the reinforcing elements are much smaller than the strains required to mobilize the strength of soil" (Anderson, Nelson, and Sampaco, 1995, p. 7).

Inextensible and extensible reinforcements also show differences with respect to their structural behavior. Extensible reinforcing elements allow substantial yielding of

the soil to occur, which induces lateral displacements near the top of the reinforced soil structure, and which mobilizes the active lateral soil pressure. Inextensible reinforcing elements, on the other hand, have small lateral displacements near the top of the wall. This seems to develop the at-rest lateral earth coefficient in the upper part of the wall, with the active state of stress developing in the lower part of the wall. The at-rest condition develops in the upper part of the wall due to overstressing from heavy compaction. The active condition develops in the lower part of the wall due to the arching effect between the base of the reinforced soil structure and the upper section of the wall (Schlosser, 1990).

The appropriate lateral earth coefficient value to use in the design process depends upon the soil reinforcement system that is chosen. Christopher et al. (1989) compiled the design envelopes of K, which are normalized with respect to the active earth pressure, K_a. These envelopes are shown in Figure 2.4.

Pullout resistance

The interaction between the soil and the reinforcement is a key parameter that needs to be considered during the design of any reinforced soil structure, and is usually accomplished by measuring the pullout resistance. The pullout resistance of welded-wire mats has been shown to be a function of three parameters: (1) the number and length of the transverse and longitudinal wires embedded behind the failure plane, (2) the diameter of the transverse and longitudinal wires, and (3) the overburden pressure (Nielsen and Anderson, 1984). Additionally, the pullout resistance is generally provided through one or a combination of two basic load transfer mechanisms: (1) friction against longitudinal

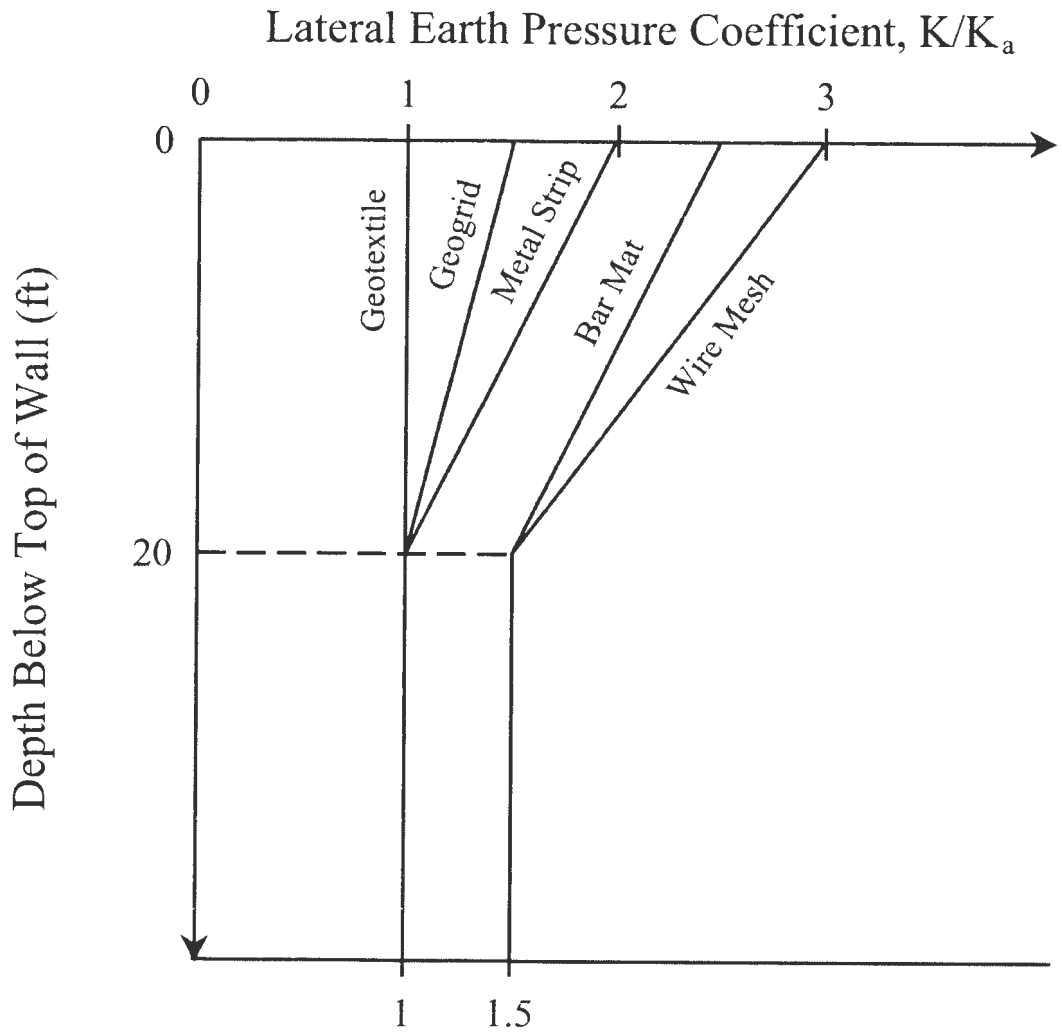

Figure 2.4. Design values of the lateral earth pressure coefficient (K) for various types of soil reinforcement systems (after Christopher et al., 1989).

elements and (2) passive soil resistance against transverse elements (Mitchell and Christopher, 1990). Figure 2.5 shows the stress transfer mechanisms for soil reinforcement. Although both load transfer mechanisms contribute to pullout resistance, one is generally dominant depending on the type of reinforcement used. The total pullout resistance, F_t, can be calculated as:

$$F_t = F_f + F_p \tag{2.1}$$

where F_f = frictional resistance of longitudinal wires,

F_p = passive resistance of transverse wires.

Frictional resistance. The frictional resistance is developed through contact between the soil particles and the longitudinal reinforcement. The magnitude of frictional resistance is a function of the overburden pressure, the coefficient of friction between the soil and the reinforcement, and the surface area of the reinforcement (Nielsen and Anderson, 1984). The frictional resistance can either be determined experimentally or theoretically. The frictional resistance, F_f, for a single longitudinal wire per unit length, L, is given by:

$$\frac{F_f}{L} = \sigma_{ave}\, \pi\, d\, \tan\delta \tag{2.2}$$

where d = diameter of wire,

$\tan\delta$ = friction coefficient between soil and reinforcement,

σ_{ave} = average stress over circumference of wire,

$$= \frac{\sigma_v + \sigma_h}{2} = \frac{\sigma_v + K\sigma_v}{2} = \frac{\sigma_v (1+K)}{2}$$

K = lateral earth pressure coefficient.

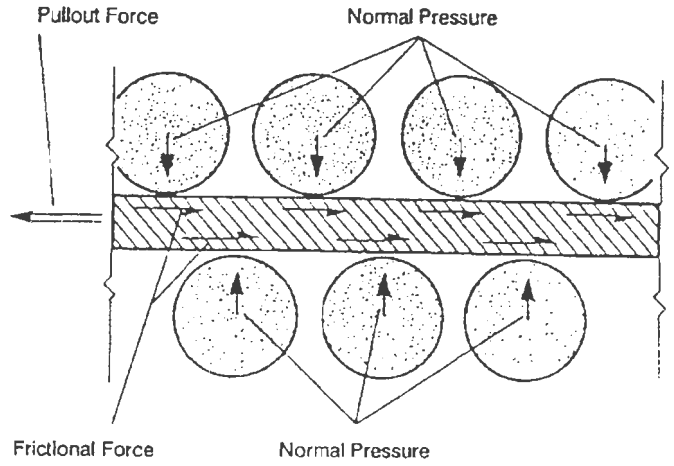

A) FRICTIONAL STRESS TRANSFER BETWEEN SOIL AND REINFORCEMENT

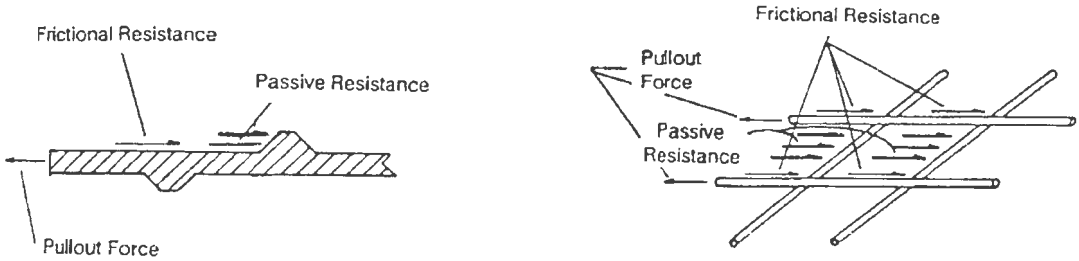

B) SOIL PASSIVE (BEARING) RESISTANCE ON REINFORCEMENT SURFACES

Figure 2.5. Stress transfer mechanisms for soil reinforcement (after Mitchell and Christopher, 1990).

Although the theoretical equation gives conservative results, it is a reasonable design approach for welded-wire walls because frictional resistance is small when compared to passive resistance of the transverse elements.

Passive resistance. The passive resistance is developed when a bearing surface normal to the pullout force is pulled into the soil. Such is the case with a welded-wire mat, where each of the transverse elements develops passive resistance along its front face. Unlike frictional resistance, however, passive resistance from the transverse elements of a welded-wire mat is not well understood due to its complexity. Despite this fact, laboratory results have been used as bases for empirical methods to quantify the magnitude of the passive resistance. Each of these methods assumes a particular failure mechanism in order to define a theoretical equation.

Peterson and Anderson (1980) provided an expression that forms the upper-bound estimation for bearing capacity, as shown in Figure 2.6(a). The bearing capacity failure mode assumes that the transverse member behaves like a strip footing rotated to the horizontal. The ratio of the grid bearing stress, σ_b', to the overall normal effective stress, σ_n', in the soil is given by (Prandtl, 1921; Reissner, 1924):

$$\frac{\sigma_b'}{\sigma_n'} = N_q = e^{(\pi \tan\phi')} \tan^2(45 + \frac{\phi}{2}) \qquad (2.3)$$

The value of N_q can then be substituted into the Terzaghi-Buissman bearing capacity equation (Dunn, Anderson, and Kiefer, 1980) to obtain the upper estimate of the transverse bearing resistance as follows:

$$Q_{ult} = B c N_c + 0.5 \sigma_n' B^2 N_\gamma + \sigma_n' B N_q \qquad (2.4)$$

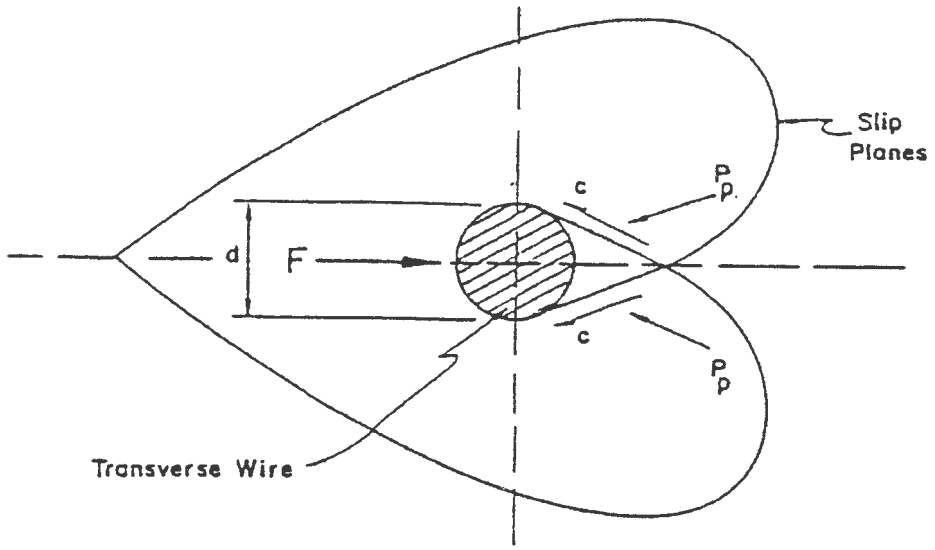

$$N_q = e^{(\pi \tan \phi')} \tan^2 (45 + \phi'/2)$$

(a) Bearing Capacity Failure (After Peterson & Anderson, 1980)

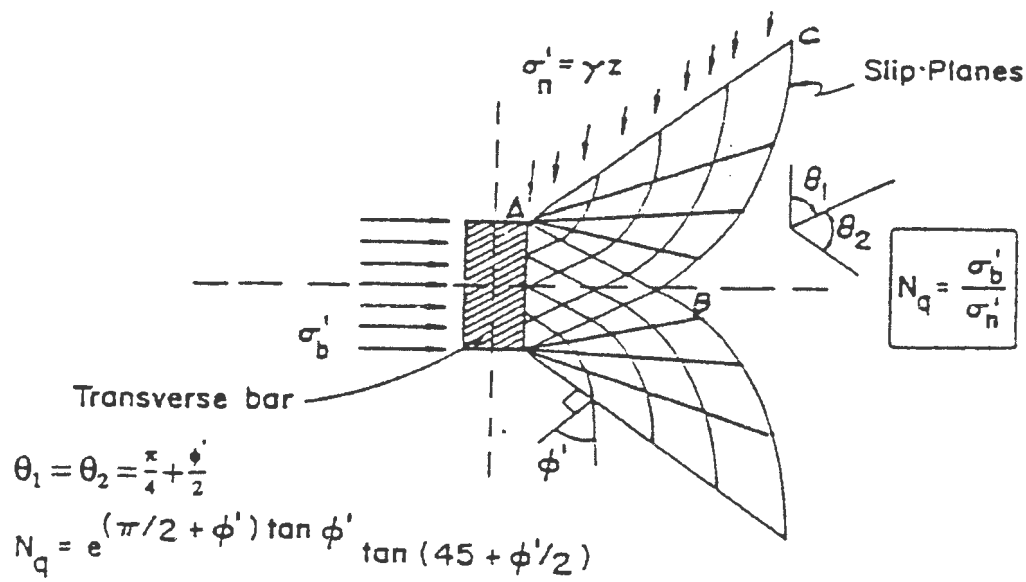

$$\theta_1 = \theta_2 = \frac{\pi}{4} + \frac{\phi'}{2}$$

$$N_q = e^{(\pi/2 + \phi') \tan \phi'} \tan (45 + \phi'/2)$$

(b) Punching Shear Failure (After Jewell et al, 1984)

Figure 2.6. Bearing failure mechanisms of grid reinforcement.

where Q_{ult} = force per unit length of the bearing member,

B = width of the bearing member,

c = soil cohesion,

$N_{c, \gamma, q}$ = bearing capacity factors.

For welded-wire reinforcement, the passive force per unit length of a single transverse wire, F_p/Nw, can be equated to Equation 2.4 to obtain an estimate of the transverse resistance as follows:

$$\frac{F_p}{N w} = B c N_c + 0.5 \sigma_n' B^2 N_\gamma + \sigma_n' B N_q \tag{2.5}$$

Jewell et al. (1984) provided an expression that forms the lower-bound estimation for bearing capacity, modeled as a punching shear failure, as shown in Figure 2.6(b). Jewell postulated that the bearing stress of the soil on the welded-wire elements is similar to the base pressure on deep foundations. The transverse members can be assumed to act like a line of anchors at some spacing, s, and diameter, d. Additionally, a high value of h/d can be assumed because the transverse elements can be considered deeply embedded. The resulting value of N_q is given by:

$$N_q = e^{(\frac{\pi}{2} + \phi') \tan \phi'} \tan(45 + \frac{\phi'}{2}) \tag{2.6}$$

The value of Nq obtained from Equation 2.6 can then be used in Equation 2.5 to obtain the lower estimate of the transverse bearing resistance.

Potential failure surface. Mechanically stabilized earth walls are quite different from classical retaining walls in both their behavior and failure mechanisms. This has been confirmed through both full-scale experiments and observations (Juran and

Schlosser, 1978). This difference can be explained by the inclusion of reinforcements that restrain deformations and change the distribution of stresses and strains in the soil (Juran, 1977: Mitchell and Villet, 1987).

The pullout resistance of the reinforcing elements must be developed behind the potential failure surface. Anderson, Nelson, and Sampaco (1995) noted that the longitudinal reinforcing elements should develop their maximum tension at the location of this failure surface, which, according to field measurements and theoretical analysis, does not necessarily correspond to the Coulomb failure plane as reported by Lee, Adams, and Vagneron (1973). This failure surface has also been reported as conforming to a parabolic surface (Schlosser and Long, 1974) and to a logarithmic spiral (Juran, 1977). The location and shape of the potential failure surface varies depending upon the geometry of wall and the type and stiffness of the reinforcing elements.

In order to formalize the design procedure for mechanically stabilized earth walls, Christopher et al. (1989) utilized the currently available field and experimental data to create two types of potential failure planes. The failure surface chosen for design purposes depends upon the stiffness of the chosen reinforcement. For inextensible reinforcement such as welded wire mats or Reinforced Earth straps, a bilinear failure surface is defined as shown in Figure 2.7(a). For extensible reinforcement such as geotextiles or geogrids, the failure surface closely resembles the Coulomb failure plane as shown in Figure 2.7(b).

The maximum tension that occurs on the failure plane can be calculated using Equation 2.7. Each longitudinal reinforcing element must be able to provide lateral

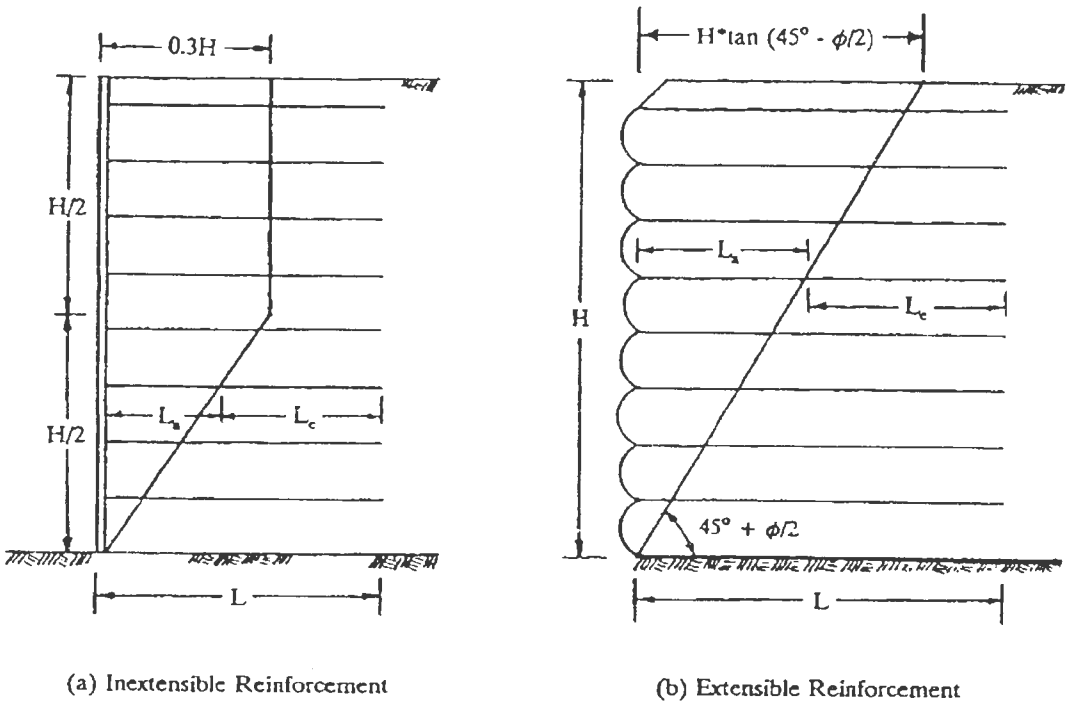

Figure 2.7. Locations of potential failure surface in reinforced soil walls (after Anderson, Nelson, and Sampaco, 1995).

restraint within the reinforced mass. Each longitudinal element is responsible for an area that extends half the distance to the adjacent wires above, below, and on both sides. Generally, the maximum tension can be expressed as:

$$T_{max} = \sigma_h S_h S_v \tag{2.7}$$

where σ_h = horizontal stress,

S_h = average horizontal spacing of longitudinal wires,

S_v = vertical spacing between layers of reinforcement.

The horizontal stress at any depth, z, from the top of the wall can be calculated using the following equation (Christopher et al., 1989):

$$\sigma_h = K(\gamma z + q + \Delta\sigma_v) + \Delta\sigma_h \qquad (2.8)$$

where K = lateral earth pressure coefficient,

γ = unit weight of the backfill material,

q = surcharge load,

$\Delta\sigma_v$ = increase in vertical stress due to concentrated vertical loads,

$\Delta\sigma_h$ = increment of horizontal stress due to horizontal concentrated surcharge loads.

The potential failure plane divides the mechanically stabilized earth wall into two zones. The zone nearest the face of the wall, called the active zone, tends to spread laterally. As the soil in this zone begins to move, stresses are transferred to the reinforcement by shear in the direction of the wall face. This can be seen in Figure 2.8. The second zone, called the resistant zone, provides the necessary resistance to prevent the reinforcement from pulling out of the backfill soil. As tensile forces are applied to the reinforcement in this zone, shear stress are mobilized in the direction of the free end of the reinforcement to counteract the tensile forces and prevent pullout (Sampaco, 1996).

Long-term pullout resistance. As part of the design process, the long-term pullout resistance of the reinforcing elements should be evaluated with respect to three criteria. First, the pullout resistance or capacity of the reinforcement should exceed the design tensile load by some factor of safety, the recommended value being 2.0. Second, the amount of reinforcement displacement with respect to the backfill material needed to

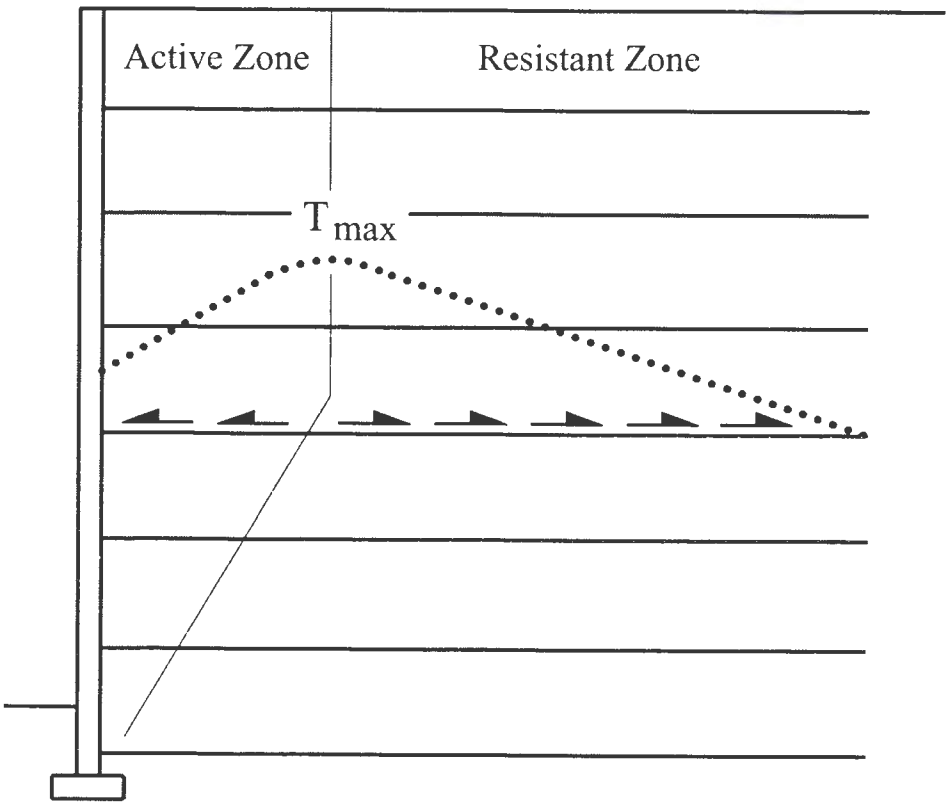

Figure 2.8. Tensile force distribution along longitudinal reinforcements in a mechanically stabilized earth wall (after Schlosser and Elias, 1978).

mobilize the design tensile load should be less than the total allowable displacement. Third, when considering long-term displacement, the pullout load should be less than the critical creep load for both the reinforcement and the backfill material (Mitchell and Christopher, 1990).

Equations for pullout resistance

In order to evaluate the pullout resistance of welded-wire reinforcement, numerous methods and design equations have been developed. Two of the most

commonly used equations that were developed for free-draining granular materials are the Federal Highway Administration equation (Christopher et al., 1989) and the Nielsen and Anderson (1984) design equations.

Federal Highway Administration equation. Christopher et al. (1989) developed a general equation that can be applied to different soil reinforcement systems. The pullout resistance per unit width of reinforcement, P_r, can be calculated as:

$$P_r = F^* \alpha \sigma_v' L_e C \qquad (2.9)$$

where L_e = embedment length in the zone behind the potential failure surface,

C = effective unit perimeter of the reinforcement (two for strips, grids, and sheets; π for nails),

F^* = pullout resistance or friction-bearing interaction factor,

α = scale effect correction factor,

σ'_v = effective vertical stress at the soil-reinforcement interface.

In order to accurately obtain the pullout resistance factor, F*, pullout tests should be performed. On the other hand, the factor can also be obtained from empirical or theoretical relationships provided by the reinforcement manufacturer or in the literature. It can also be estimated using the following equation:

F^* = passive resistance + frictional resistance

$$F^* = F_q \alpha_\beta + K \mu^* \alpha_f \qquad (2.10)$$

where F_q = embedment or surcharge bearing capacity factor,

α_β = structural geometric factor for passive resistance,

K = ratio of actual normal stress to the effective vertical stress; dependent on the geometry of the reinforcement,

μ^* = apparent friction coefficient,

α_f = structural geometric factor for frictional resistance.

The α-term in the equations reflects the non-linearity of the P_r - L_e relationship and depends primarily on the extensibility of the reinforcement element. For inextensible reinforcement it can be approximated as one; however, for extensible reinforcement it can be significantly less than one (Christopher et al., 1989).

Using some of the experimental results reported by Nielsen and Anderson (1984), the factor F* was derived for welded-wire reinforcement. The equation is:

$$F^* = 18.5\frac{D_T}{S_T} + 0.475\frac{D_L}{S_L} \tag{2.11}$$

where D_T = diameter of transverse wires

S_T = spacing of transverse wires

D_L = diameter of longitudinal wires

S_L = spacing of longitudinal wires

Nielsen and Anderson (1984) design equations. Ninety-three pullout tests were conducted by Nielsen and Anderson (1984) at the buried structures test facility at Utah State University. Using the plotted results from the pullout tests, prediction equations were developed for the best-fit line. The equations were derived as a function of the overburden pressure, mesh spacing, wire diameter, soil type, and number of longitudinal

and transverse wires. The pullout resistance per unit width of reinforcement, P_r, for silty sand can be calculated as:

For $N\sigma_v D_T > 113.6$ lb/ft:

$$P_r = \frac{F_t}{W} = 2143 + \sigma_v D_T (\pi L_e M \tan\delta + 17.61N) \quad (2.12)$$

For $N\sigma_v D_T < 113.6$ lb/ft:

$$P_r = \frac{F_t}{W} = \sigma_v D_T (\pi L_e M \tan\delta + 36.47N) \quad (2.13)$$

Additionally, the pullout resistance per unit width of reinforcement, P_r, for washed sand and pea gravel can be calculated as:

Washed sand:

$$P_r = \frac{F_t}{W} = 633 + \sigma_v D_T (\pi L_e M \tan\delta + 36.8N) \quad (2.14)$$

Pea gravel:

$$P_r = \frac{F_t}{W} = 712 + \sigma_v D_T (\pi L_e M \tan\delta + 38.1N) \quad (2.15)$$

where σ_v = vertical overburden pressure,

D_T = diameter of transverse wires,

L_e = embedment length,

M = number of longitudinal wires per unit width,

$\tan\delta$ = friction factor between soil and reinforcement,

N = number of transverse wires.

CHAPTER 3

PARAMETRIC STUDY

Introduction

In order to design both the pullout box and the pullout test program used in this study, a parametric study was undertaken to investigate how certain factors affect pullout resistance. By using the finite element computer program Plaxis, four pullout test parameters were investigated: overburden pressure, gap width, height of pullout box, and distance of transverse bars from pullout box face. First, the overburden pressure was investigated using seven different overburdens that varied from 1000 psf to 7000 psf. Second, the gap width was evaluated using six different widths that varied from 0.5 inches to 3 inches. Third, the height of the pullout box was studied using five different heights that varied from 6 inches to 6 feet. Finally, the horizontal distance of the first transverse bars from the pullout box face was examined using six distances that varied from 3 inches to 5 feet.

Plaxis finite element program

Development of the Plaxis finite element computer program began in 1987 at the Technical University of Delft to analyze river embankments on the soft soils of the lowlands of Holland. Over the past several years, Plaxis has been expanded to cover most other areas of geotechnical engineering, and is now principally used for deformation and stability analyses. Plaxis uses a plane strain two-dimensional analysis for structures with a relatively uniform cross section, stress state, and loading system (Plaxis, 1998).

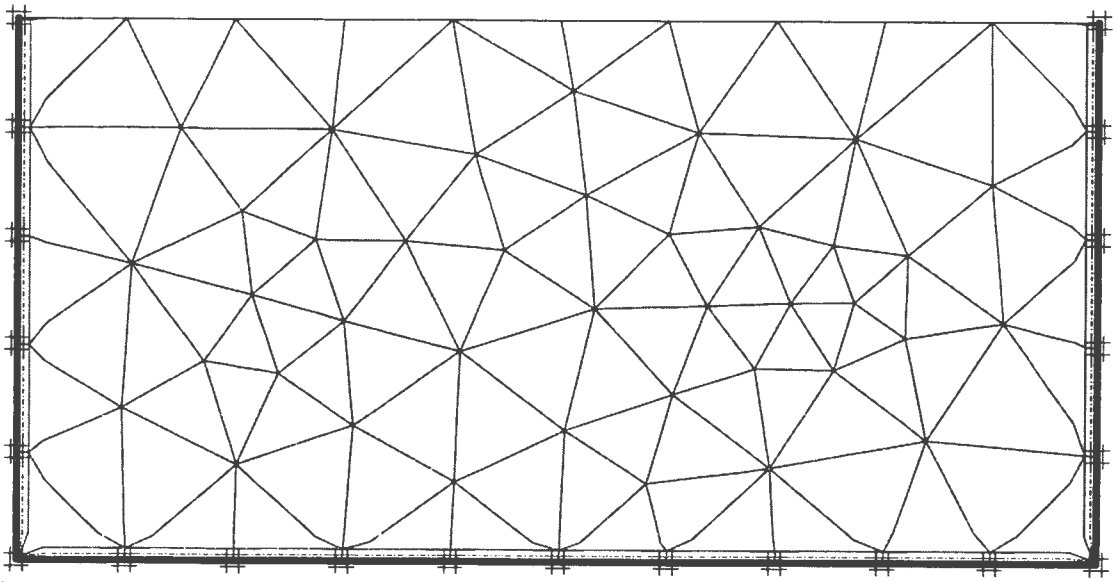

Figure 3.1. Typical finite element mesh composed of 15-node triangular elements.

The plane strain models are calculated over a length running perpendicular to the cross section.

Finite element mesh. Before calculations could begin, the geometry of the soil in each model was divided into a finite element mesh composed of basic 15-node triangular soil elements, as shown in Figure 3.1. The 15-node elements provide a fourth order interpolation for displacements. Numerical integration was used to evaluate the element stiffness matrix using a total of 12 Gauss stress points. Plaxis automatically generates the finite element mesh for each input model. The resulting disorderly mesh usually performs better numerically than regular or structured meshes (Plaxis, 1998). Figure 3.2 shows the position of the nodes in a 15-node triangular element.

Finite element meshes were also generated for each of the two basic structural objects used in the Plaxis pullout test models: beams and geotextiles. For the 15-node

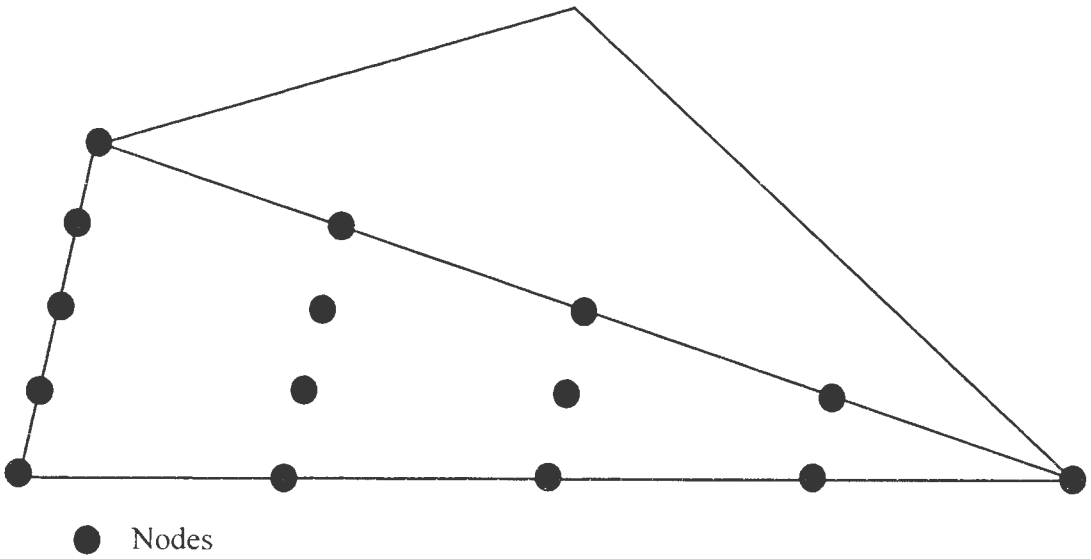

Figure 3.2. Distribution of nodes in a 15-node triangular element.

soil elements, 5-node beam elements are utilized where each node has three degrees of freedom (two translational and one rotational). Each 5-node beam element also contains four pairs of stress points that are spaced equally about the beam centerline. These stress points are used to evaluate the bending moments and axial forces. Figure 3.3 shows the position of the nodes and stress points in a 5-node beam element. For 15-node soil elements, 5-node geotextile elements are used. Figure 3.4 shows the position of the nodes and stress points in a 5-node geotextile element. The stress points for the geotextile elements, where the axial forces are evaluated, are located at the nodes (Plaxis, 1998).

Structural objects. The first structural object utilized in the models was a beam, which has both a significant bending stiffness and a normal stiffness. In Plaxis, beams

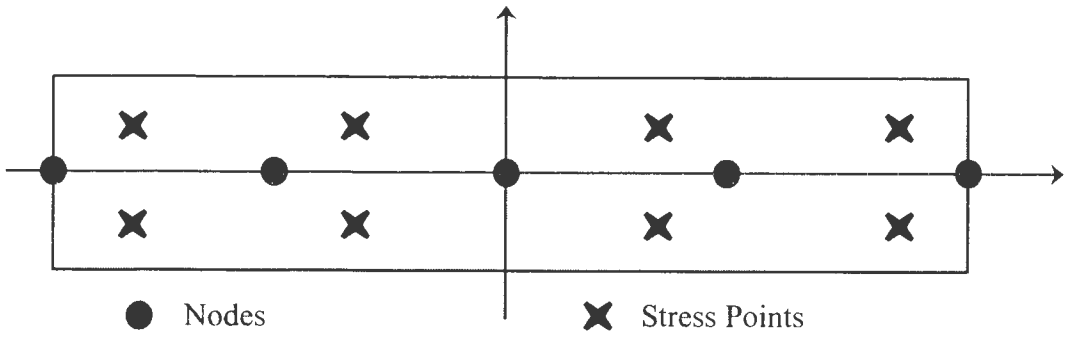

Figure 3.3. Distribution of nodes and stress points in a 5-node beam element.

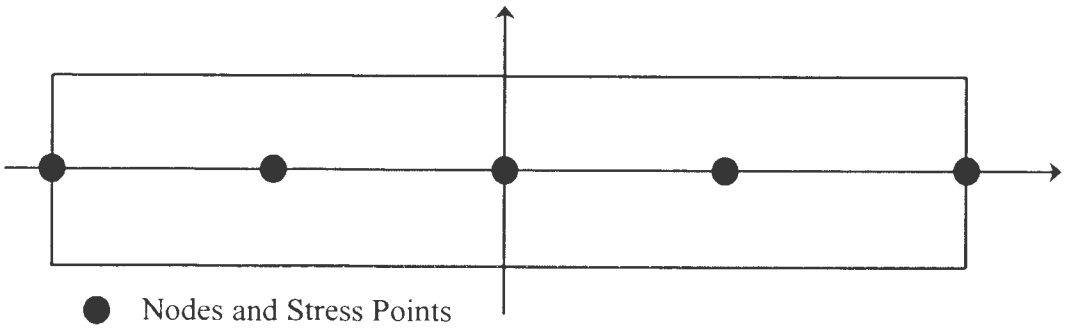

Figure 3.4. Distribution of nodes and stress points in a 5-node geotextile element.

can represent plates running perpendicular to the cross section. Thus, they can be used to model walls, boxes, and plates (Plaxis, 1998). Beams were used in the pullout test models to represent the pullout box, the loading plate, and the transverse elements.

The second structural object used in the models was a geotextile, which only has the property of elastic axial stiffness. Geotextiles can only sustain tensile forces, and are normally used in Plaxis to model geogrids, woven fabrics, or other extensible soil reinforcements (Plaxis, 1998). However, in the pullout models the axial stiffness was

increased so that the geotextile became inextensible. Geotextiles were used in the pullout test models to represent the longitudinal bars of the welded-wire mats.

Interfaces. In order to model the soil-structure interaction, Plaxis utilizes what is termed an interface. An interface can be placed on both sides of a geometry line or structural element to enable full interaction between the object and the surrounding soil. Figure 3.5 shows how the interface elements are connected to the 15-node soil elements. In the figure the interface nodes are shown at some finite distance from the soil element; however, the coordinates or position of each node pair are identical during generation of the finite element mesh. Simply put, the interface element has a zero thickness. In the pullout test computer models, an interface was used along all soil-structure boundaries (pullout box, transverse and longitudinal elements, and loading plate). Because the values of the interface friction angle and adhesion are not necessarily the same as the values of the friction angle and cohesion for the surrounding soil, the interface strength, R_{inter}, can be modified in the Plaxis program. The interface is generally weaker and more flexible than the soil for real soil-structure interaction; therefore, the R_{inter} value is usually a value less than one. The value may be assumed to be two-thirds for sand-steel or sand-geotextile contact (Plaxis, 1998).

Fixities. Additional items from the Plaxis model worth noting are the horizontal and vertical fixities. Fixities allow the user to prescribe areas of zero displacement within the finite element model. Total fixities (no horizontal or vertical movement) were applied to the pullout box to ensure that all deformations occurred within the soil matrix.

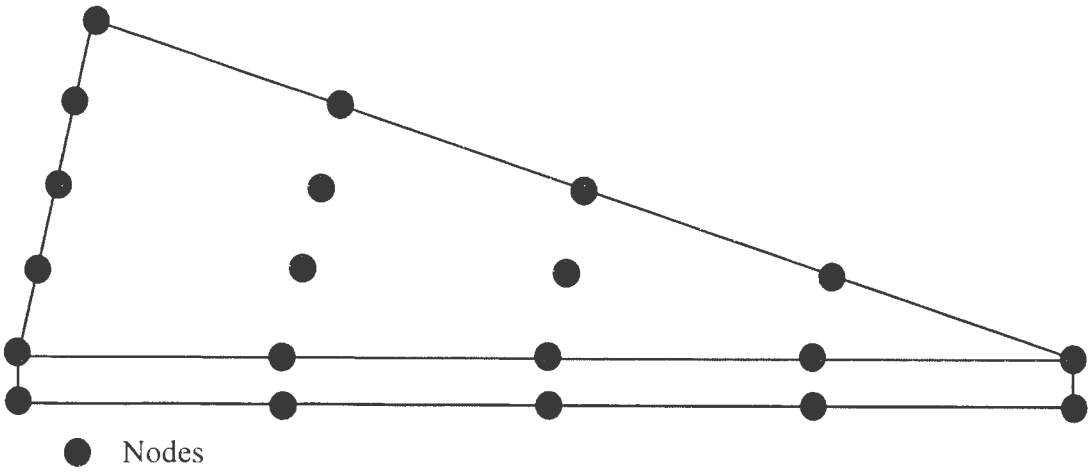

Figure 3.5. Distribution of nodes in an interface element connected to a soil element.

Finite element models

The Plaxis computer program was utilized to investigate four parameters that deal with pullout testing: overburden pressure, gap width, height of pullout box, and distance of transverse bars from box face. Each parametric model is described and the respective results and conclusions are given. Figure 3.6 shows an idealized diagram of the pullout box configuration used in each of the computer models. The "surcharge" was a soil of variable unit weight that was used to apply the overburden pressure. The "fill" was used to model the soil used in the pullout box. Both the "surcharge" and the "fill" are described in the following section. The "gap width" was the width of the opening in the face of the pullout box. The "point load" and "uniform load" were utilized to apply the pullout forces, and are described in more detail later. The "welded-wire mat", which was modeled using a continuous geotextile sheet, and the "transverse bars," which were modeled using beam elements, were used to represent actual welded-wire mats used in

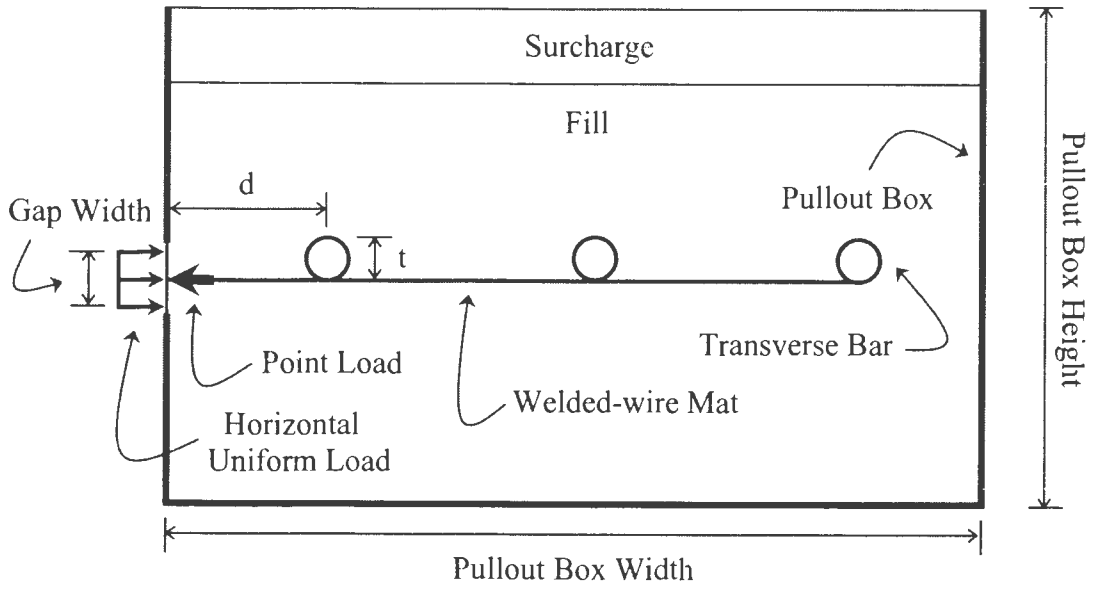

Figure 3.6. Idealized diagram of pullout box configuration.

pullout tests. The "pullout box height" and the "pullout box width" were used to define the size of the model pullout boxes.

Finite element model parameters. The soil, reinforcement, and interface properties used in the Plaxis computer models can all be found in Table 3.1. Several items from the parameters table are worth noting. First, the deformations or displacements of the backfill soil (noted as "fill") used in the pullout box were calculated using a hardening-soil model. Though the hardening- soil model is a type of hyperbolic model, it varies in three distinct ways: (1) it uses the theory of plasticity in lieu of elasticity, (2) it includes soil dilatancy, and (3) it utilizes a yield cap (Plaxis, 1998).

A second material model was used for the "surcharge" in the pullout box models. The vertical stresses were applied to several of the models via a surcharge load rather

Table 3.1. Soil, reinforcement, and interface properties used in Plaxis models

Material property description	Fill	Surcharge	Beam elements	Geotextile elements
Material model	Hardening Soil	Liner Elastic	--	--
Materail type	Drained	Drained	Elastic	--
Dry unit weight, γ_{dry}	130 lb/ft^3	Variable	--	--
Horizontal permeability, k_x	0 ft/day	0 ft/day	--	--
Vertical permeability, k_y	0 ft/day	0 ft/day	--	--
Initial void ratio, e_0	1.0	1.0	--	--
Plastic straining due to primary deviatoric loading, E_{50}^{ref}	20000 lb/ft^2	--	--	--
Plastic straining due to primary compression, E_{oed}^{ref}	20000 lb/ft^2	--	--	--
Young's modulus, E_{ref}	--	2000 lb/ft^2	--	--
Poisson's ratio, ν	--	0.3	0.2	--
Stress dependent stiffness according to a power law, m	0.5	--	--	--
Cohesion, c_{ref}	0 lb/ft^2	--	--	--
Friction angle, φ	38°	--	--	--
Dilatancy angle, Ψ	0°	--	--	--
Interface strength reduction factor, Rinter	0.6	0.6	--	--
Axial stiffness, EA	--	--	6.0E+09 lb/ft	6.0E+09 lb/ft
Flexural rigidity, EI	--	--	6.0E+09 lb-ft^2/ft	--

than a uniform load. Plaxis only allows two simultaneous load arrangements; whether it be uniform load A and uniform load B, point load A and point load B, or some combination thereof. As will be explained later, a uniform load A and point load B were used to model the pullout performance of the longitudinal wires. This necessitated the use of a surcharge to provide the required vertical stresses or loads. The surcharge material was defined as a linear elastic soil. Only two elastic stiffness parameters are

included in this model: Young's modulus, E, and Poisson's ratio, ν. The linear elastic model was deemed appropriate for the surcharge material because, as noted, it was used only as a means to apply vertical stress.

Two more parameters were included in the finite element models to deal with water. First, both the fill and surcharge materials were defined as "drained." This means that no excess pore pressures were generated, which was the case for the pullout models in that no phreatic water line or water pressures were included. Second, the permeability of both soils was equal to zero. In Plaxis, the permeability parameters are only required for consolidation calculations or for groundwater flow analyses (Plaxis, 1998). Once again, since no water pressures were included in the models, permeability was ignored.

Overburden pressure. The first parameter that was investigated using Plaxis was the effect of overburden pressure on pullout resistance. The dimensions of the pullout box for this model were 3 feet by 6 feet (height by width), with one additional foot of overburden. The welded-wire reinforcement was modeled using a 5-foot long inextensible and continuous geotextile sheet. Due to limitations within the Plaxis program, no transverse elements were included in this model, but were studied in later models. The width of the opening in the pullout box face, or gap width, was set at 1.2 inches.

The trial runs of the pullout test model proved to be erroneous. Initially, a horizontal point load was applied to the end of the geotextile to simulate the pullout force and a vertical uniform load was applied to the top of the box to simulate the overburden pressure (no surcharge material). The soil at the opening in the pullout box face failed

before any tension could be applied to the longitudinal reinforcement. There was, however, a simple solution to the problem. The uniform load was removed from the top of the box and applied horizontally to the opening in the pullout box. In order to apply an overburden pressure, a surcharge was added to the top of the pullout box to replace the vertical uniform load. This change allowed the longitudinal reinforcement to develop tensile forces and it forced the failure to occur within the fill material.

Seven overburden models were evaluated. All parameters from Table 3.1 were held constant except for the unit weight of the overburden. The unit weight was varied in 1000 psf increments starting with a 1000-psf and ending with a 7000-psf overburden. Figure 3.7 shows the load displacement curves for the finite element models. As can be seen, the pullout resistance is a function of overburden pressure. When the overburden pressure is increased, the pullout resistance of the soil reinforcement also increases.

Gap width. The second parameter that was investigated using Plaxis was the effect of the width of the opening of the pullout box face (gap width) on pullout resistance. The dimensions and parameters of this model were the same as those for the overburden model. However, for this model the overburden was held constant and the gap width was varied to measure the pullout resistance. Six models were run with this configuration. The gap width was varied in 0.5-inch increments starting with a 0.5-inch and ending with a 3-inch gap. Figure 3.8 shows the load displacement curves for the finite element models. As can be seen, the size of the opening in the face of the pullout box, the gap width, has little effect on the pullout resistance of the reinforcement.

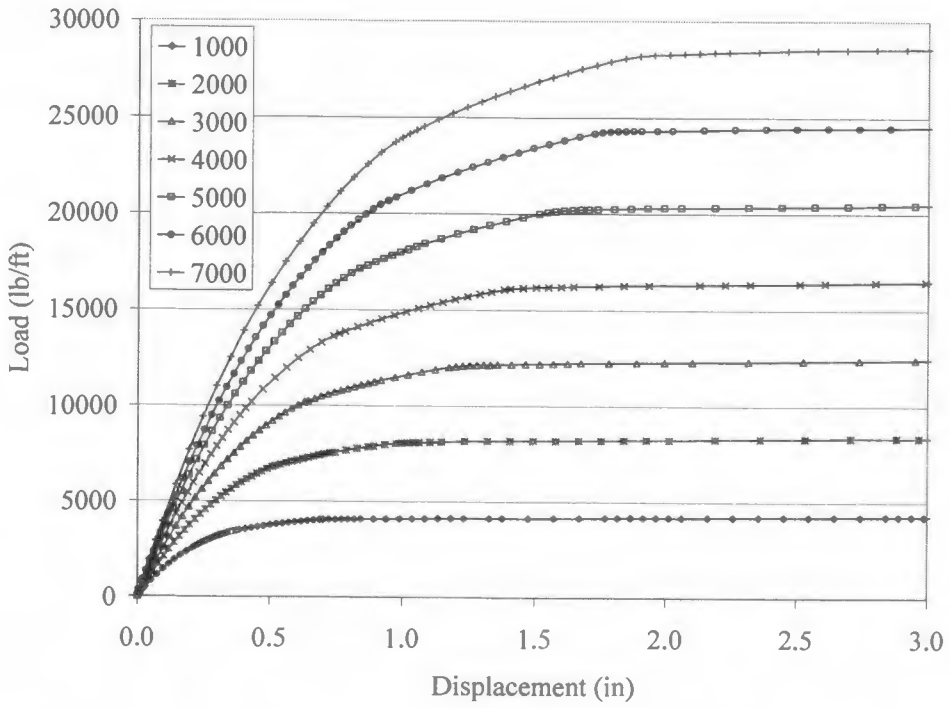

Figure 3.7. Effect of overburden pressure on pullout resistance.

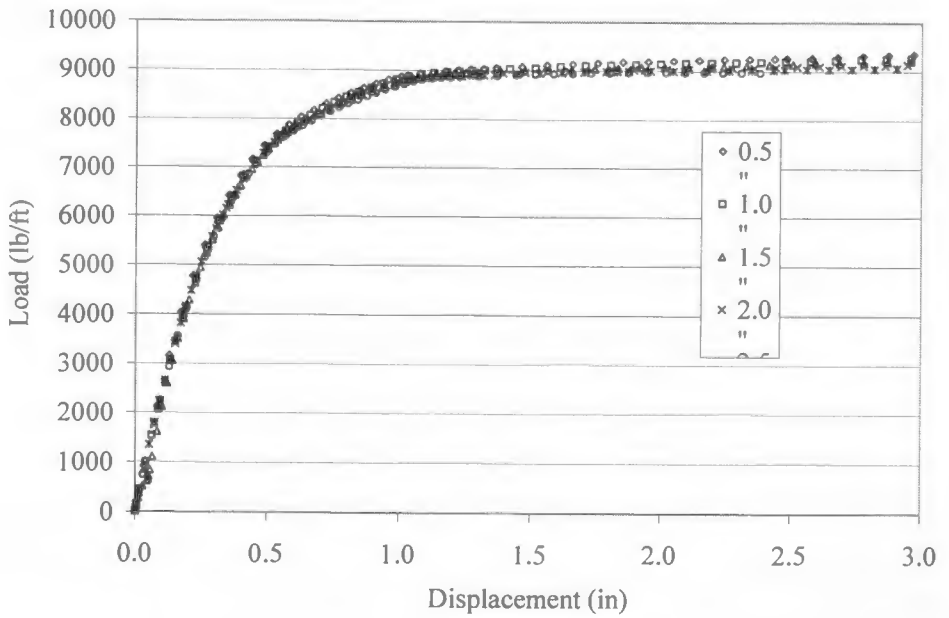

Figure 3.8. Effect of the width of the opening of the pullout box face (gap width) on pullout resistance.

Height of pullout box. The third parameter that was investigated using Plaxis was the height of the pullout box and whether boundary effects would change the pullout resistance. For this model the overburden and gap width were held constant and the height of the pullout box was varied. Additionally, a loading plate was added between the surcharge and the fill materials. This was to ensure that any boundary effects would be modeled and evaluated on all sides of the pullout box. Five models were run with this configuration. The various heights of the pullout box that were modeled were 6 inches, 1 foot, 2 feet, 4 feet, and 6 feet. Figure 3.9 shows the load displacement curves for the finite element models. The pullout force at a displacement of 0.2 inches, 0.6 inches, and 1.0 inch for the five pullout box heights was obtained from Figure 3.9 and the results are plotted on Figure 3.10. As can be seen, the height of the pullout box can adversely affect the measured pullout resistance, though the effects are greater at low strains. Concerns should be raised when the size of the pullout box is less than 3 feet in height. The stress interaction between the pullout box and the reinforcement can increase the pullout resistance and give inaccurate results.

Horizontal distance of transverse bars from pullout box face. The fourth parameter that was investigated using Plaxis was the effect that the distance from the first transverse bar to the pullout box face had on pullout resistance. This can be seen graphically as the dimension "d" in Figure 3.6. The reason that this parameter was investigated is that as the dimension "d" decreases, the pullout resistance could increase due to greater passive resistance against the pullout box face.

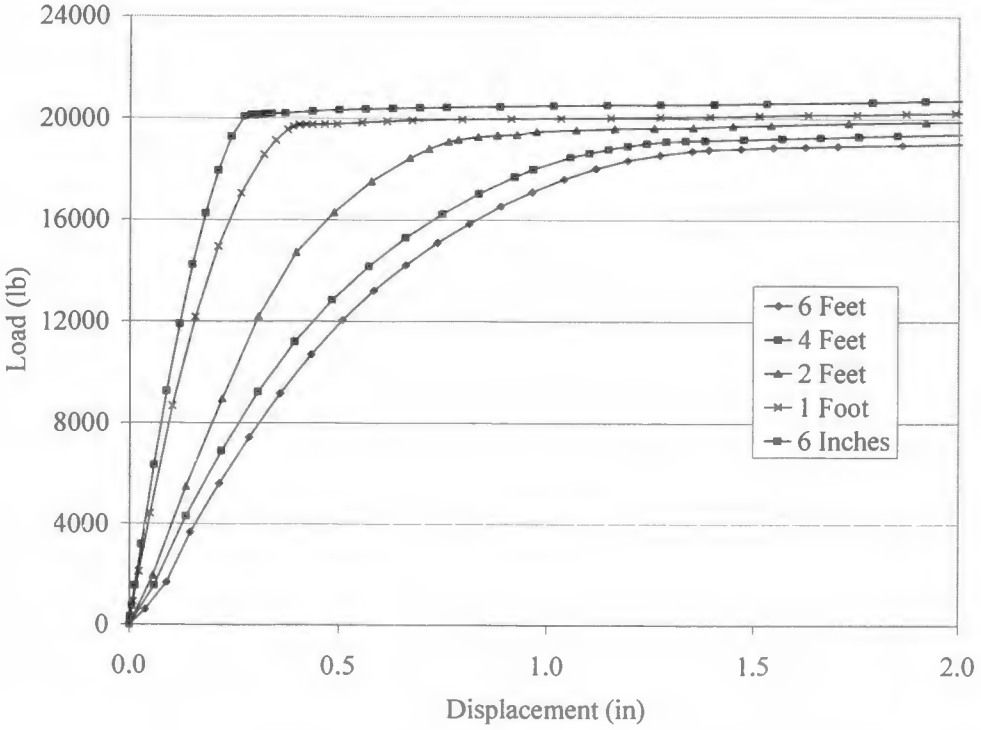

Figure 3.9. Boundary effects as a result of the pullout box height.

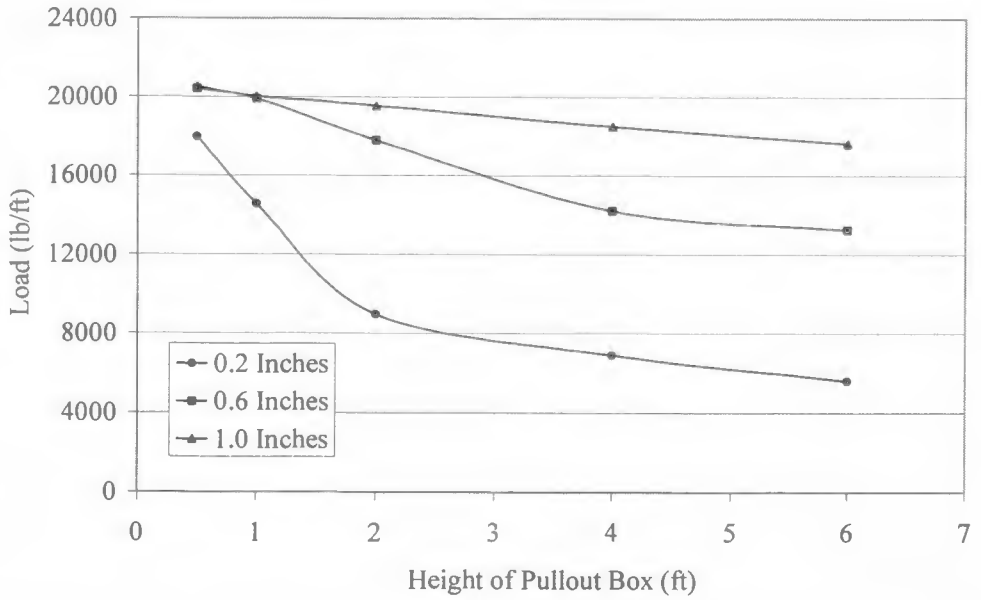

Figure 3.10. Required pullout force as a function of pullout box height for a displacement of 0.2 inches.

This was a very simple model geometrically. The dimensions of the pullout box for this model were 6 feet by 6 feet (height by width), with no added overburden. The transverse bar of the welded-wire reinforcement was modeled using a 2.5-inch long vertical beam element. Additionally, there was no opening in the pullout box face. A single point load was applied to the center of the vertical beam element to provide the pullout force. In total, six models were run with this configuration. The vertical beam element was spaced horizontally from the pullout box face at distances, d, of 3 inches, 6 inches, 1 foot, 2 feet, 3 feet, and 5 feet. Figure 3.11 shows the load displacement curves for the finite element models. Another graph was prepared using the results of the transverse element models. In order to generate this graph, a displacement of 0.4 inches was selected, the corresponding pullout force for each of the box sizes was noted, and this force was then plotted against the normalized value of the horizontal distance from the pullout box face over the height of the transverse bar (the ratio of d/t as shown on Figure 3.6). This graph is shown in Figure 3.12. When considering the model results, care needs to be taken to ensure that the first transverse bar of a welded-wire mat is spaced far enough horizontally from the pullout box face so that the pullout resistance is not adversely increased. Figure 3.12 suggests that a ratio of the horizontal distance over the height of the transverse element (a ratio of d/t) of six is sufficient.

Conclusions and guidelines for pullout testing

As mentioned, in order to design both the pullout box and the pullout test program used in this study, a parametric study was completed to investigate how certain factors

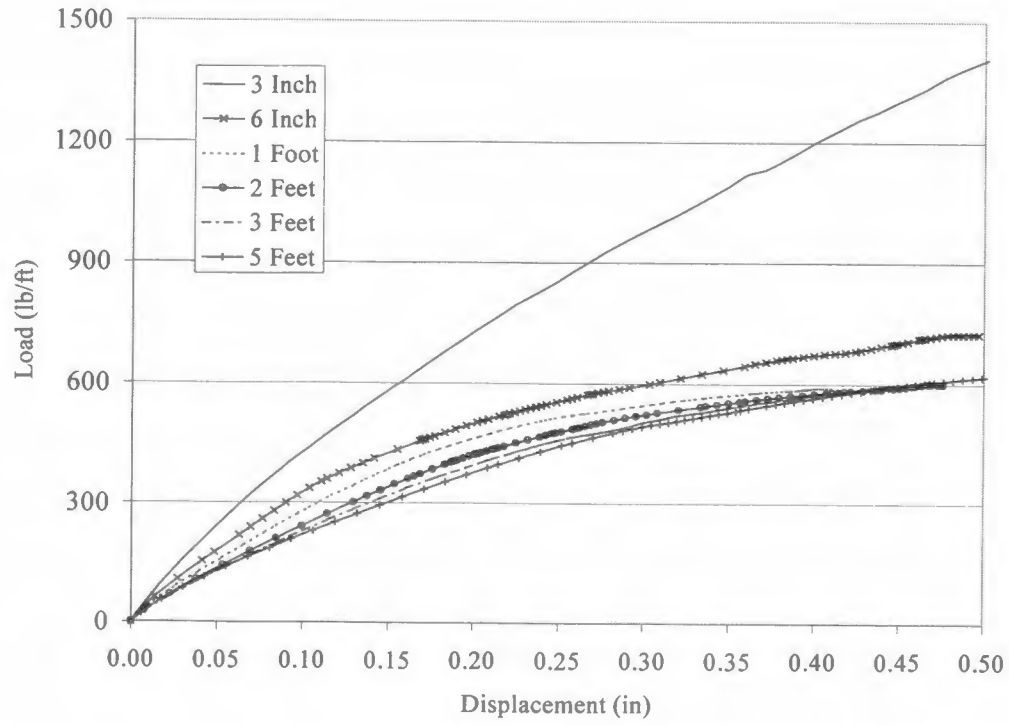

Figure 3.11. Effect of the horizontal spacing of the first horizontal transverse element with respect to the pullout box face.

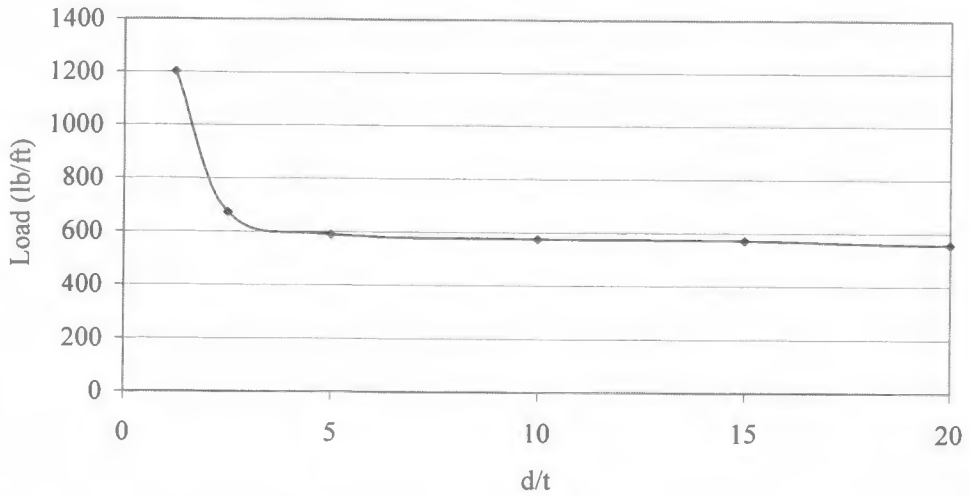

Figure 3.12. Required pullout force as a function of the ratio of horizontal distance of transverse bar from pullout box front to bar height for equivalent displacements (ratio of d/t).

affect pullout resistance. The conclusions from this study can be used as basic guidelines for pullout testing. The finite element computer program Plaxis was utilized to study four pullout test parameters. First, the effect of the overburden pressure on pullout resistance was investigated using seven different overburdens that varied from 1000 psf to 7000 psf. Figure 3.7 shows that pullout resistance is a function of the overburden pressure. As the overburden pressures increase, so does the pullout resistance of the reinforcement. When performing actual pullout tests, therefore, the overburden should be varied to measure the change in pullout resistance.

Second, the effect of the width of the opening of the pullout box face, or gap width, on pullout resistance was evaluated using six different widths that varied from 0.5 inches to 3 inches. Figure 3.8 shows that the gap width has little effect on the pullout resistance of the reinforcement (for gap widths less than or equal to approximately 3 inches as modeled in this study). Therefore, there is no need to consider the gap width when performing actual pullout tests.

Third, the effect of the height of the pullout box on pullout resistance was studied using five different heights that varied from 6 inches to 6 feet. Figure 3.10 shows that boundary effects between the pullout box and the reinforcement can affect the measured pullout resistance. When the pullout box is less than 3 feet in height, the stress interaction between the pullout box and the reinforcement can increase the pullout resistance and give inaccurate results. For that reason, when performing actual pullout tests, the pullout box should be a minimum of 3 feet high.

Finally, the effect of the horizontal distance of the first transverse bars from the pullout box face was examined using six distances that varied from 3 inches to 5 feet. Figure 3.12 shows that the first transverse bar of a welded-wire mat needs to be spaced horizontally a sufficient distance from the pullout box face so that the pullout resistance is not adversely increased. The ratio of the horizontal distance over the height of the transverse element (the ratio of d/t) of six should be sufficient, as shown in Figure 3.6, and should be followed for actual pullout tests.

CHAPTER 4

PULLOUT TEST PROCEDURE

Introduction

To further evaluate the pullout resistance of the welded-wire mats, specifically the pullout resistance of the lap zone, pullout tests were performed. In order to complete the tests, scale model welded-wire mats and a scale model pullout box were constructed. The welded-wire mats were fabricated using ty wire. A 1-foot square pullout box was constructed utilizing aluminum plates. A metal frame was erected which housed the pullout box and the hardware that applied the pullout forces to the welded-wire mats. Finally, a sand rainer was assembled in order to more uniformly fill the scale pullout box with sand.

In order to perform the tests, a general procedure was followed for all of the test configurations as explained later in this chapter. First, the pullout box was filled using the sand rainer and then placed into the pullout box frame. Next, proving rings and dial gages were attached to the mats, box, and frame in order to measure the pullout forces and displacements. Finally, an overburden was applied to the top the pullout box and the pullout tests were performed.

Pullout box components

The length of the lap zone in the Hilfiker retaining walls built at Kennecott Copper Mine was 10 feet. In order to correctly model the lap during pullout testing, a pullout box of at least 10 feet or more in length would have been needed. As this was not

feasible for this study, it was decided to perform pullout testing on 1:10 scale models of the lap zone. This created a scale lap zone length of 12 inches. The welded-wire mats, pullout box, pullout box frame, and sand rainer were all constructed at Utah State University to facilitate the scale pullout testing.

Welded-wire mats. In order to evaluate the pullout resistance of the lap zone, 1:10 scale models of the welded-wire mats were fabricated. The scale mats were constructed using nominal 1/16-inch ty wire for both the longitudinal and transverse reinforcement. In order to reduce the boundary effects during the pullout tests, two sizes of mats were constructed: (1) eights mats that were 6 inches wide and 13-1/2 inches long and (2) 16 mats that were 2-1/2 inches wide and 13-1/2 inches long. The 2-1/2-inch wide mats were placed on either side of the 6-inch wide mats and spaced 1/2-inch apart, thus creating a total reinforcement width of 12 inches. Figure 4.1 shows the finished mats and how they are positioned relative to one another. During the actual pullout tests, the three mats were connected to the loading plate (which is described in detail in the section titled "Pullout box frame"). The two smaller mats were connected to the loading plate using threaded rod and turnbuckles, whereas a proving ring connected the larger mat to the loading plate (also described in the section titled "Pullout box frame"). In this way, only the pullout resistance of the larger mat, which had no contact with the sides of the pullout box, would be measured, and boundary effects would be reduced.

The ty wire was purchased in small rolls, thus making it necessary to straighten the wire before constructing the reinforcing mats. In order to accomplish this, the wire was drawn through a small diameter groove fashioned inside two halves of a wooden jig.

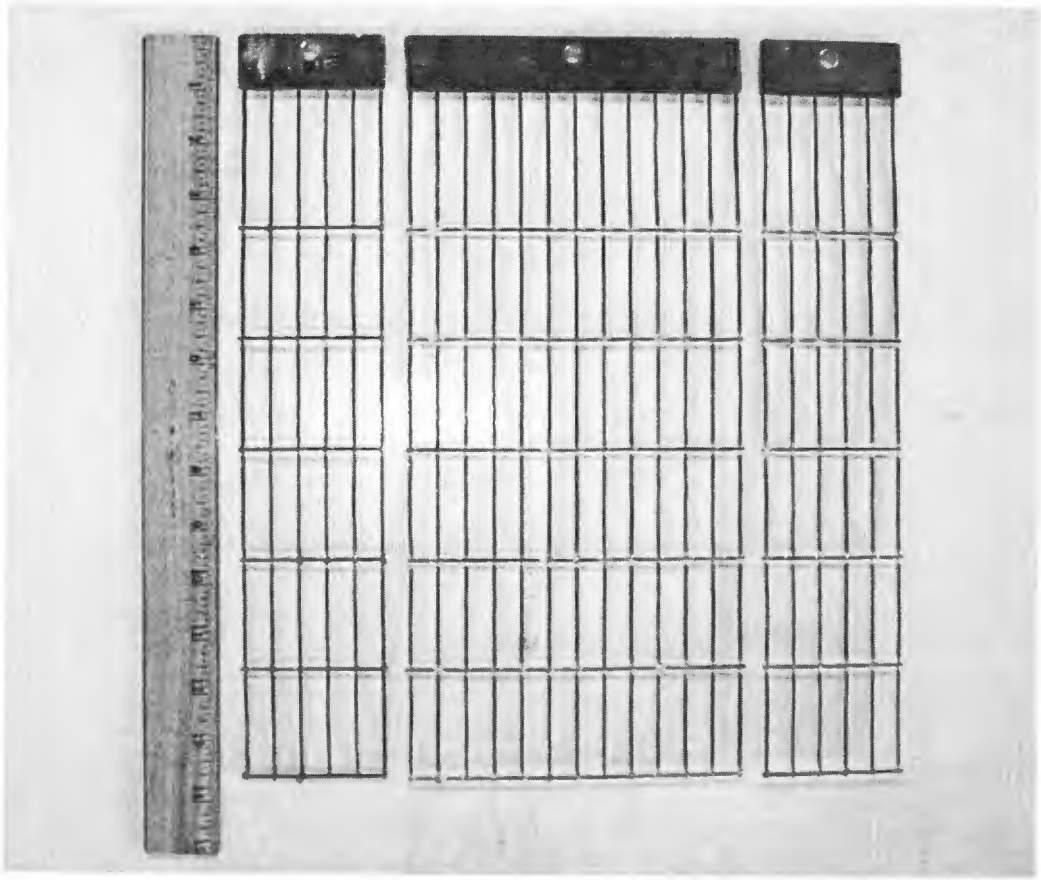

Figure 4.1. Completed scale models of welded-wire mats.

The two halves of the wooden jig were held tightly together using a table vise. The ty wire was then drawn through the jig and cut to length to form the longitudinal and transverse wires.

To ensure that the transverse and longitudinal wires would be square, an aluminum jig was fabricated. The aluminum jig was 1/2 inch thick, 3 inches wide, and 8-1/2 inches long. Two 1/16-inch wide by 1/8-inch deep grooves were cut lengthwise into the jig to accommodate the transverse wires. These two grooves were spaced 2 inches

apart and 1/2 inch from each edge of the jig. Next, sixteen 1/16-inch wide by 1/16-inch deep grooves were cut perpendicular to the transverse grooves to accommodate the longitudinal wires. Finally, 3/8-inch diameter holes were drilled 1/2 inch deep at each point where the transverse and longitudinal grooves crossed. These holes allowed sufficient space between the wires and the jig so the mats would not fuse to the jig during brazing.

The first step in the construction of the scale mats was to place the wires into the jig. For each 6-inch wide mat, two transverse wires were placed in the jig, followed by 13 longitudinal wires. When constructing the 2-1/2-inch wide mats, the width of the aluminum jig accommodated the construction of two mats simultaneously. For each 2-1/2-inch mat, two transverse wires were placed in the jig, followed by six longitudinal wires. A heavy square metal stock was then positioned across the longitudinal wires to hold them in place in the jig. Figure 4.2 shows the wires for a 6-inch mat positioned in the jig with the metal stock on top. Next, flux was applied to each of the joints that required brazing, as seen in Figure 4.3. The wires were then brazed using an oxyacetylene torch and silver-alloy brazing rod, as shown in Figure 4.4. Brazing rod was chosen over silver solder for two reasons: (1) it had higher tensile strength and (2) the amount of material needed to braze the transverse and longitudinal wires together at each joint would be minimized, reducing the effect on pullout resistance.

After the first two transverse wires were brazed to the longitudinal wires, the mat was removed from the jig. In order to ensure equal spacing between all of the transverse bars, a single transverse bar was first placed into the jig. Next, one of the two brazed

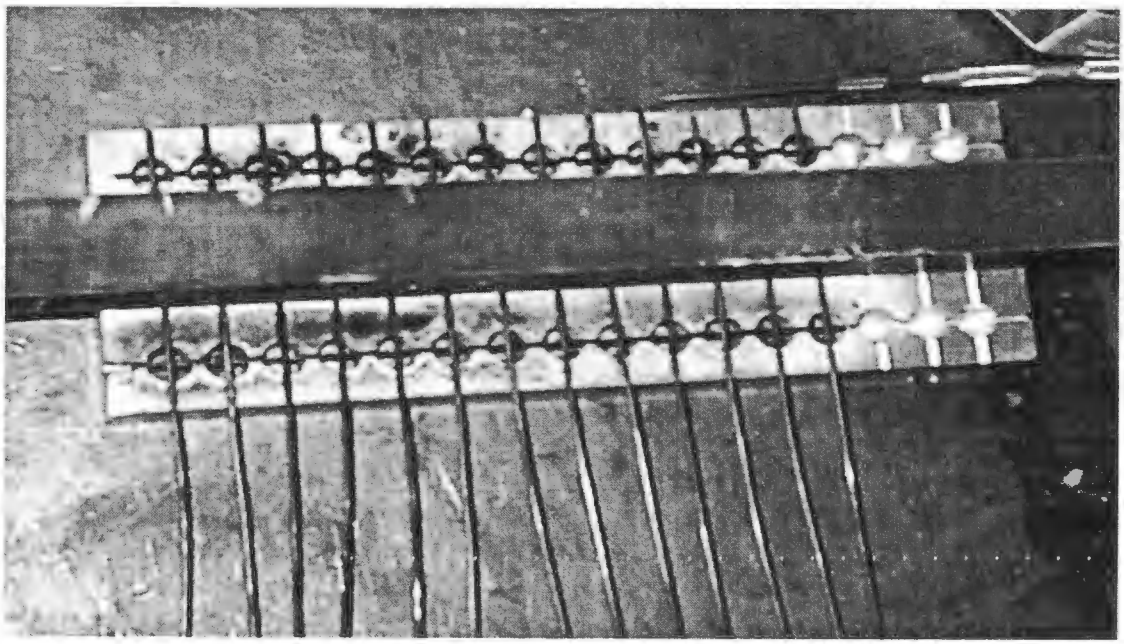

Figure 4.2. Position of ty wires in aluminum jig with the metal stock on top.

Figure 4.3. Application of flux using a brazing rod.

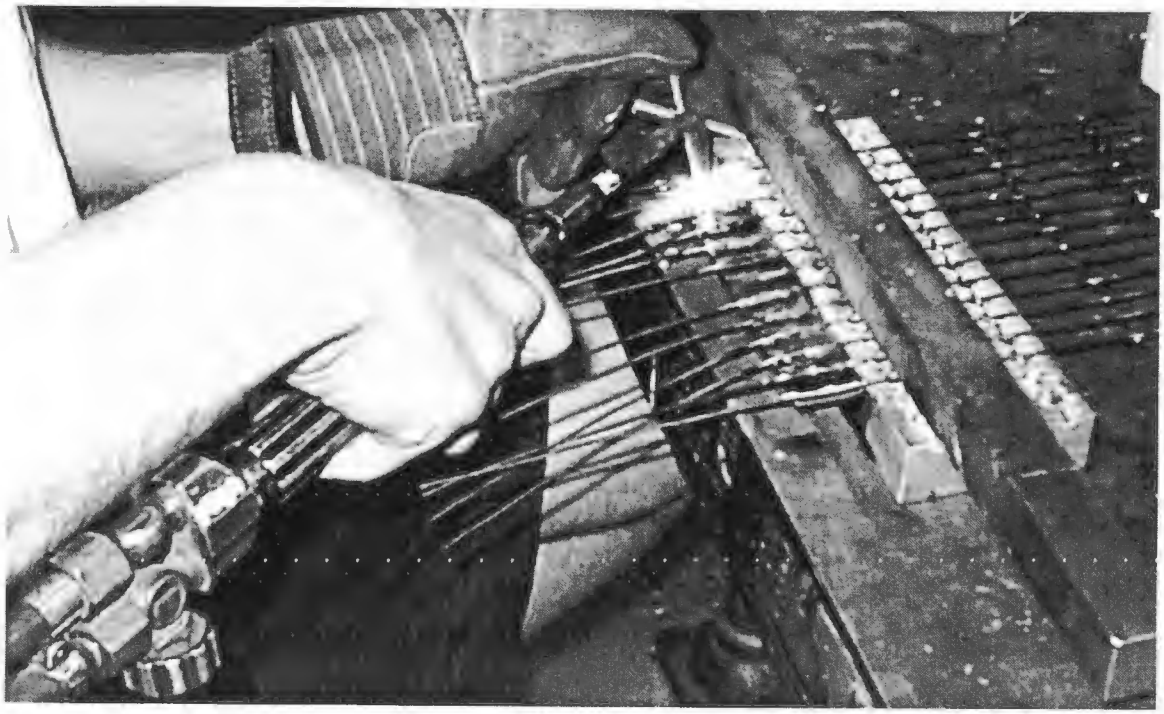

Figure 4.4. Brazing the ty wires using an oxyacetylene torch and brazing rod.

transverse bars was placed into the remaining groove in the jig. The metal stock was again placed atop the wires for weight, flux was applied to the joints, and the single transverse wire was brazed to the mat. This process was repeated until a total of six transverse wires were brazed to the longitudinal wires at an equal spacing of 2 inches.

The next step in the construction of the scale welded-wire mats was to attach 1/8 inch thick by 1-inch wide hot-rolled steel plate to the end of the longitudinal wires. One side of the plate was cleaned using a grinder to remove a thin residue. The thin plates were then cut into 6-1/8-inch and 2-5/8-inch lengths using a band saw. The mats were placed into the jig once again, and the thin plates were temporarily attached using metal clamps, as shown in Figure 4.5. This ensured that the plates were brazed square to the

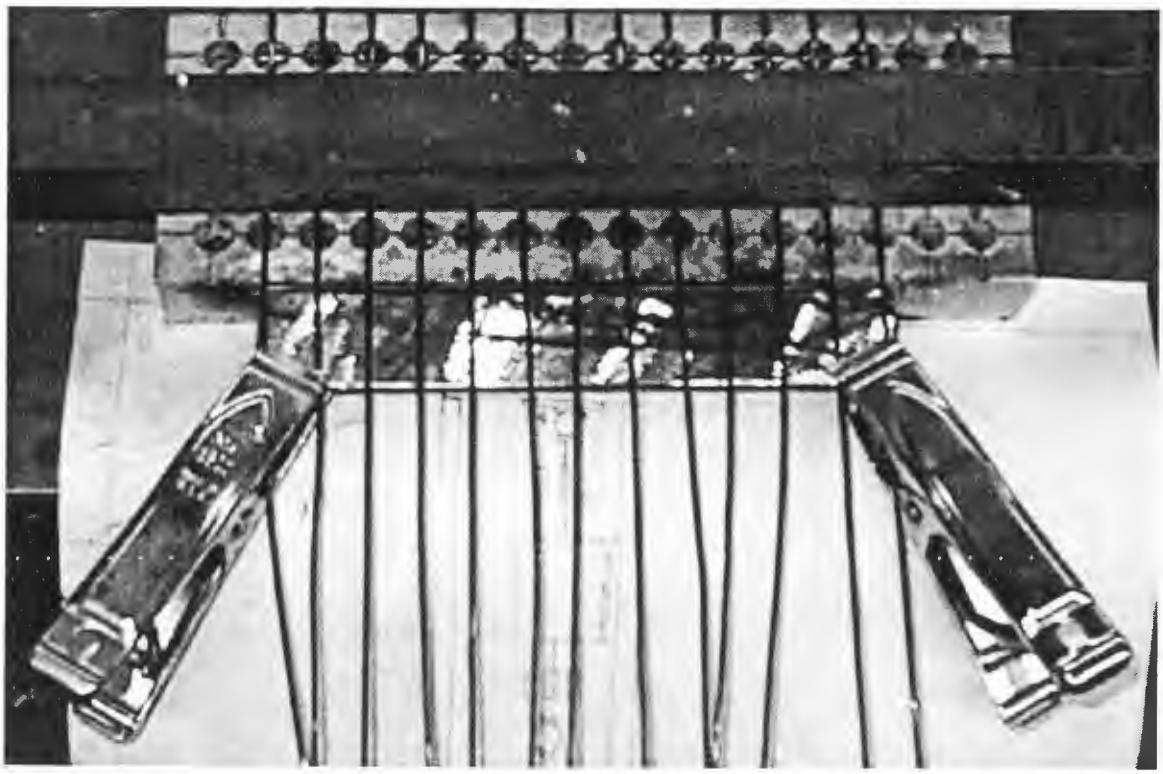

Figure 4.5. Clamps used to temporarily attach thin plates to mat.

rest of the mat and that they were spaced 2-1/2 inches from the nearest transverse wire. The plates and longitudinal wires were then painted with flux using a brush and, after brazing several wires to the plates, the clamps were removed and the remaining wires were brazed. A 5/16-inch hole was then drilled in the middle of each plate, centered 5/16 from the front edge of the plate.

The final step was to trim and clean the mats. Because the transverse and longitudinal wires were initially cut long, the added wire length was trimmed to create the final dimensions of the mats. The tips of every wire and the edges of every plate were then lightly buffed using a drum sander to remove any sharp points or corners. The

mats were then scrubbed using a wire brush and water to remove the remaining flux residue. Figure 4.1 shows the completed mats.

Pullout box. In order to test the scaled down lap zone, a pullout box was constructed to accommodate the 1:10 scale welded wire mats. Figure 4.6 shows the completed pullout box. The inside dimension of the pullout box was 12 inches by 12 inches by 12 inches. The four walls of the box were constructed of 3/8-inch aluminum plate. Two of the walls on opposing sides of the pullout box were milled with six 1/4-inch high by 12-inch long slots, or gaps, spaced 1-1/4 inches vertically on center. The numerous levels of gaps were milled to allow different pullout test configurations to be investigated. The base of the pullout box was constructed of 1/2-inch cold rolled steel plate. Two shallow 1/2-inch semicircular linear races were then milled into the bottom of the base plate. A second 1/2-inch steel plate was milled to 11-7/8 inches by 11-7/8 inches to act as an overburden plate. A 3/8-inch hole was tapped into the loading plate, and a removable eye-screw was added to enable the plate to be lifted on and off the box. This overburden plate was used to apply overburden pressures to the soil in the pullout box.

Pullout box frame. In order to apply the pullout forces to the welded-wire mats embedded in the pullout box, a pullout box frame was constructed. The base of the pullout box frame was a 40-inch long by 8-inch wide by 2-1/4 inch high steel channel. Two 27-inch long by 6-inch wide by 2-inch high steel channels were welded vertically to each end of the 40-inch long channel. At the top of the pullout box frame, a 40-inch long by 1-1/2 inch square steel tube connected both ends of the 27-inch long channels. The

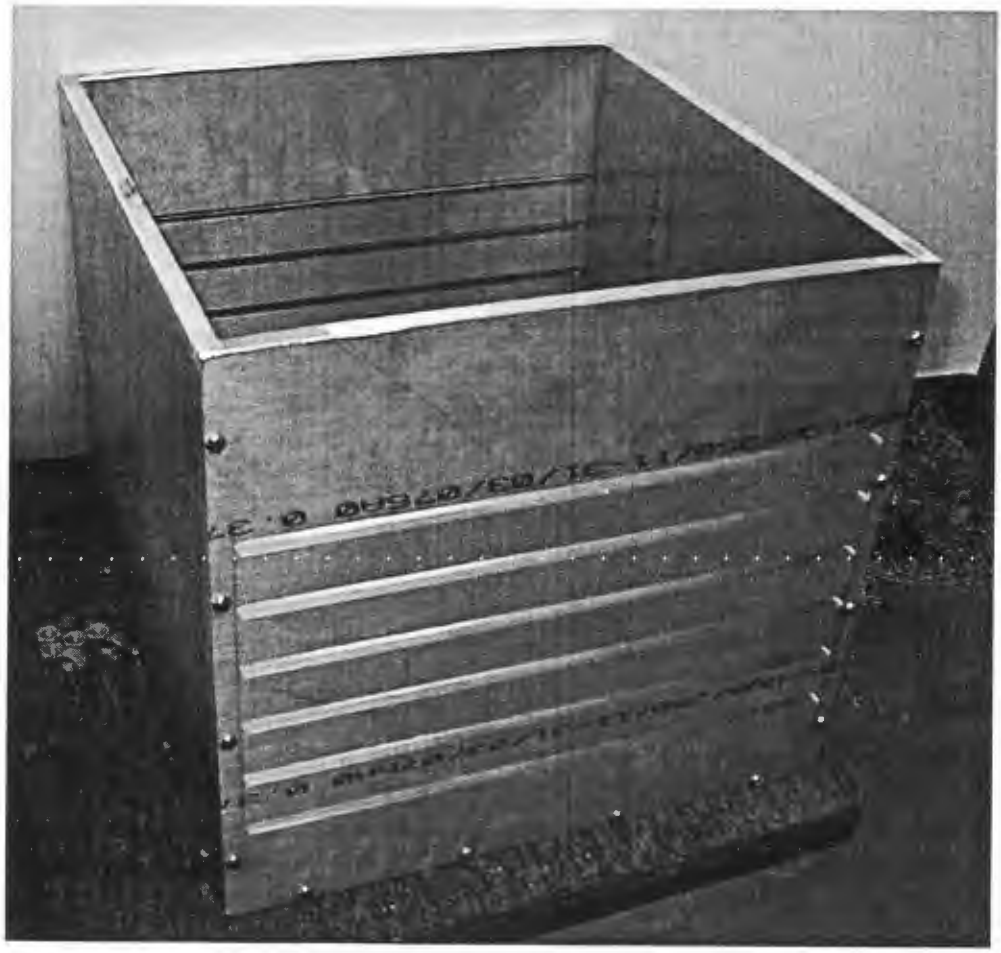

Figure 4.6. Completed pullout box.

pullout box frame is shown in Figure 4.7. The pullout box was not attached directly to the bottom steel channel. Instead, a third 1/2-inch steel bearing plate was cut to the exact dimensions of the base plate in the pullout box and attached to the bottom channel. Two shallow 1/2-inch semicircular linear races were then milled into the bearing plate that matched those milled into the base plate in the pullout box. The linear races in both the base plate and bearing plate were used to encase 1/2-inch steel ball bearings, as seen in

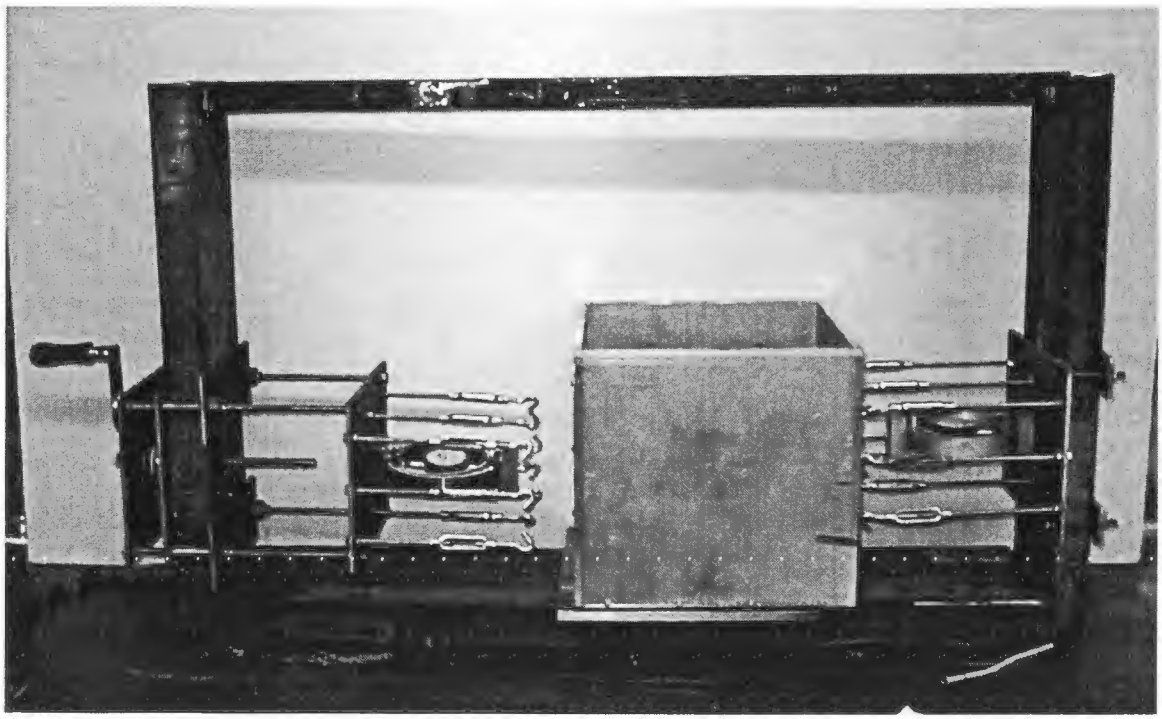

Figure 4.7. Completed pullout box frame.

Figure 4.8. In this way, the pullout box was in contact with the frame only through the ball bearings, and the box was free to roll only in the direction parallel to the direction of the applied pullout force.

In order to attach the welded-wire mats to the pullout box frame, two loading plates were bolted to the two vertical channel sections. The loading plates were 10 inches long by 8-1/2 inches wide by 1/4-inch thick. On the right side of the pullout box frame, the loading plate was completely stationary. This is shown in Figure 4.9. The right loading plate was secured to the inside of the vertical channel by means of four 3/8-inch diameter bolts and two 8-inch long by 2-inch wide by 1/4-inch thick securing plates. The

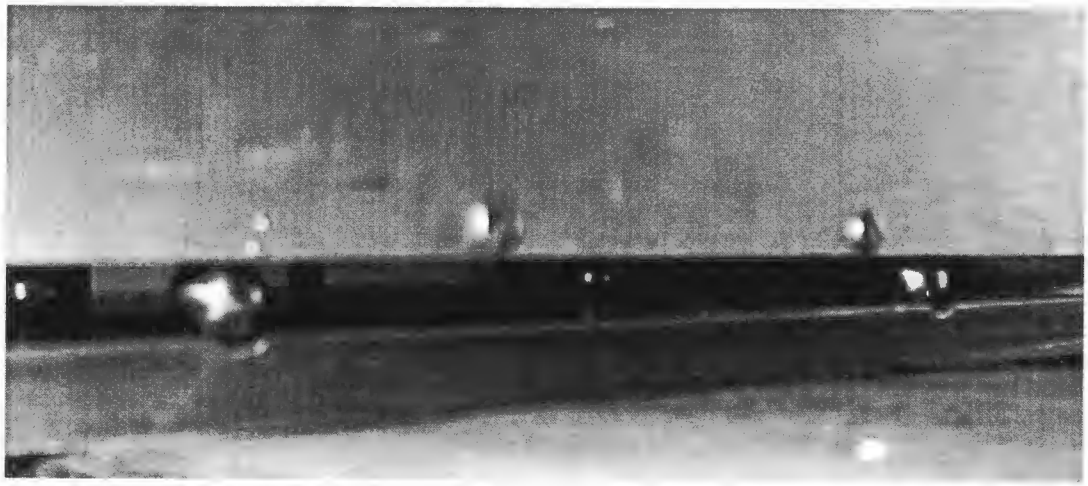

Figure 4.8. Pullout box resting on ball bearings in semicircular races.

Figure 4.9. Loading plate connection on right side of pullout box frame.

four bolts passed through the four corners of the loading plate. The top two bolts then attached to the top securing plate on the outside of the vertical channel, and the bottom two bolts attached to the bottom securing plate. This setup, when tightened, "sandwiched" the channel between the plates, securing the loading plate in position. This setup also allowed the loading plate to be adjusted vertically up or down to match the position of the reinforcing mats in the pullout box.

On the left side of the pullout box frame, the loading plate setup was a bit more complicated, as seen in Figure 4.10. On the left side of the pullout box the two securing plates were on the inside of the vertical channel, and were attached to a large sandwich plate on the outside of the vertical channel using 5/8-inch bolts. This sandwich plate had roughly the same dimensions as the loading plate. A 7/16-inch diameter hole was machined completely through each of the four 5/8-inch bolts to create a simple bushing. Four 3/8-inch diameter rods were then inserted into the simple bushings. On the inside of the pullout box frame, the four rods attached to the right-hand loading plate. On the outside of the frame, the four rods attached to a third plate (which also had roughly the same dimensions as the loading plate) that housed the hand-crank. This hand crank was used to apply the pullout force to the welded-wire mats.

The hand crank was very simple in its construction. A 5/8-inch wide by 5-1/2 inch long slot was cut into the vertical channel section. This slot allowed the hand crank to be adjusted vertically up or down with the loading plate. Additionally, 7/16-inch holes were drilled in the center of the sandwich plate and the third plate outside of the pullout box frame. A 1/2-inch diameter nut was then welded over the hole in the sandwich plate.

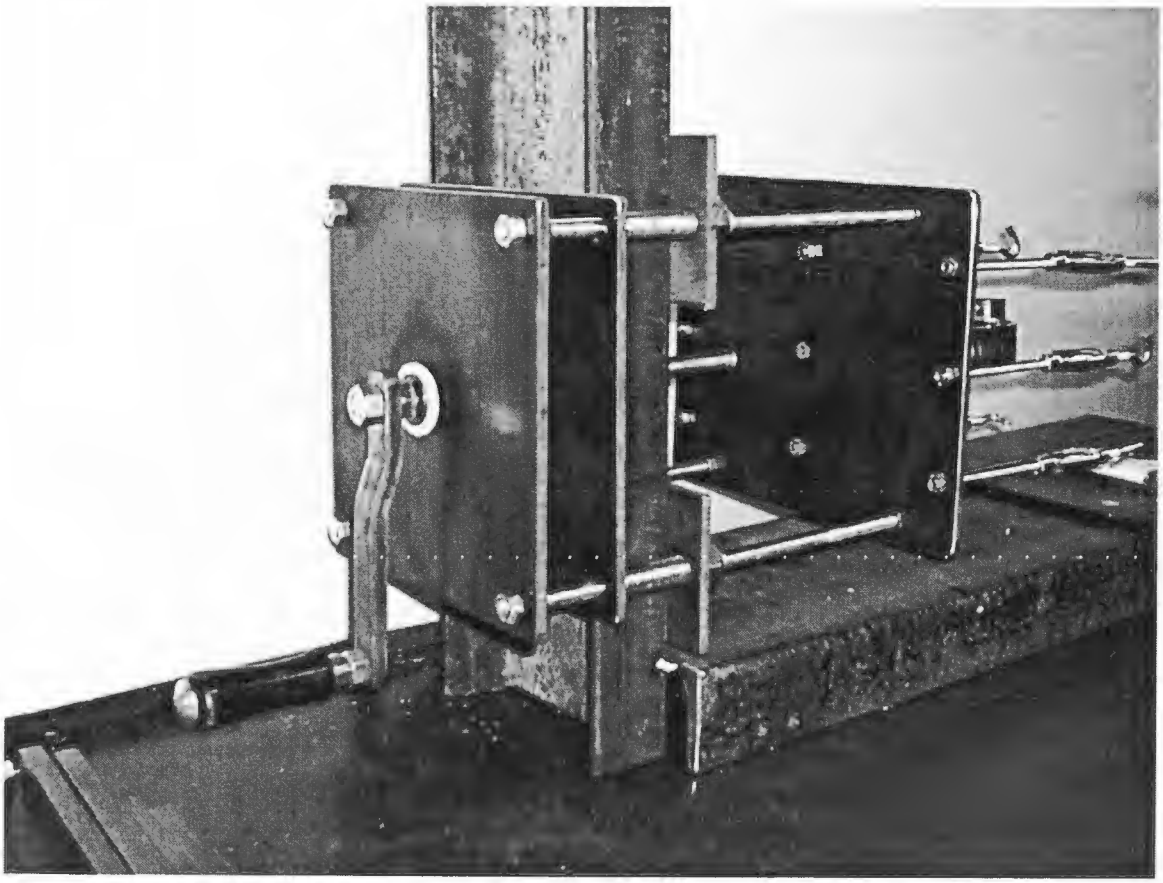

Figure 4.10. Loading plate connection on left side of pullout box frame.

A 1/2-inch diameter fine-threaded rod (20 threads per inch) was then passed through the two holes and the nut. On either side of the third plate, Teflon and steel washers were slipped over the rod and held in position by two 1/2-inch diameter nuts. Finally, a handle with a 7-inch lever arm was attached to the end of the fine-threaded rod to complete the hand crank.

In order to attach the welded-wire mats to the loading plates, a straightforward solution was realized, as shown in Figure 4.11. Nine 5/16-inch holes were drilled

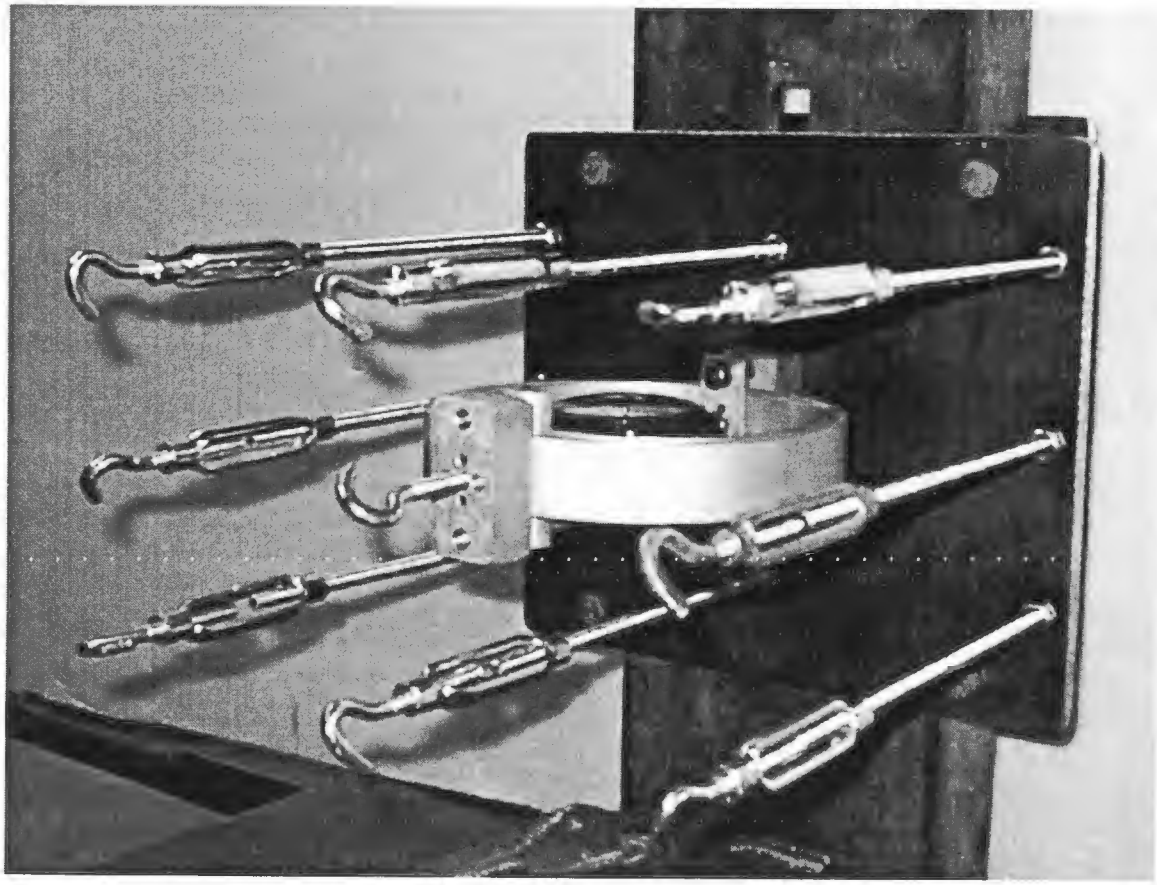

Figure 4.11. Layout of turnbuckles and proving ring on loading plate.

through each loading plate, with three holes spaced across each of the three levels. Eight 1/4-inch diameter threaded rods passed through the holes in each of the two loading plates: three rods in the top and bottom rows, and two rods in the middle row. Each rod was secured to the loading plate using two 1/4-inch diameter nuts, one on either side of the plate. 3-inch long turnbuckles were then attached to the free end of each of the 6 inch long threaded rods. A small hook on the end of each turnbuckle was used to finish the connection to the 5/16-inch holes drilled in the thin plates of each welded-wire mat. The

turnbuckles were used to take up any uneven slack between each of the welded-wire mats and the loading plates. This helped to ensure that initially the pullout forces were evenly distributed through all of the mats. Finally, a calibrated proving ring was attached to the ninth hole in the middle of each loading plate using a 1/4-inch screw. A small hook was attached to the free end of the proving rings that, in turn, attached to the welded wire mats.

Proving rings. In order to measure the tensile force applied to the welded-wire mats during the pullout tests, two proving rings were utilized. The dial gages in the proving rings were accurate to 0.0001 inches. Before using the two proving rings for the pullout tests, they were calibrated to obtain calibration curves. The proving rings were suspended from large I-beams in the basement of the engineering building at Utah State University, as shown in Figure 4.12. Metal weights were suspended from the proving ring in succession and the respective displacements were recorded. From the known masses and displacements, the calibration curves in Figure 4.13 and Figure 4.14 were created. The equation for the best-fit line was obtained to calculate the pullout force following each pullout test using the recorded proving ring displacement.

Sand rainer

In traditional pullout tests, the size of the pullout box normally permits the fill material to be compacted using a jumping jack, vibratory plate, or other compaction equipment. However, due to the small size of the pullout box used in the pullout testing at Utah State University, compaction equipment could not be used. In order to obtain a relatively consistent density of fill material in the box, a "sand rainer" was constructed.

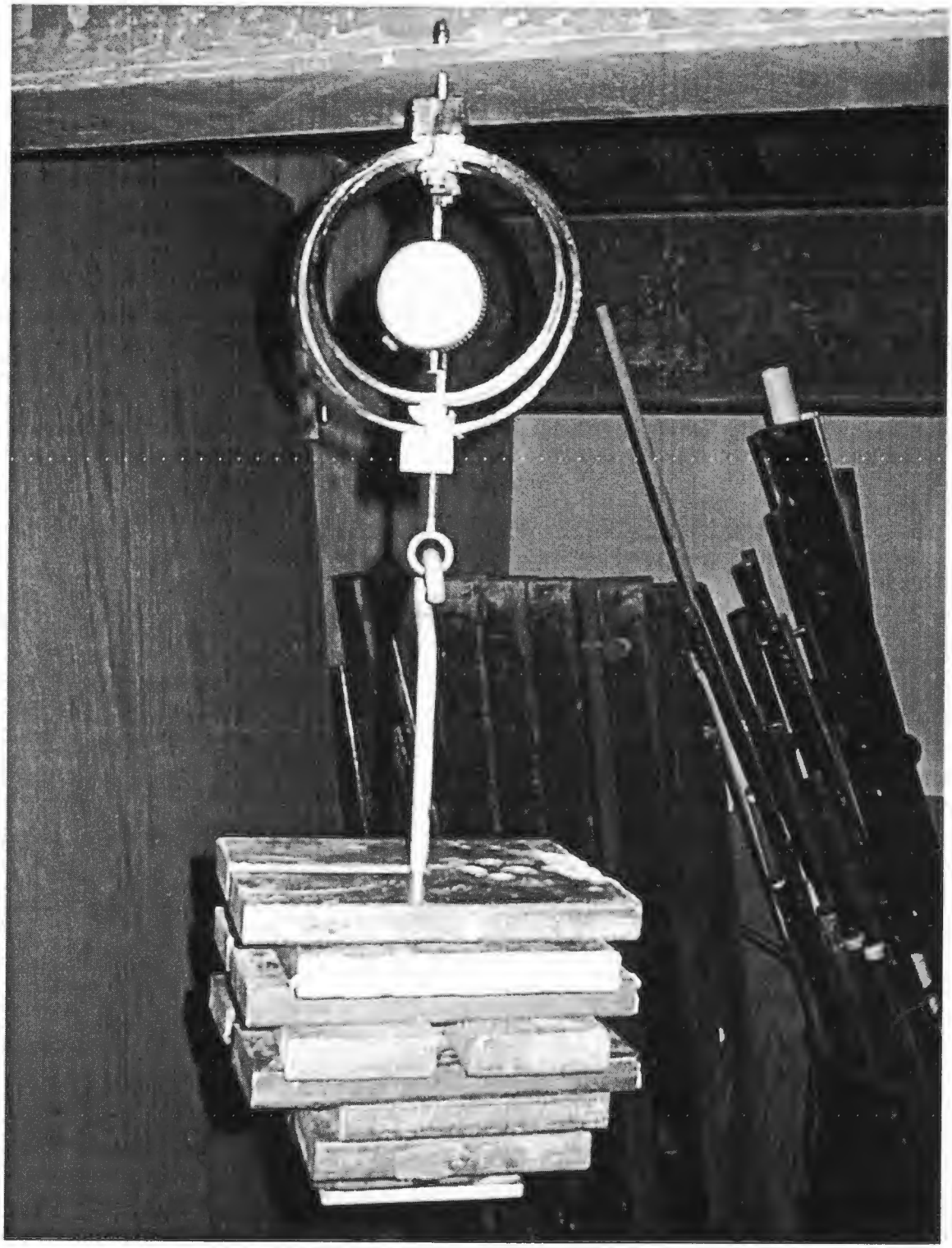

Figure 4.12. Calibration of proving ring.

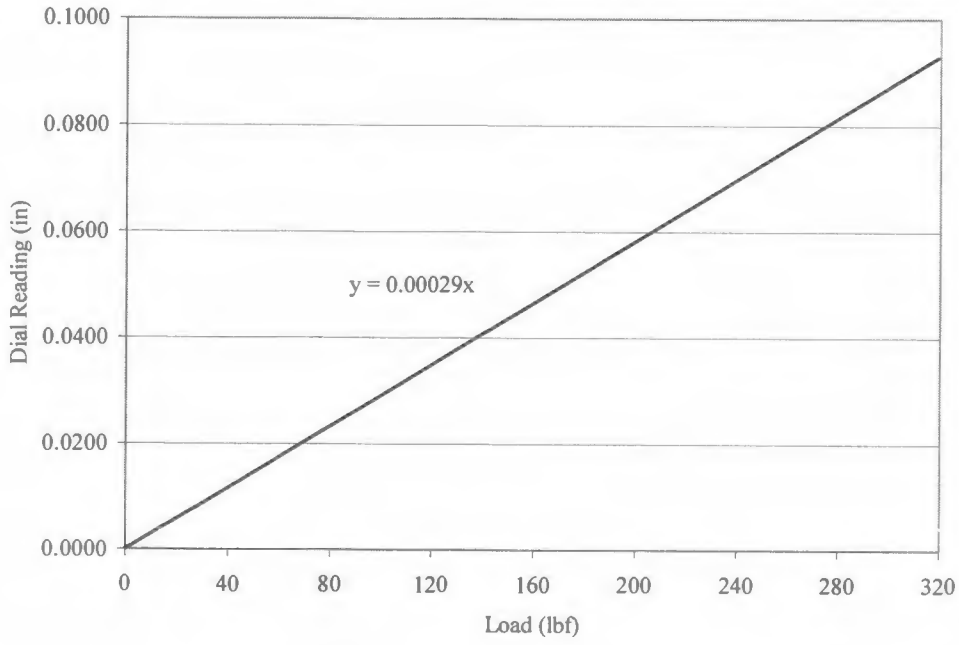

Figure 4.13. Calibration curve for proving ring #2110.

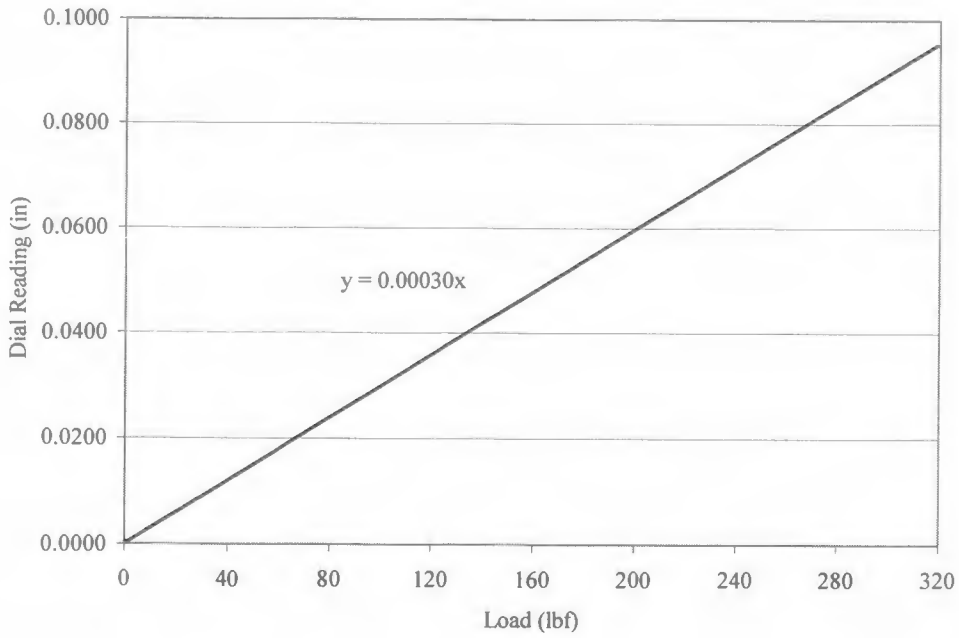

Figure 4.14. Calibration curve for proving ring #4982.

The sand rainer was used by continuously passing back and forth across the top of the pullout box, raining a thin lift of soil into the box with each pass.

The sand rainer was constructed using a 15-inch long piece of angle steel. Figure 4.15 shows the initial sand rainer configuration. The two flanges of the angle steel were 3-1/2 inches wide and 1/4-inch thick. Two triangular pieces were welded to each end of the angle steel to complete the rainer. A 3/32-inch slot was cut through the middle of the angle steel where the two flanges connected, and the edges of the slot were then slightly beveled. This slot was slightly larger than the largest soil grain size used during pullout testing (grains passing a number 10 sieve). Additionally, a thin sheet of Teflon tape was applied to the inside flanges of the rainer to allow the soil grains to slide more easily through the slot.

In order to keep the sand rainer steady during the pullout box filling, two rails were welded to the bottom of the rainer. The rails were made of 8-inch long by 3/4-inchwide by 1/2-inch high steel. A 3/8-inch wide by 1/4-inch high notch was cut on the inside edge of the rails. The two rails were spaced so that the notches cut into the rails rested on the outside edges of the pullout box. The notches and the top edges of the pullout box were covered with a thin sheet of Teflon tape so the rainer would slide easily across the top of the pullout box during filling. Unfortunately, when the sand rainer was initially tested it did not function as planned. The major reason for this was that some of the soil particles accumulated on top of the pullout box during filling. This made it difficult to slide the sand rainer across the top of the pullout box, and ultimately the Teflon tape began to rip. This, in turn, made it even more difficult to slide the rainer

Figure 4.15. Initial sand rainer configuration.

back and forth on the rails. The second reason the sand rainer did not function as planned was that the soil grains did not rain continuously through the slot. It was necessary to rhythmically tap the trough with a metal bar to keep a somewhat steady flow of soil raining into the box.

To overcome these two problems, a new solution was formulated as shown in Figure 4.16. Two 1/4-inch holes were drilled in the each of the two end triangular pieces of the rainer, and an S-hook was inserted into each hole. Two ropes were fixed to the

Figure 4.16. Modified sand rainer suspended from ceiling with chains and rope.

rafters of the ceiling, a short piece of chain was tied to the bottom of each rope, and the S-hooks were attached to each chain to suspend the sand rainer in the air. The short piece of chain was used so small adjustments could easily be made to the height of the sand rainer. With the sand rainer suspended from the ceiling, the metal rails were no longer required and the first problem was solved. To fix the second problem, a small jigsaw (with the blade removed) was fixed to the side of the sand trough using C-clamps. The jigsaw provided steady high-frequency vibration to the trough, helping to rain the soil into the box at a more consistent rate.

Soil data

In order to obtain the properties of the soil used during the pullout tests, several laboratory tests were performed. These tests included grain size distribution, dry density calculations, and consolidated-drained triaxial tests.

Grain-size distribution. The first laboratory test performed to determine the properties of the soil was a grain-size distribution. Initially, a number 10 sieve was used to remove all grain sizes larger than 2 mm. This size of sieve was chosen because the relative grain size of the soil in relation to the size of the ty wire used in the welded-wire mats was important, and any grains larger than 2 mm could adversely affect the pullout resistance of the mats. A grain-size distribution test was performed with the remaining soil that passed the number 10 sieve. The results of this laboratory test are shown in Figure 4.17.

Dry density. In order to determine the dry density of the soil used in the pullout tests, a second laboratory test was performed. Since all soil used in each of the pullout tests would be dry, only the dry density was required. First, the empty pullout box was weighed. After filling the pullout box completely using the sand rainer, the pullout box was weighed a second time. The weight of the empty box was subtracted from the weight of the full box to obtain the total weight of the soil. The inside dimensions of the pullout box were measured to obtain the total volume of the box. The weight of the soil was then divided by the volume of the box to obtain a dry density of 115.4 pcf.

Triaxial tests. The final test performed on the soil was a consolidated-drained (CD) triaxial test. In order to determine the soil friction angle, ϕ, and the Young's

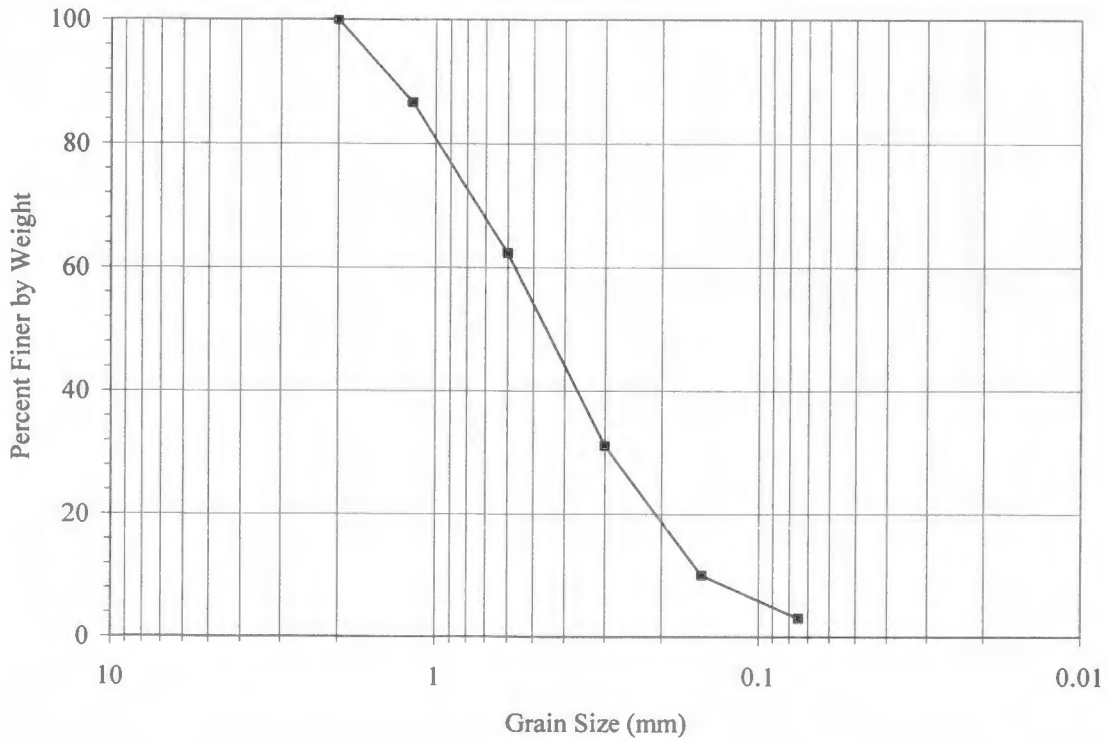

Figure 4.17. Grain-size distribution for sand used in scale model pullout testing.

Modulus, E, three triaxial tests were performed at cell pressures of 0.5, 1, and 2 psi. A friction angle of 35.7 degrees and a Young's Modulus of 22,900 psf were calculated. Figure 4.18 shows the results of the triaxial tests.

Pullout test methodology

A pullout test program was conducted to compare the pullout resistance of welded-wire mats with a lap zone to those without a lap zone. Though each of the test configurations varied slightly, all of the pullout tests followed the same basic setup and test procedure.

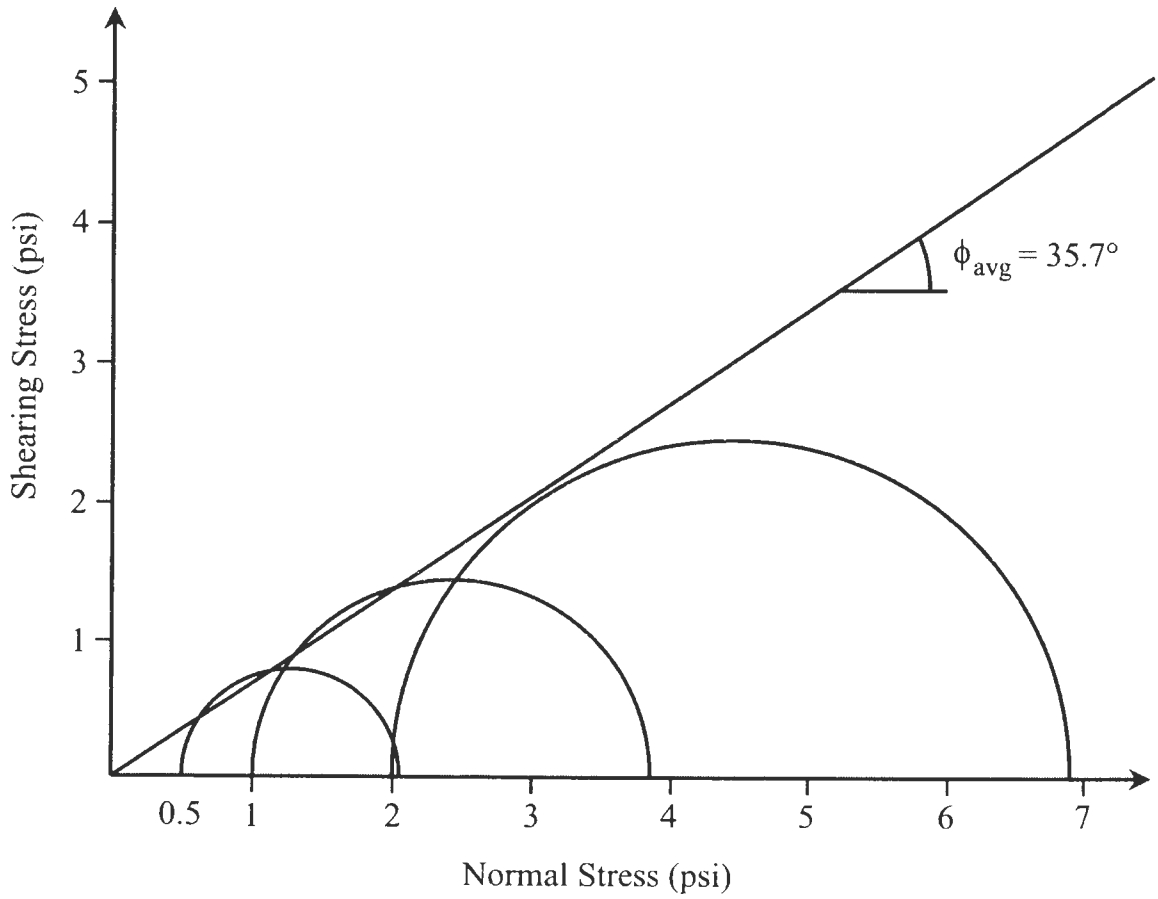

Figure 4.18. Mohr's circles from the consolidated-drained triaxial tests on sand used in scale model pullout tests.

Filling the pullout box. The first step was to tape shut any gap in the pullout box that was not used during the pullout tests. For example, for test configuration one (as explained in Chapter 5), 11 gaps were taped shut because only a single gap was used. For test configuration two, nine gaps were taped shut because only three gaps were used. Next, the sand rainer was used to place soil into the pullout box up to the height of the first open gap, making certain the soil was level. The welded-wire mats were slipped in through the gap and positioned within the pullout box so that the thin plates on the end of

each mat were square to the face of the box, as seen in Figure 4.19. If the lap zone was being investigated, the second set of mats was slipped through the gap in the opposite face of the pullout box, and laid directly on top of the other mats. The transverse bars on the lower lapped mat faced down, whereas the transverse bars on the upper lapped mat faced up. This was so the transverse bars from the lapped mats would never come into contact with each other if large displacements occurred during a pullout test. If three layers of welded-wire mats needed to be added to the box, this process was repeated two more times. After the final layer of welded-wire mats was added, the pullout box was filled with soil to within 1/2 inch of the inside top edges. Any loose soil was removed from the top edges, and the overburden plate was placed on the soil in the box.

Placing pullout box in frame. The next process was to place the pullout box into the pullout box frame. In order to ensure that little, if any, soil entered the ball bearing races, a wet towel was used to remove any soil particles that accumulated in the races of both the base of the pullout box and the plate on the bottom channel of the pullout box frame. Once the races were clean, ball bearings (an equal number in each race) were placed on the plate in the pullout box frame. They were temporarily held in position using small strips of sheet metal, one strip placed on either side of each ball bearing. The box was then lifted into position in the pullout box frame. Often, as the pullout box was lifted into position, a few grains of soil slipped out of the gaps between the welded-wire mats. A high-pressure air hose was used to remove these loose grains from the pullout box frame and the ball bearing races.

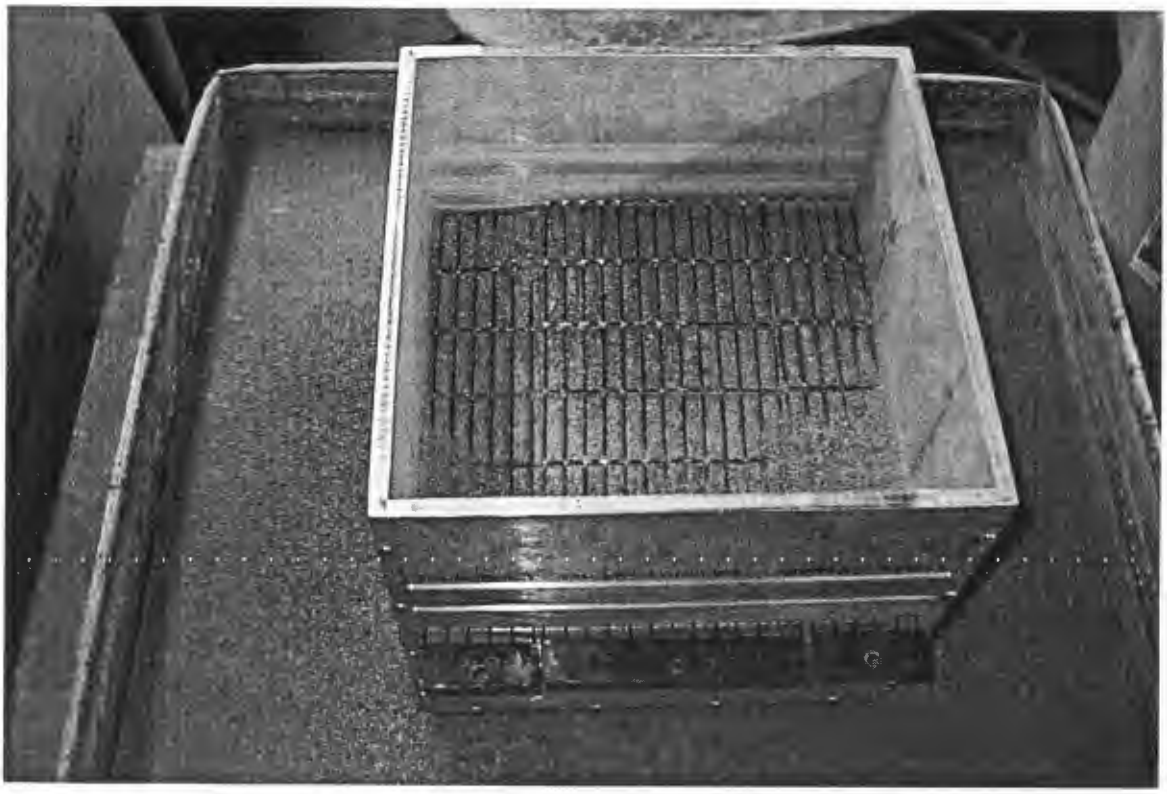

Figure 4.19. Placement of a single layer of welded-wire mats in pullout box.

The first few attempts at lifting the pullout box into the frame and placing it onto the ball bearings in the races proved very difficult. Therefore, two handles were fastened to the sides of the pullout box to make this job more manageable.

Once the pullout box was in the frame, the welded-wire mats were attached to the loading plates. This step varied depending upon the pullout test configuration. For tests run on welded-wire mats with no lap zone, it was necessary to block the pullout box into position to simulate traditional pullout tests. In this case, the ball bearings and races were used simply to keep the pullout box square with the pullout box frame. Both the top and bottom of the pullout box were blocked using pieces of wood cut to length to prevent any

vertical rotation or tipping. This blocking is shown in Figure 4.20. The welded-wire mats were then attached to the left loading plate using the turnbuckles and the proving ring, and the right loading plate was left unused.

For tests run on welded-wire mats with a lap zone, it was not necessary to block the pullout box into position. In this case, the welded-wire mats were simply attached to both the right and left loading plates, and the pullout box was free to roll along the ball bearings in the races.

For tests run with a single level of mats, whether a lap zone was present or not, only one proving ring and two turnbuckles were needed per loading plate. The top and bottom layers of turnbuckles were removed to avoid any possibility of interference. For tests run with three levels of mats, whether a lap zone was present or not, the proving ring and all of the turnbuckles were used from each loading plate.

Placement of dial gages. In order to develop load displacement curves for each pullout test, dial gages were needed—in addition to the proving rings—to measure pullout displacements. For pullout tests performed on welded-wire mats with no lap zone, a single dial gage was required. This gage, which was accurate to 0.001 inches, was positioned against the left loading plate. As the hand crank was turned, the movement of the left loading plate was equivalent to the displacement of the welded-wire mats, and was recorded by the dial gage.

For the initial set of pullout tests performed on welded-wire mats with lap zones (as explained in Chapter 5), two dial gages were required. The left dial gage was set up exactly as described above. The right dial gage, however, was positioned against the

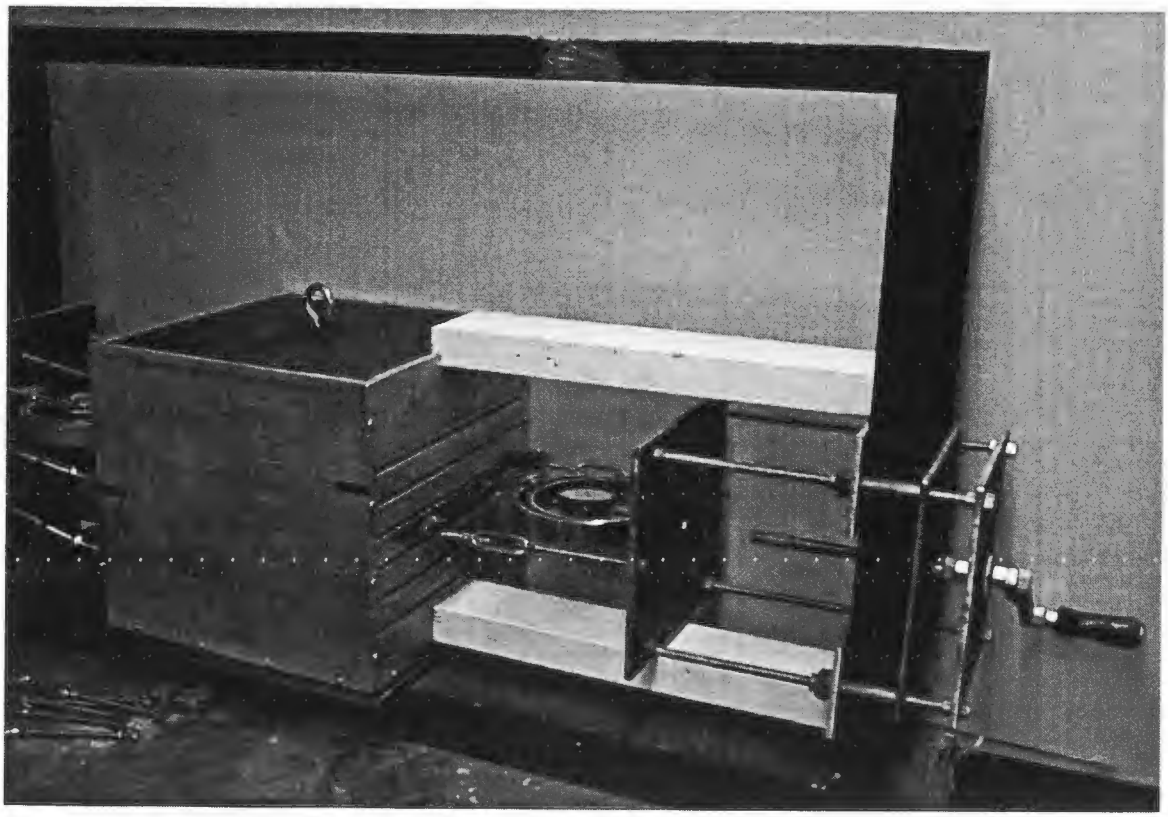

Figure 4.20. Pullout box blocked in place for pullout tests with no lap zone.

pullout box. Since the right loading plate was fixed and the pullout box was free to roll, any movement of the pullout box was equivalent to the displacement of the welded-wire mats on the right side. The right dial gage, therefore, was used to measure the displacement of the right mats directly. In order to calculate the displacement of the left mats, the reading on the right dial gage was subtracted from the reading on the left dial gage.

For the final pullout test configurations (as explained in Chapter 5), an approach similar to that used for the tests with no lap zone was adopted in that a single dial gage

was positioned against the left loading plate. The forces in both the right and left mats of each lap zone could then be plotted using the same displacement.

Running the pullout tests. Once the dial gages were in place, the specified overburden was applied to the pullout box. This was accomplished by simply stacking weights on top of the overburden plate. Once the overburden was applied, the hand crank was used to take up the remaining slack between the proving ring hooks and the welded-wire mats. Then, each of the turnbuckles was adjusted to take up the remaining slack between the loading plates and the welded-wire mats. The dial gages were then all zeroed, and the pullout tests were ready to begin.

For the pullout tests performed on welded-wire mats with no lap zone, only two people were required. One person turned the hand crank at a constant rate to apply the pullout force while simultaneously watching the left dial gage. Each time the left dial gage moved 0.01 inches the second person took a reading on the proving ring. The hand crank was turned continuously until the reading on the proving ring dial gage held fairly constant or dropped off.

For the pullout tests performed on welded-wire mats with a lap zone, four people were required. One person turned the hand crank at a constant rate to apply the pullout force and watched the left dial gage. The other three people watched the two proving ring dial gages and the right dial gage. Just as with the test procedure described above, every time the left dial gage moved 0.01 inches, the remaining three people took readings on their respective dial gages until the pullout force leveled off.

With several of the test configurations, some tests were run at two overburdens without refilling the pullout box. When this was the case, once a pullout test was complete and the pullout force had leveled off, the hand crank was turned backward to release all of the tension in the welded-wire mats. The extra overburden was then applied to the overburden plate by adding more weights. Then the setup and testing procedure was repeated.

Once the pullout test was complete for a given test configuration, the overburden was removed, the pullout box was completely emptied, and the box was removed from the pullout box frame. The pullout box was then refilled using the sand rainer, and the entire setup and testing procedure was repeated.

Modified pullout box components

An initial set of pullout tests was completed using the scale model pullout apparatus and the testing procedures described above. However, it became necessary to alter the pullout box before a final set of pullout tests could be finished. The pullout box was modified by splitting it into two equal halves along the cross section without the 1/4-inch wide gaps. The reasons for this modification are explained in detail in Chapter 5.

The pullout test setup procedures for the final set of tests were very similar to those explained above, though several new obstacles had to be overcome. The first major obstacle was how to keep soil from spilling out of the pullout box during testing as the two halves of the box split apart. The solution was to attach a highly elastic rubber membrane to the inside of the pullout box in order to bridge the gap between the two halves as seen in Figure 4.21.

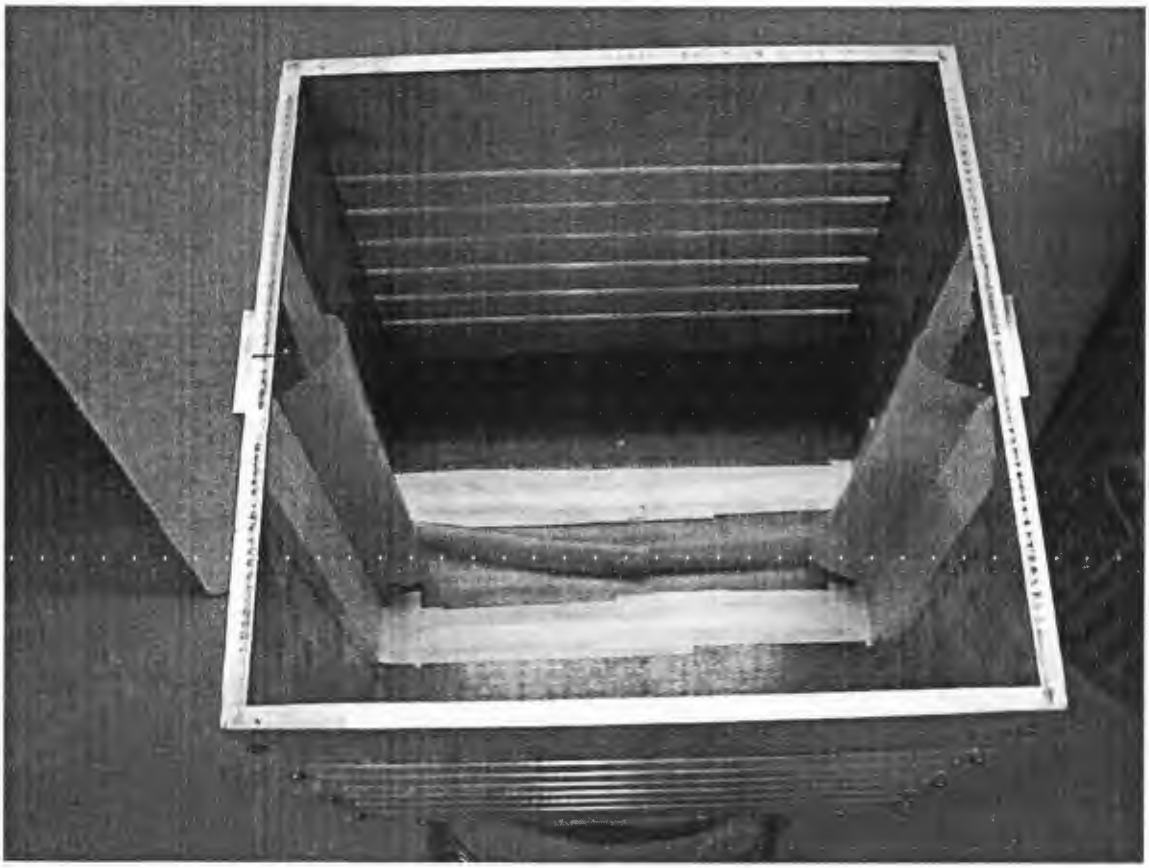

Figure 4.21. Rubber membrane encasing inside of split pullout box.

A second major concern was how to keep the pullout box together until the testing began. In order to fill the pullout box with soil using the sand rainer, it was necessary to keep the box intact. More critically, as the box was transferred into the pullout box frame, any differential movement between the two halves of the pullout box needed to be eliminated. The solution was to attach two removable plates that screwed onto the outside of the box, securing the two halves of the box together as seen in Figure 4.22. These two plates kept the box rigid until it was filled and until it had been transferred to the frame. They were also easily removed before the pullout tests began.

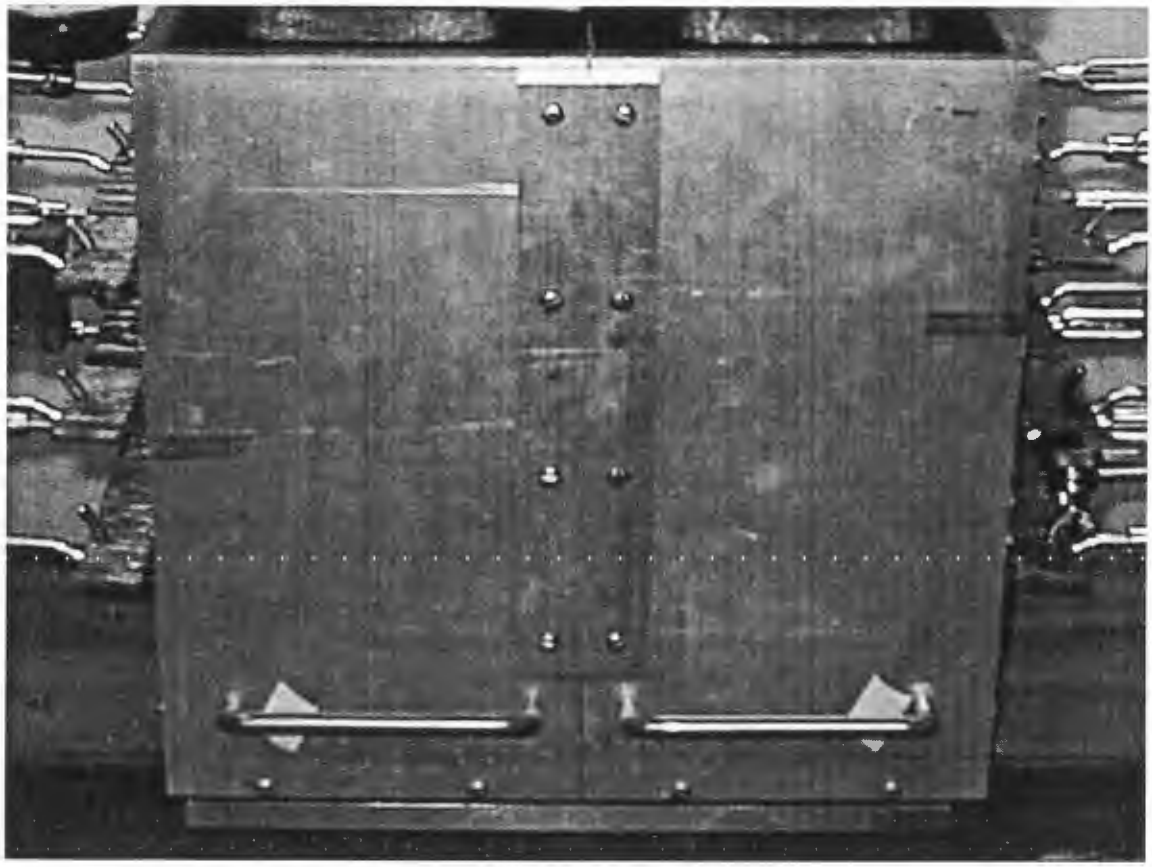

Figure 4.22. Removable plate securing the two halves of the split pullout box.

A third obstacle was how to apply the overburden pressures to a split pullout box with a solid overburden plate. The purpose behind splitting the pullout box into two halves was to eliminate any effect the box may have on the transfer of stresses between the two lapped mats. A solid overburden plate would, in effect, diminish the effectiveness of the split pullout box, as additional boundary effects would be added to the top layer of soil. The solution was to also split the overburden plate in half. Steel plates of equal mass and size were stacked on each half of the split overburden plate to apply the required overburden pressures, as shown in Figure 4.23.

Figure 4.23. Overburden being applied to split pullout box using steel plates of equal mass and size.

Similar to the test procedure described in the previous section, once the pullout test was complete for a given test configuration, the overburden was removed, the pullout box was emptied, and the box was removed from the pullout box frame. The pullout box was then refilled using the sand rainer, and the entire setup and testing procedure was repeated.

CHAPTER 5

PULLOUT TEST RESULTS

Introduction

Based on the pullout test apparatus and procedures described in the previous chapter, two sets of pullout tests were performed. An initial round of tests was performed using four different pullout test configurations: (one) a single level of mats with no lap zone; (two) three levels of mats with no lap zone; (three) a single level of mats with one lap zone; and (four) three levels of mats with three lap zones. Once the initial round of test was completed, and after the pullout box had been modified as described in Chapter 4, a final round of pullout tests was performed. Five different configurations were used for these final pullout tests (numbered in sequence from the previous four tests): (five) three levels of mats with three lap zones, free split box; (six) three levels of mats with three lap zones, fixed split box; (seven) three levels of mats with three lap zones, fixed box, pullout forces applied to left side only; (eight) three levels of mats with three lap zones, fixed box, right mats free; and (nine) three levels of mats with no lap zone, fixed box. All of the nine test configurations are summarized in Table 5.1. In conjunction with the scale pullout tests, a final set of Plaxis models was completed that closely modeled the dimensions and parameters of the scale pullout box and welded-wire mats.

Initial pullout tests

An initial set of pullout tests was performed in an attempt to study the lap zone. Four different configurations were used for the pullout tests: (one) a single level of mats

Table 5.1. Summary of the nine test configurations

Test configuration	Number of welded-wire mat layers	Number of lap zones in pullout box	Pullout box fixed or free to roll on linear bearings	Pullout box solid or split	Right welded-wire mats fixed or free
One	One	--	Fixed	Solid	--
Two	Three	--	Fixed	Solid	--
Three	One	One	Free	Solid	--
Four	Three	Three	Free	Solid	Fixed
Five	Three	Three	Free	Split	Fixed
Six	Three	Three	Fixed	Split	Fixed
Seven	Three	Three	Fixed	Solid	Fixed
Eight	Three	Three	Free	Solid	Free
Nine	Three	--	Fixed	Solid	--

with no lap zone; (two) three levels of mats with no lap zone; (three) a single level of mats with one lap zone; and (four) three levels of mats with three lap zones. These four initial test configurations are shown in Figure 5.1. Four different overburden pressures were also used during the pullout testing: 77, 212, 326, and 581 psf.

Single level of mats with no lap zone. This test configuration is shown as test configuration one in Figure 5.1. For this test configuration, only a single level of welded-wire mats was used and no lap zone was included. The first three pullout tests were completed at overburden pressures of 77, 212, and 326 psf. Initially, the lower bound for overburden pressure was chosen to be 77 psf, and the upper bound 326 psf. It was decided, however, that a higher upper bound overburden was desirable; therefore, a fourth pullout test was performed at an overburden pressure of 581 psf. Figure 5.2 shows this test configuration and Figure 5.3 shows the same configuration with 581 psf of added

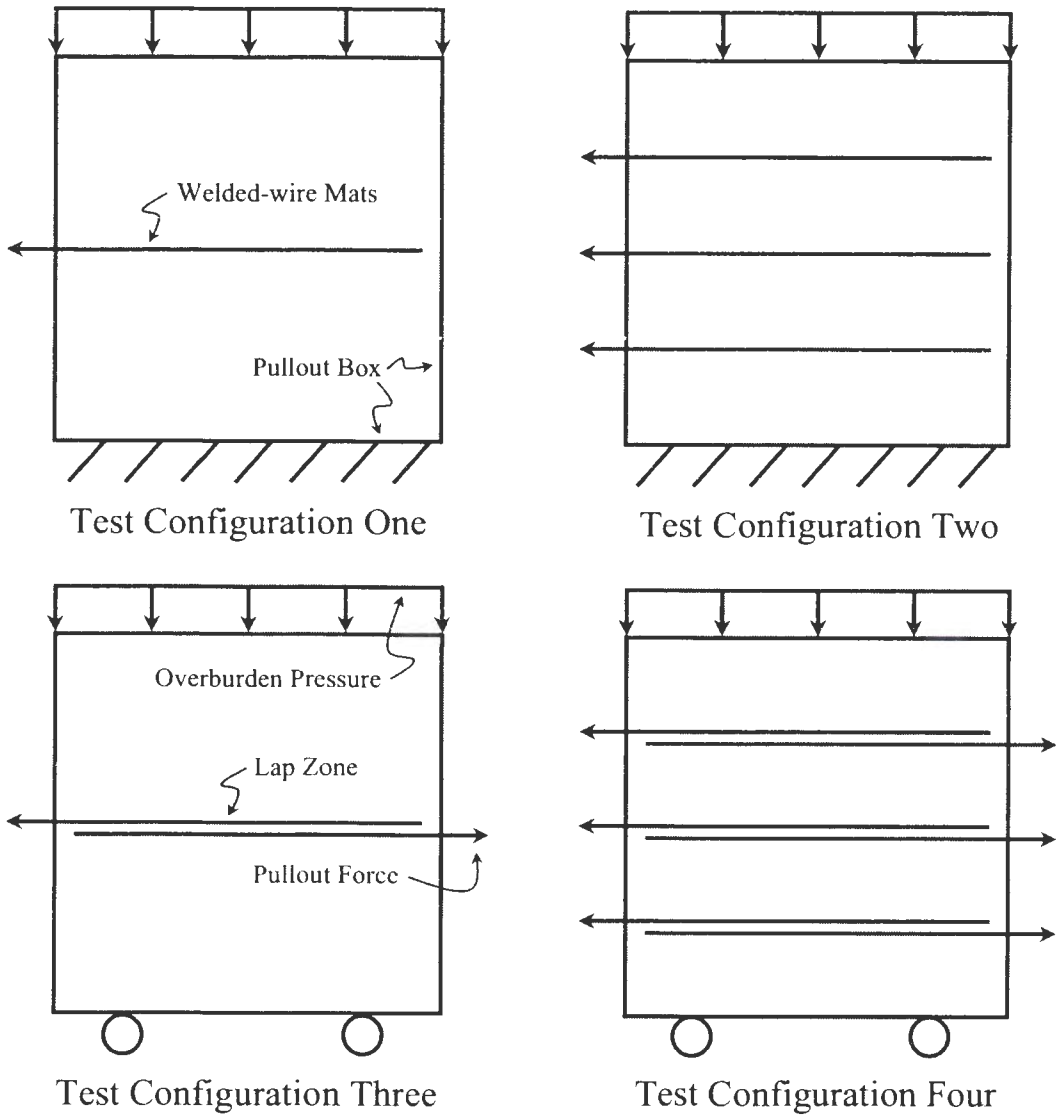

Figure 5.1. Simplified models of initial pullout test configurations.

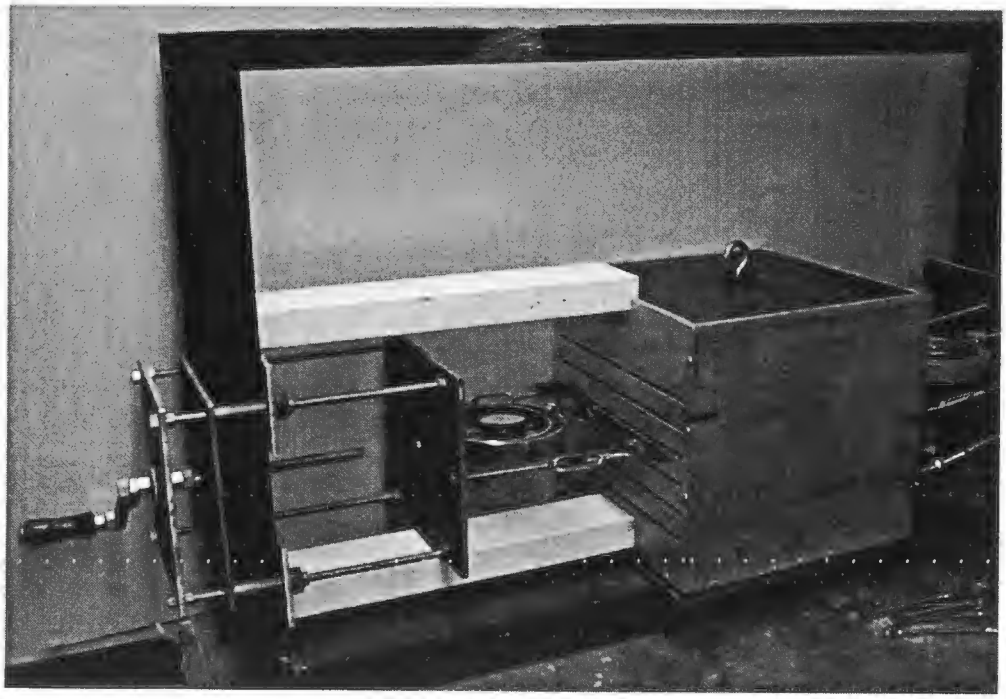

Figure 5.2. Single level of mats with no lap zone (test configuration one).

Figure 5.3. Single level of mats with no lap zone (test configuration one) with 581 psf of added overburden pressure.

overburden pressure. Figure 5.4 shows the load displacement curves for this test configuration.

Three levels of mats with no lap zone. This test configuration is shown as test configuration two in Figure 5.1. For this test configuration, three levels of welded-wire mats were used with no included lap zone. These pullout tests were performed to study how the addition of extra levels of mats affects the pullout resistance. They were completed at overburden pressures of 77, 212, and 326 psf. No pullout tests were performed at higher overburdens for this test configuration because of the difficulty of applying the pullout forces and the desire to not deform or break the pullout box frame. Figure 5.5 shows this test configuration before addition of overburden pressure. Figure 5.6 shows the load displacement curves for this test configuration.

Single level of mats with one lap zone. This test configuration is shown as test configuration three in Figure 5.1. For this test configuration, only a single level of welded-wire mats was used and one single lap zone was included. These pullout tests were completed at overburden pressures of 212, 326, and 581 psf. Figure 5.7 shows this test configuration with 212 psf of added overburden pressure. Figure 5.8 shows the load displacement curves for this test configuration.

Three levels of mats with three lap zones. This test configuration is shown as test configuration four in Figure 5.1. For this test configuration, three levels of welded-wire mats were used with three included lap zones. These pullout tests were completed at overburden pressures of 212, 326, and 581 psf. Figure 5.9 shows the left loading plate

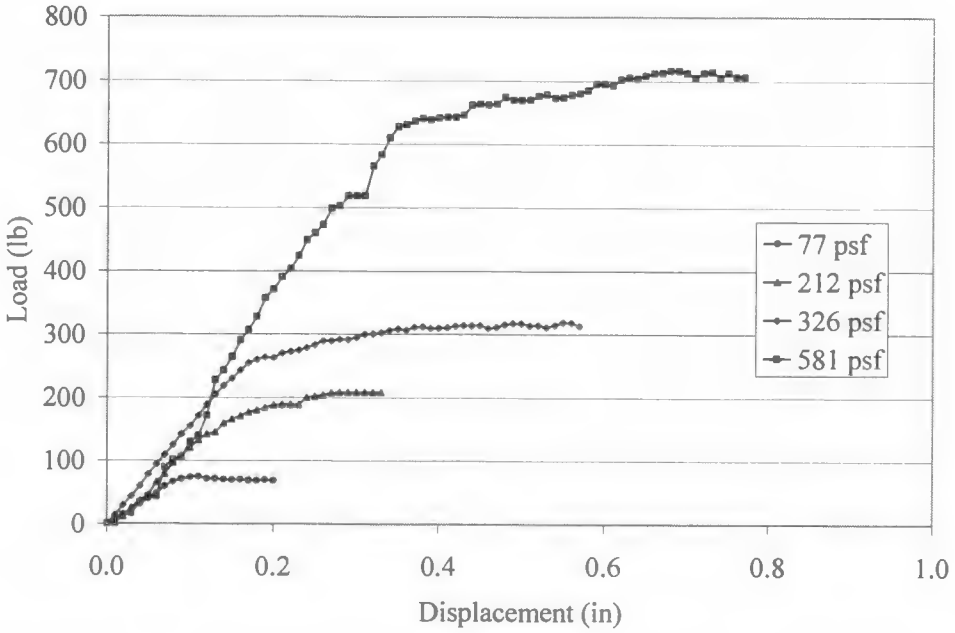

Figure 5.4. Load displacement curves for a single level of mats with no lap zone (test configuration one) at overburdens of 77, 212, 326, and 581 psf.

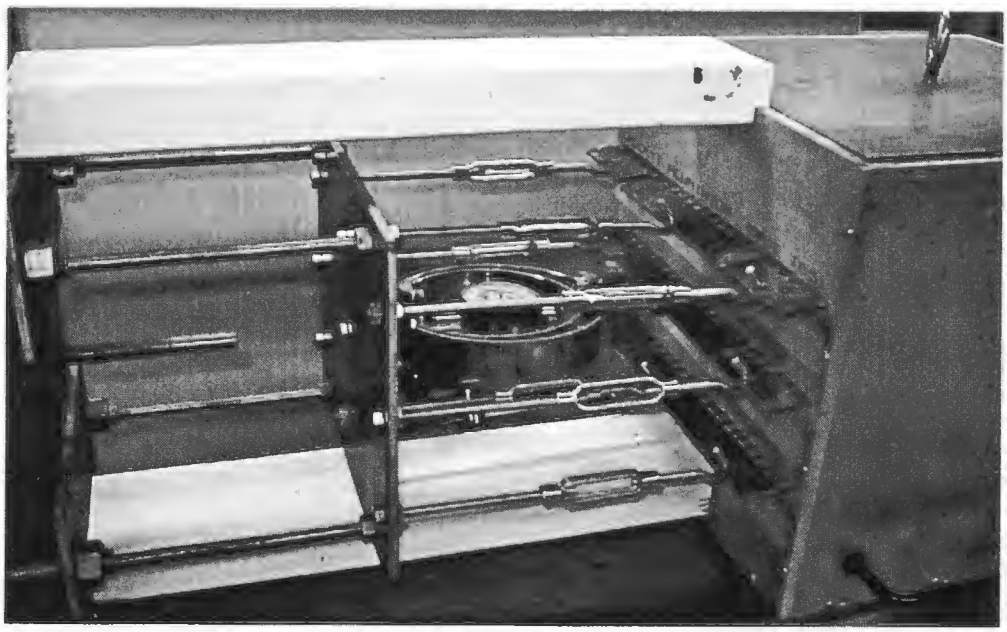

Figure 5.5. Three levels of mats with no lap zone (test configuration two) before addition of overburden pressure.

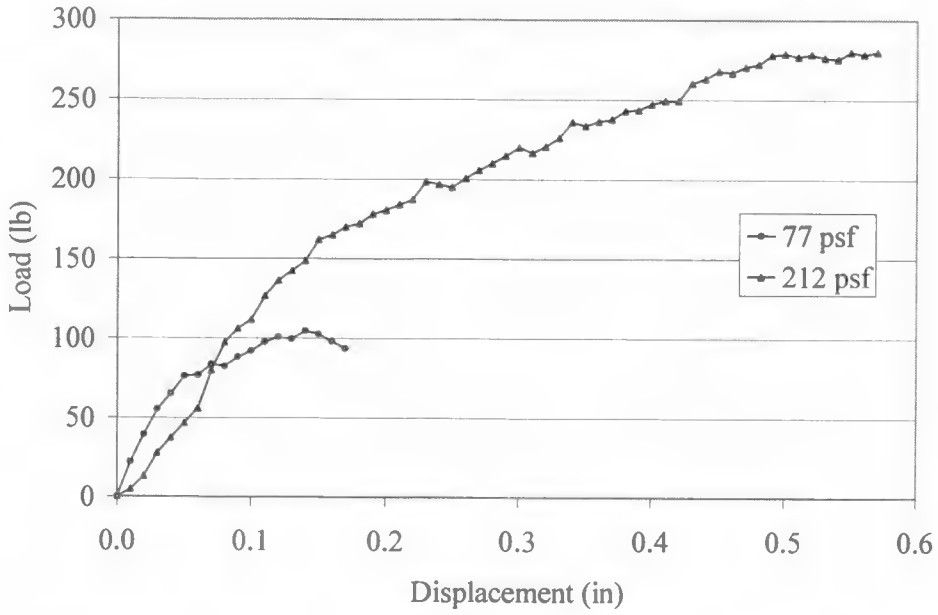

Figure 5.6. Load displacement curves for three levels of mats with no lap zone (test configuration two) at overburdens of 77 and 212 psf.

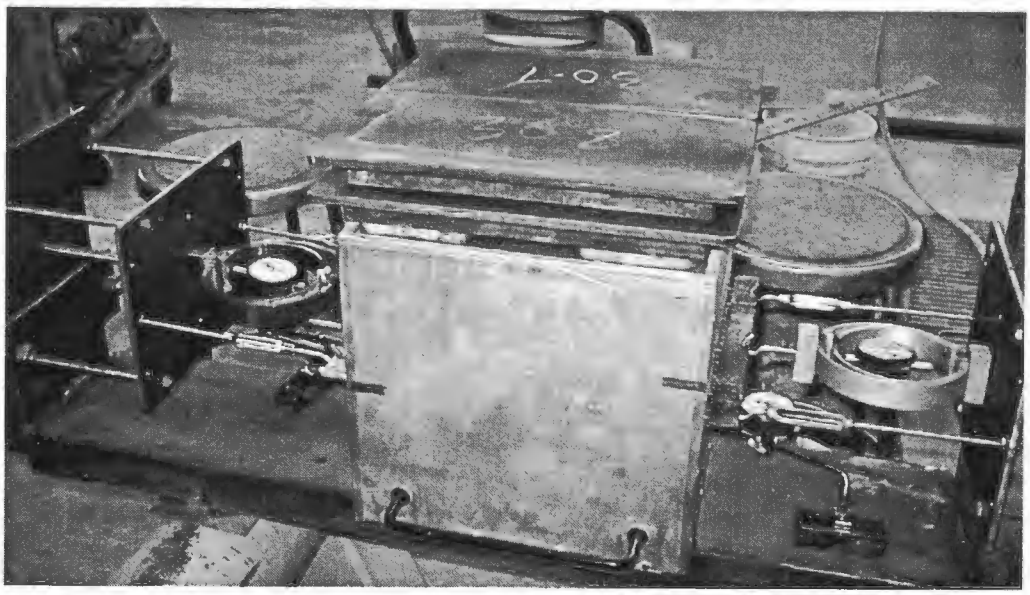

Figure 5.7. Single level of mats with one lap zone (test configuration three) with 212 psf of added overburden pressure.

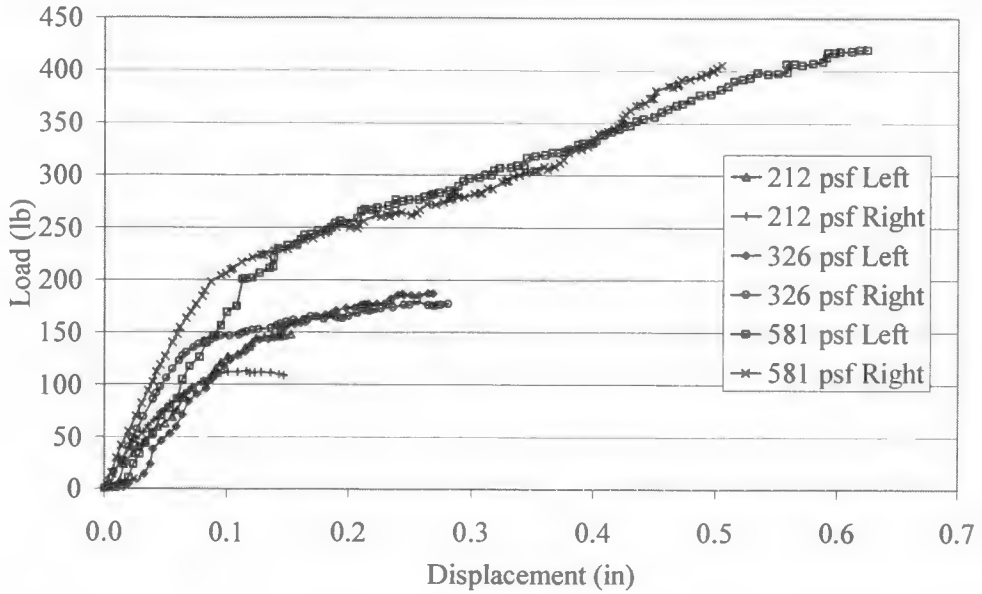

Figure 5.8. Load displacement curves for single level of mats with one lap zone (test configuration three) at overburdens of 212, 326, and 581 psf.

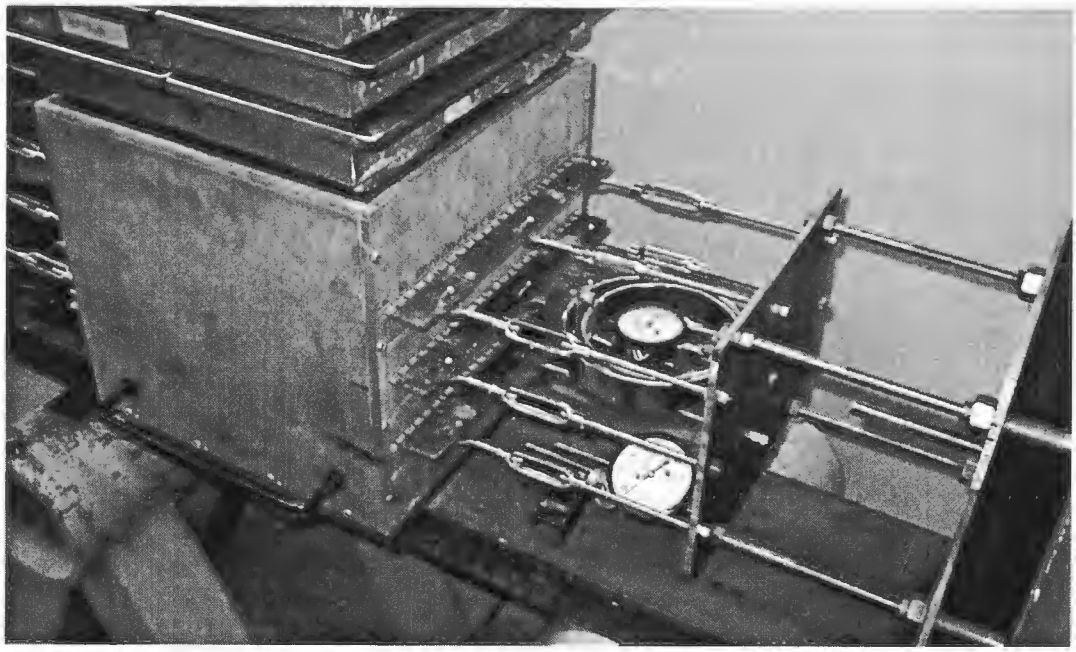

Figure 5.9. Three levels of mats with three lap zones (test configuration four) with 581 psf of added overburden pressure.

for this test configuration with 581 psf of added overburden pressure. Figure 5.10 shows the load displacement curves for this test configuration.

Final pullout tests

The objective for performing the pullout tests was to investigate the lap zone and to determine whether it could effectively transfer stress between the two lapped mats. Using the first four test configurations, this objective was not entirely realized. This point is better illustrated using Figure 5.11. The pullout box is free to roll horizontally on the nearly frictionless steel ball bearings in the direction of the applied pullout forces. In the case of three levels of mats with three lap zones, nearly equal and opposite pullout forces are applied to the right and left welded-wire mats at all times during the pullout tests. Similarly, if the mats are simply butted end-to-end, the same static principles apply. The opposing forces applied to the right and left welded-wire mats will be nearly equal and will yield results similar to pullout tests utilizing a lap zone (though the pullout forces may be lower for mats butted end to end). Thus, the four initial test configurations did not answer the question of whether the lap zone could effectively transfer stresses.

In order to correctly study the lap zone, a final set of pullout tests was performed. Before the final set of tests was begun, however, the pullout box was modified by splitting it into two equal halves along the cross section without the 1/4-inch wide gaps. With the pullout box split, both halves were free to move independently of one another during the pullout tests, making it possible to note whether the stresses in the left-hand mat were being transferred through the lap zone to the right-hand mat. As the pullout

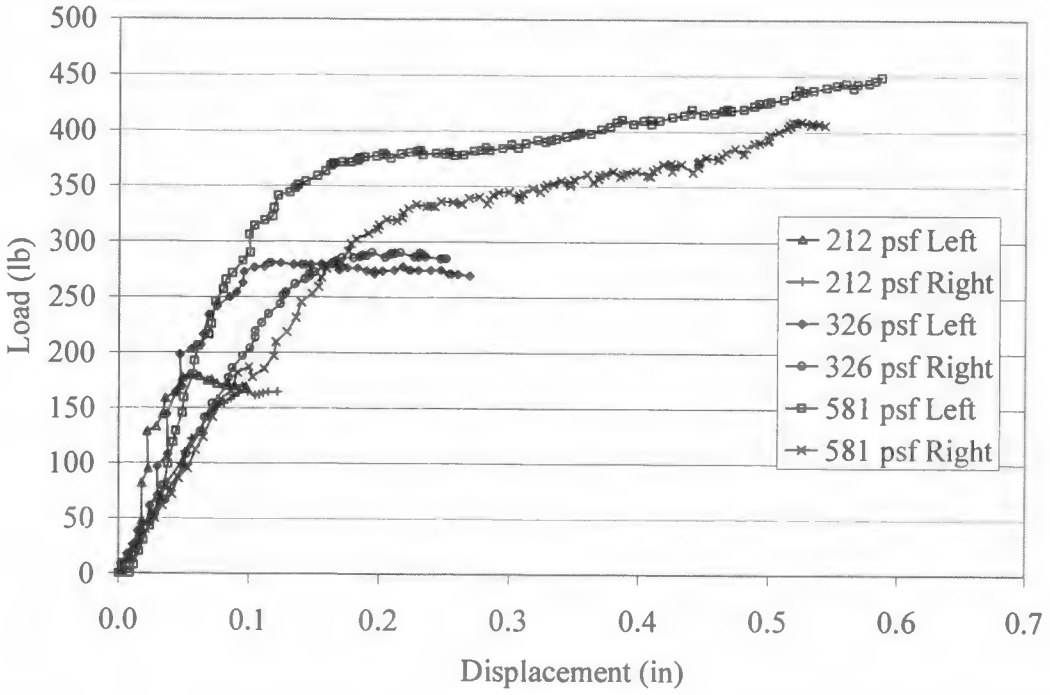

Figure 5.10. Load displacement curves for three levels of mats with three lap zones (test configuration four) at overburdens of 212, 326, and 581 psf.

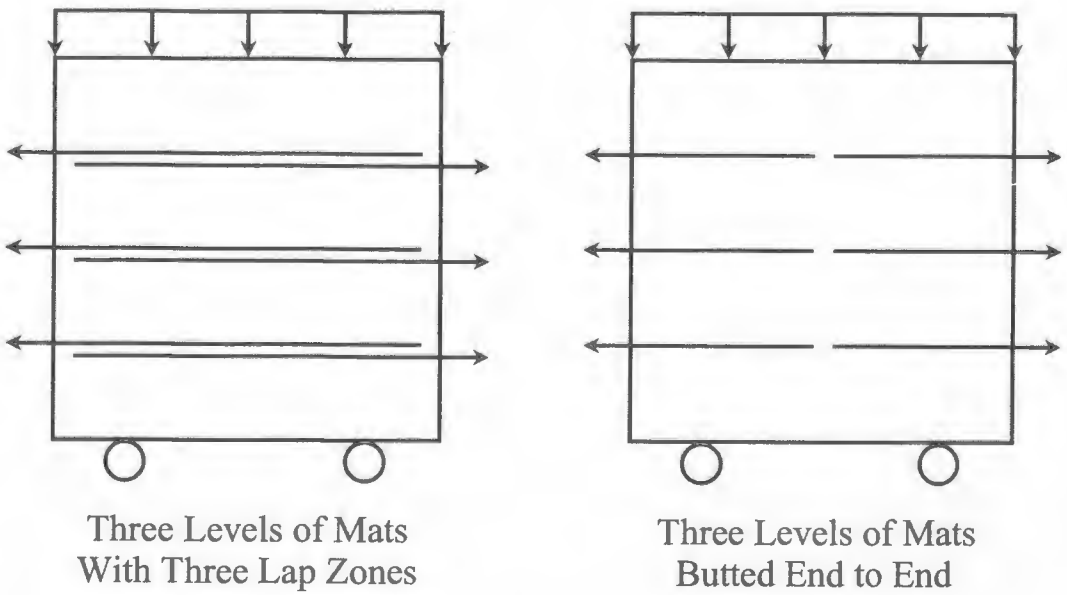

Figure 5.11. Visual explanation why initial test configurations were unsuccessful.

force was applied to the left welded-wire mat, the force in the right welded-wire mat was not necessarily equal and opposite. If no stresses were being transferred through the lap zone, the left half of the pullout box would simply pull away from the right half of the box. On the other hand, if 100 percent of the stresses were being transferred, then the pullout box would not split apart. Instead, both halves of the pullout box would simply slide in unison towards the applied pullout force. Thus, with this final pullout box configuration, we were able to begin to correctly investigate the transfer of stresses through the lap zone.

Five different configurations were used for the pullout tests (numbered in sequence from the previous four tests): (five) three levels of mats with three lap zones, free split box; (six) three levels of mats with three lap zones, fixed split box; (seven) three levels of mats with three lap zones, fixed box, pullout forces applied to left side only; (eight) three levels of mats with three lap zones, free box; (nine) three levels of mats with no lap zone, fixed box. These five final test configurations are shown in Figure 5.12. All of the pullout tests for the final test configurations were performed at the overburden pressure of 326 psf.

Three levels of mats with three lap zones and a free split box. This test configuration is shown as test configuration five in Figure 5.12. For this test configuration, three levels of welded-wire mats were used with three included lap zones. The pullout box was free to roll horizontally in the direction of the applied pullout forces along the ball-bearing grooves. Additionally, this was the first test run with a split box configuration. This pullout test was completed at an overburden pressure of 326 psf.

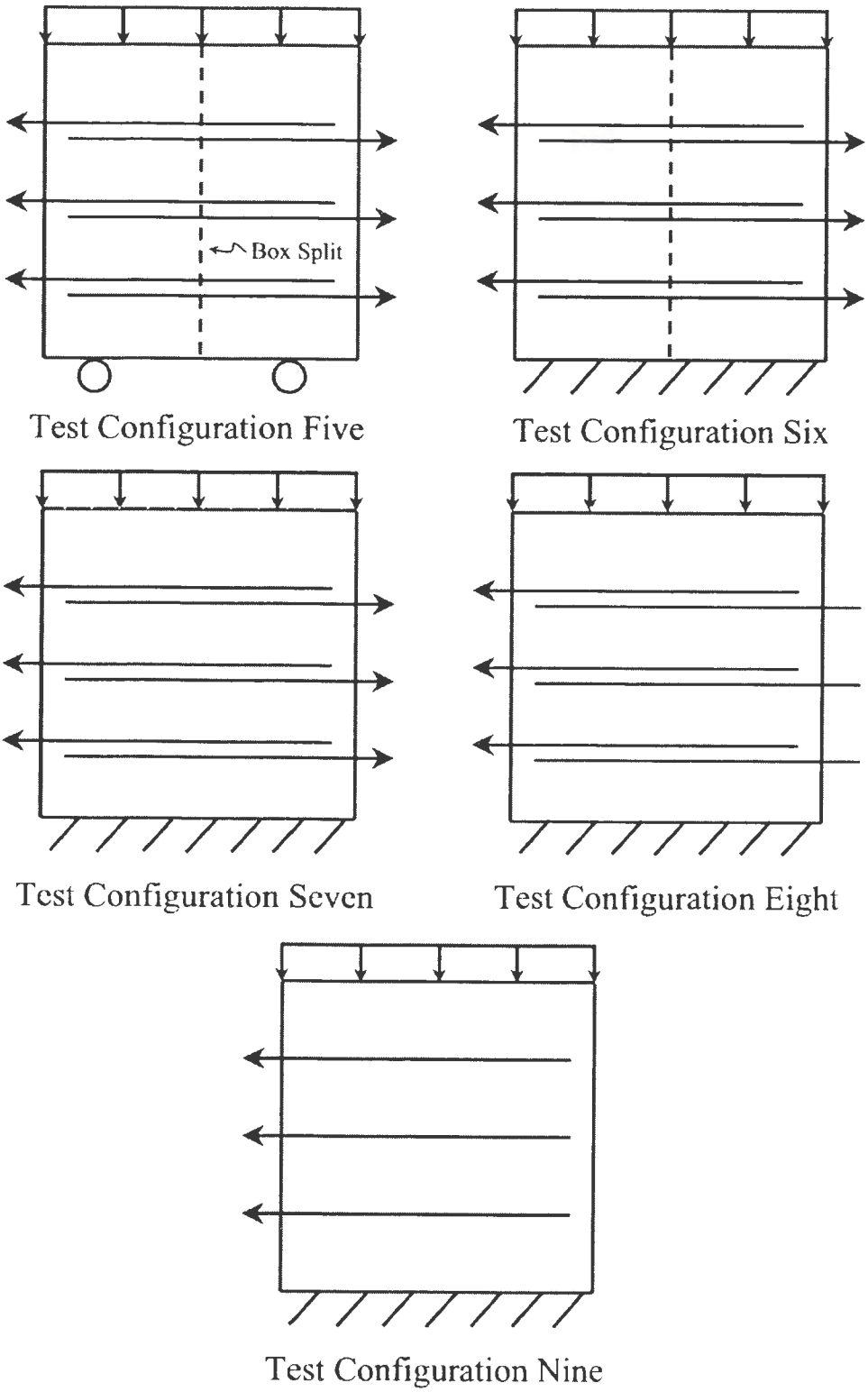

Figure 5.12. Simplified models of final pullout test configurations.

Figure 5.13 shows the pullout box with 326 psf of added overburden pressure after completion of the pullout test (note how the box split apart and exposed the rubber membrane). Figure 5.14 shows the load displacement curves for this test configuration.

Three levels of mats with three lap zones and a fixed split box. This test configuration is shown as test configuration six in Figure 5.12, and was actually a continuation of test configuration five. Once the pullout tests were concluded for test configuration five, the box was fixed in place so that it could no longer move horizontally in the direction of the applied pullout forces. This was accomplished by attaching the pullout box to the pullout box frame using pipe clamps. Once the box was fixed, the pullout test was completed at an overburden pressure of 326 psf. Figure 5.15 shows the load displacement curves for this test configuration.

Three levels of mats with three lap zones, a fixed box, and pullout forces applied to left side only. This test configuration is shown as test configuration seven in Figure 5.12 and was nearly the same as test configuration six. This test was run, however, with the removable plates attached to the sides of the pullout box to keep the two halves of the box from separating. Instead of bar clamps, a length of rope and two blocks of wood were used to fix the pullout box in place so that it could not move horizontally in the direction of the applied pullout forces. For this test configuration, three levels of welded-wire mats were also used with three included lap zones. This pullout test was completed at an overburden pressure of 326 psf. It is important to note that because the pullout box was fixed, the pullout forces on the right and left welded-wire mats did not necessarily need to be equal, as verified by statics principles. In addition to the pullout box being

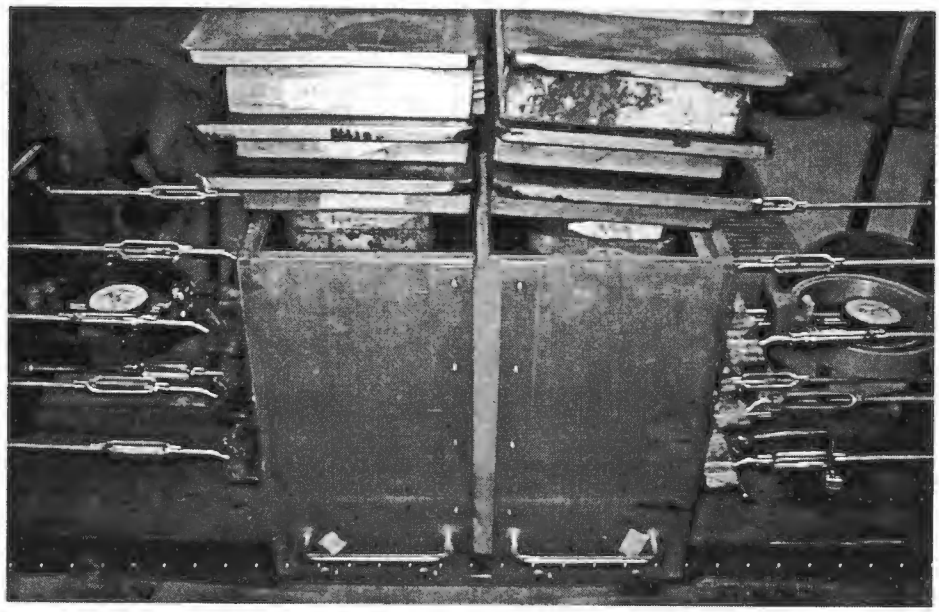

Figure 5.13. Three levels of mats with three lap zones and a free split box (test configuration five) after completion of pullout tests showing exposed rubber membrane between the two halves of the split pullout box.

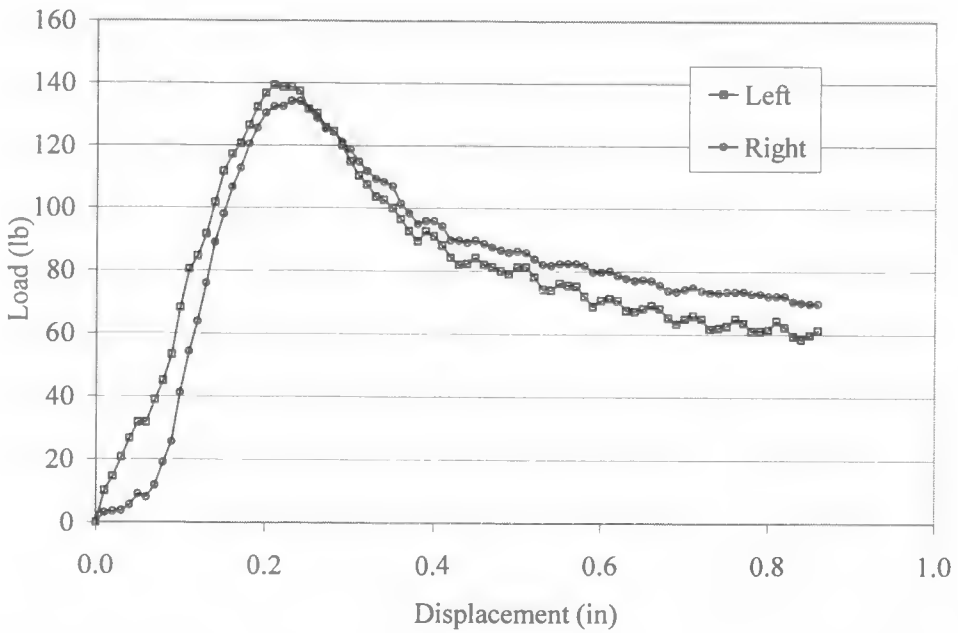

Figure 5.14. Load displacement curves for three levels of mats with three lap zones and a free split box (test configuration five) at an overburden of 326 psf.

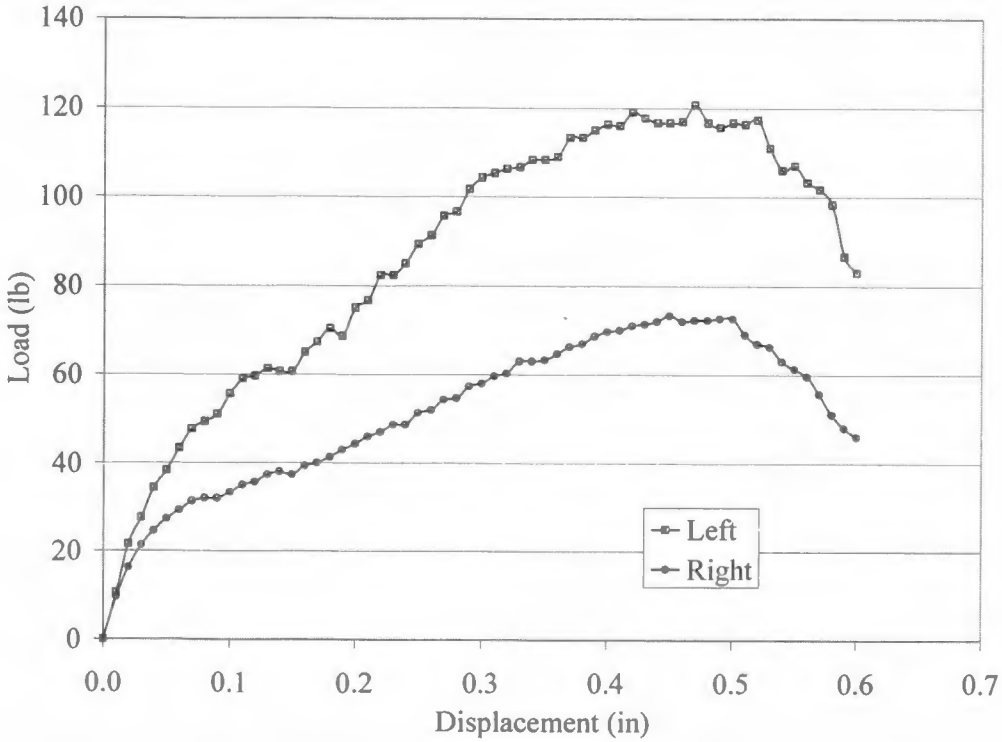

Figure 5.15. Load displacement curves for three levels of mats with three lap zones and a fixed split box (test configuration six) at an overburden of 326 psf.

fixed, the right welded-wire mat was also fixed, and the forces transferred between the mats in the lap zone were measured. Figure 5.16 shows how this test was configured and how the pullout box was fixed in place. Figure 5.17 shows the load displacement curves for this test configuration.

Three levels of mats with three lap zones and a free box. This test configuration is shown as test configuration eight in Figure 5.12 and the test setup was exactly the same as for test configuration seven except that the right mats were not fixed to the right loading plate. Instead, the right mats were free to displace during pullout testing. This

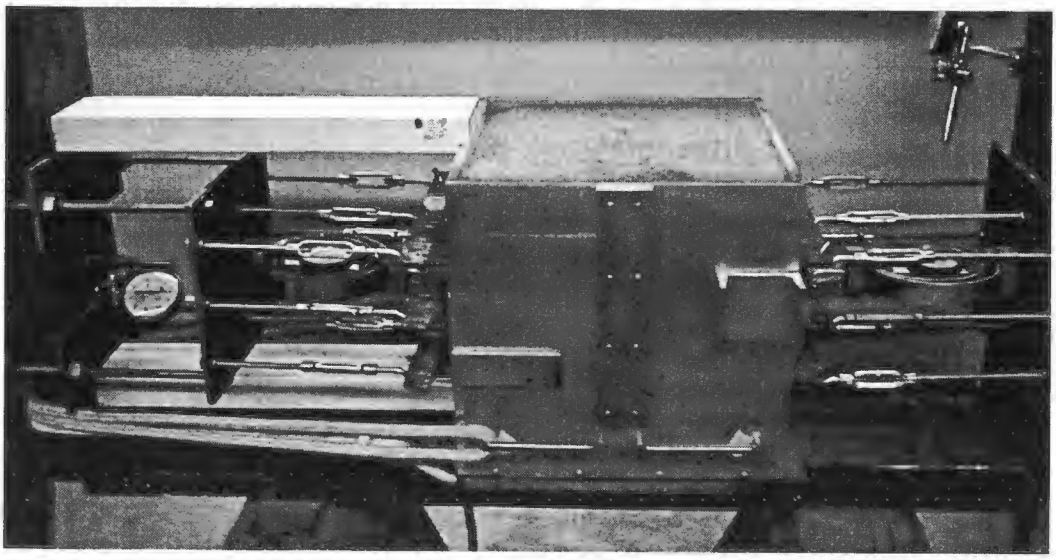

Figure 5.16. Pullout test setup showing three levels of mats with three lap zones, a fixed box, and pullout forces applied to left side only (test configuration seven).

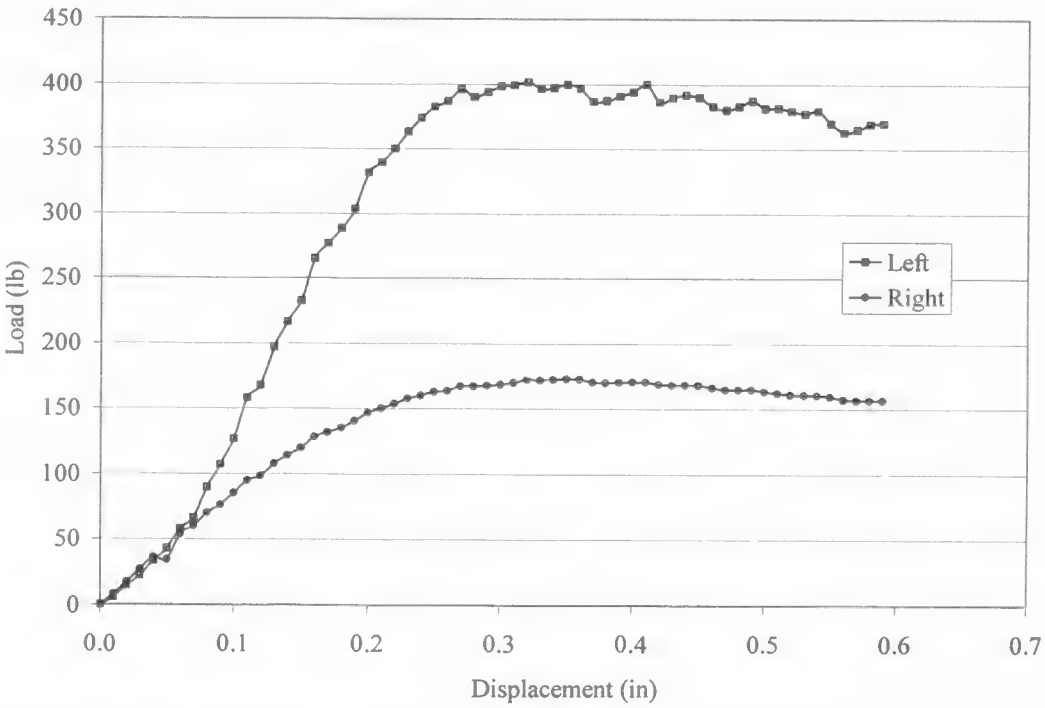

Figure 5.17. Load displacement curves for three levels of mats with three lap zones, a fixed box, and pullout forces applied to left side only (test configuration seven) at an overburden of 326 psf.

pullout test was also completed at an overburden pressure of 326 psf. Figure 5.18 shows how the pullout box was fixed for this test configuration, and how the right welded-wire mats are not attached to the right loading plate. Figure 5.19 shows the load displacement curves for this test configuration.

Three levels of mats with no lap zone and a fixed box. This test configuration is shown as test configuration nine in Figure 5.12 and was set up exactly the same as for test configuration two except that an additional overburden pressure of 326 psf was used. For this test configuration, three levels of welded-wire mats were used with no included lap zone. Figure 5.20 shows this test configuration with 326 psf of added overburden. Figure 5.21 shows the load displacement curves for this test configuration.

Composite pullout test results

In order to aid in the analysis and comparison of the pullout test results from both the initial and the final set of pullout tests, a composite load displacement curve was developed. Figure 5.22 is a composite plot of all the initial and final pullout test data for the overburden pressure of 326 psf. This overburden pressure was chosen because it was the only overburden pressure used for all of the final pullout test configurations. This overburden pressure was also used for all of the initial pullout test configurations except for test configuration two—three levels of mats with no lap zone. However, test configuration nine was a continuation of test configuration two at the higher overburden pressure of 326 psf, so it can be concluded that all of the test configurations are included in Figure 5.22.

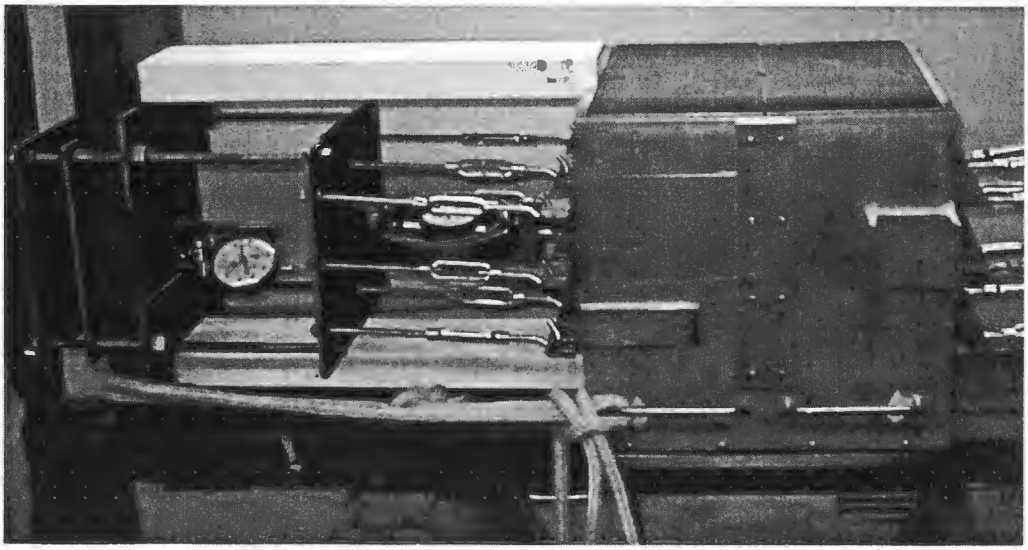

Figure 5.18. Pullout test setup showing three levels of mats with three lap zones, a free box, and the right mats free (test configuration eight).

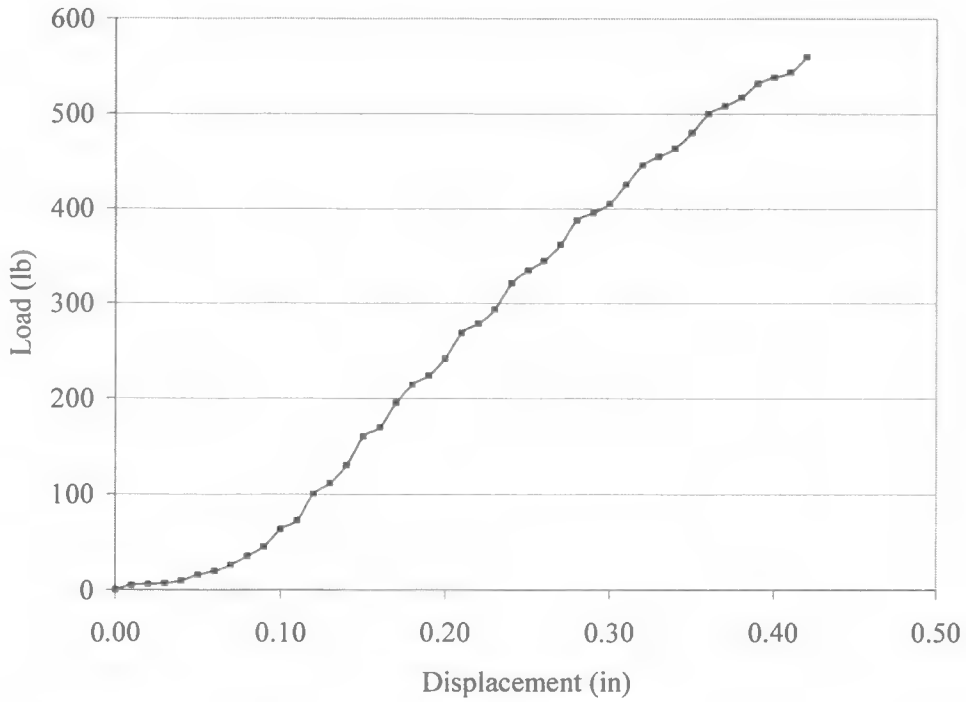

Figure 5.19. Load displacement curves for three levels of mats with three lap zones, a fixed box, and the right mats free (test configuration eight) at an overburden of 326 psf.

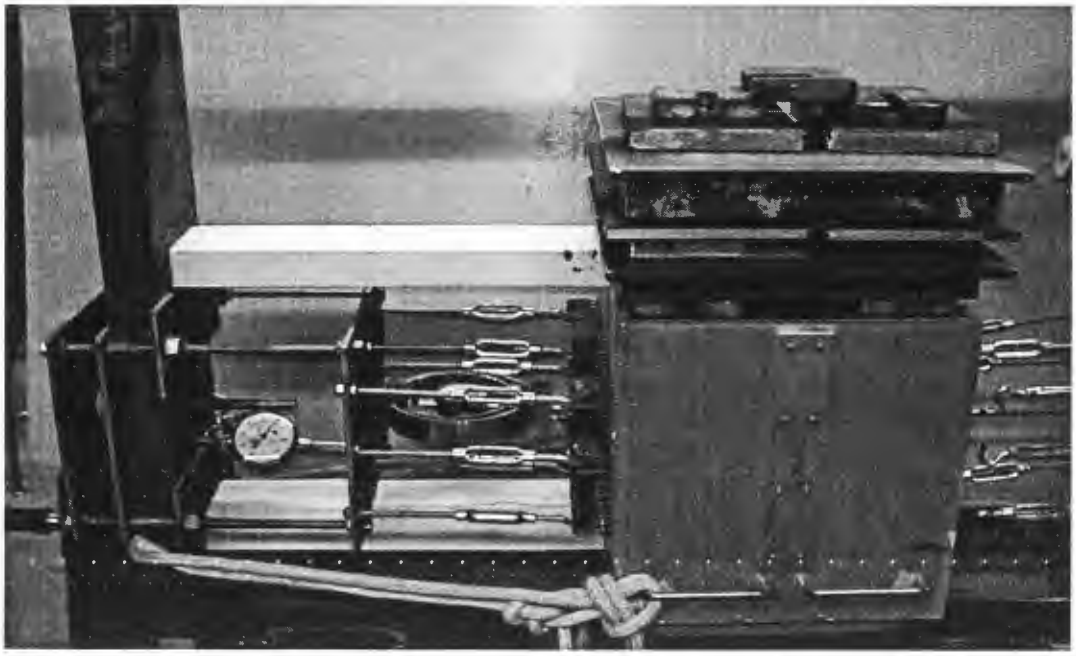

Figure 5.20. Pullout test setup showing three levels of mats with no lap zone and a fixed box (test configuration nine) with 326 psf of added overburden pressure.

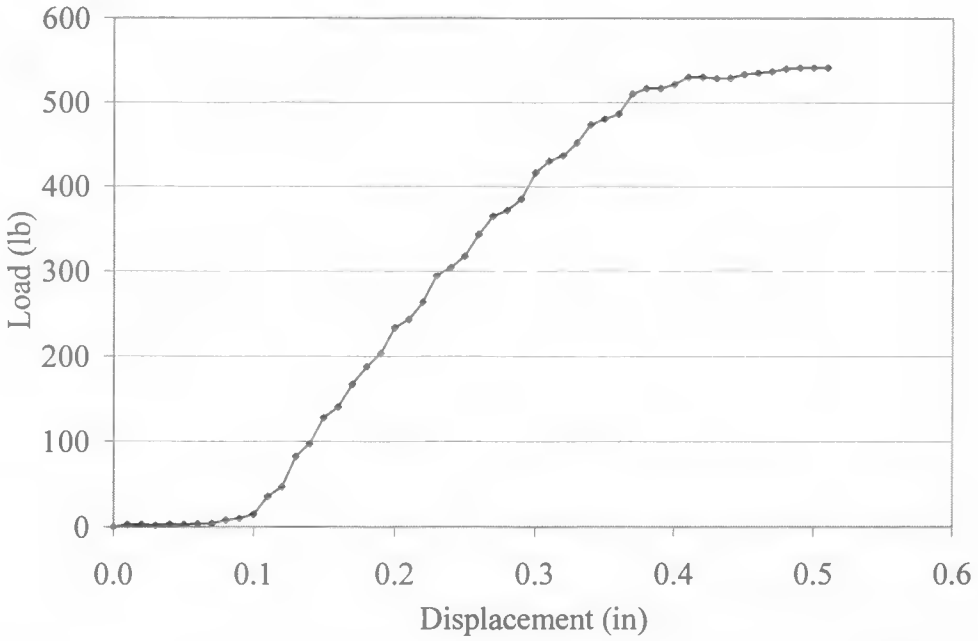

Figure 5.21. Load displacement curves for three levels of mats with no lap zone and a fixed box (test configuration nine) at an overburden of 326 psf.

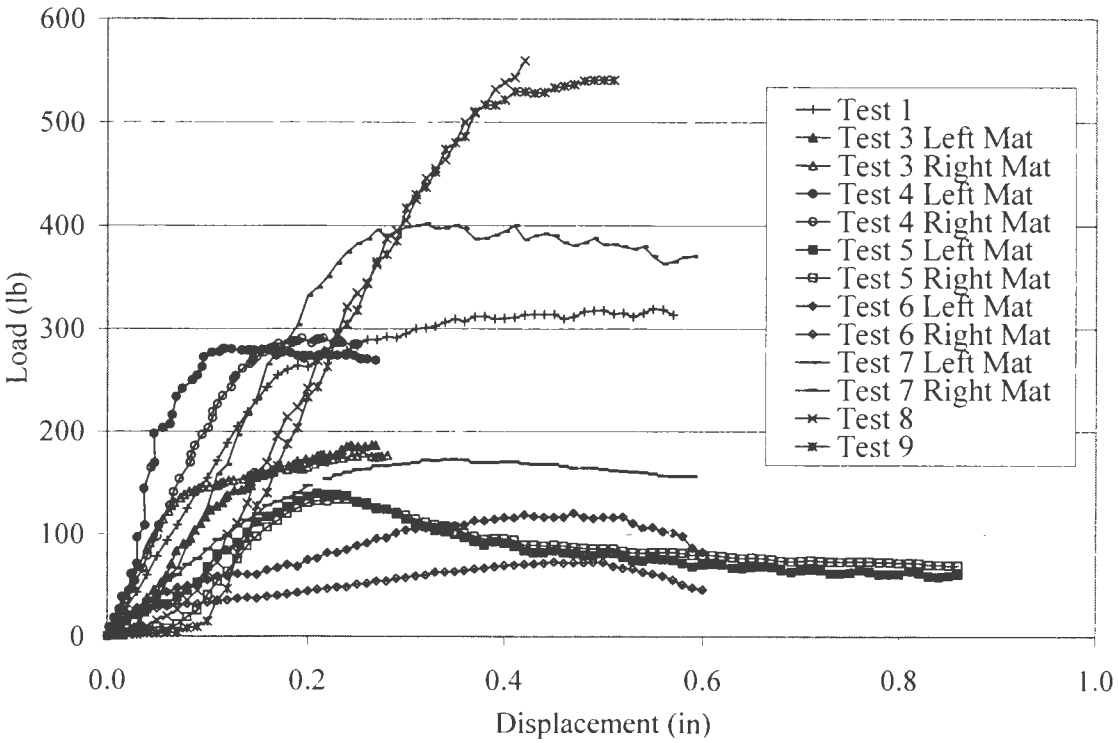

Figure 5.22. Composite load displacement curves for all of the initial and final pullout test data at an overburden of 326 psf.

Proving ring displacement

One item that needs to be addressed in subsequent scale pullout tests is the fact that the proving rings added flexibility to the pullout force measurement system. The flexibility of the proving rings made it so that all mats did not experience the same deflection. Mats connected to proving rings experienced less deflection and, hence, less force than those connected to turnbuckles. In future pullout tests, a more rigid pullout measurement system should be used.

Table 5.2 compares the displacement of the proving ring to the displacement of

Table 5.2. Displacement of the proving ring to the displacement of the welded-wire mats at failure for the final set of pullout test configurations

Test configuration	Mat displacement (in)	Left proving ring displacement (in)	Right proving ring displacement (in)
Five	0.86	0.0190	0.0202
Six	0.60	0.0249	0.0138
Seven	0.59	0.1110	0.0470
Eight	0.42	0.1680	--
Nine	0.51	0.1623	--

the welded-wire mats at failure for the final set of pullout test configurations. It is important to note that the proving ring deflection was subtracted from the measured displacement in order to obtain the actual displacement of the scale welded-wire mats.

Final set of Plaxis comparison models

In order to verify that the Plaxis computer program could accurately predict the pullout resistance, and that the previous computer models were valid, a final set of models was completed. The final models were much more robust and complicated than the simplified models described in Chapter 3.

Model parameters. The parameters used for the final Plaxis models closely reproduce the known parameters from the scale pullout tests. The pullout box was modeled using beam elements, and the dimensions of the box matched those of the actual

scale model test: 12 inches square. The longitudinal bars of the welded-wire mats were modeled using 12-inch long geotextile elements. For the final models, transverse bars were also included. They were modeled using short vertical beam elements fixed to the geotextile elements. To keep the transverse elements from rotating, moment fixities were used at the point where the beam and geotextiles attach. These fixed rotations, or moment fixities, fix the rotational degree of freedom of a beam (Plaxis, 1998). The remainder of the model parameters can be found in Table 5.3. Once the Plaxis models were built, a fine finite element mesh was generated. The same calculation procedures were then followed as explained in Chapter 3.

Model descriptions and results. Two different computer models were completed whose results were similar to those obtained during the scale pullout testing, and represent test configurations one and two. Unfortunately, no finite element models were successfully completed that represent lap zone models. The reason for this lies with limitations within the Plaxis program itself. Plaxis has a programmed maximum limit on the number of iterations that can be completed during the calculation phase. Due to the complexity of the lap models, the maximum number of iterations was quickly reached at the beginning of the calculation phase, and no pullout forces could be developed. No data could be collected from the computer models to compare to the scale pullout tests performed in the pullout box.

The results for the final set of finite element models are shown in Figure 5.23 and Figure 5.24. Figure 5.23 shows the results for the model that closely resembles test configuration one (a single level of mats with no lap zone). Figure 5.24 shows the results

Table 5.3. Properties used in final set of Plaxis models

Material property description	Fill	Surcharge	Beam elements	Geotextile elements
Material model	Hardening Soil	Liner Elastic	--	--
Materail type	Drained	Drained	Elastic	--
Dry unit weight, γ_{dry}	115 lb/ft^3	Variable	--	--
Horizontal permeability, k_x	0 ft/day	0 ft/day	--	--
Vertical permeability, k_y	0 ft/day	0 ft/day	--	--
Initial void ratio, e_0	1.0	1.0	--	--
Plastic straining due to primary deviatoric loading, E_{50}^{ref}	22920 lb/ft^2	--	--	--
Plastic straining due to primary compression, E_{oed}^{ref}	22920 lb/ft^2	--	--	--
Young's modulus, E_{ref}	--	2000 lb/ft^2	--	--
Poisson's ratio, ν	--	0.3	0.2	--
Stress dependent stiffness according to a power law, m	0.5	--	--	--
Cohesion, c_{ref}	4.2 lb/ft^2	--	--	--
Friction angle, φ	35.7°	--	--	--
Dilatancy angle, Ψ	2°	--	--	--
Interface strength reduction factor, Rinter	0.6	0.6	--	--
Axial stiffness, EA	--	--	6.0E+09 lb/ft	6.0E+09 lb/ft
Flexural rigidity, EI	--	--	6.0E+09 lb-ft^2/ft	--

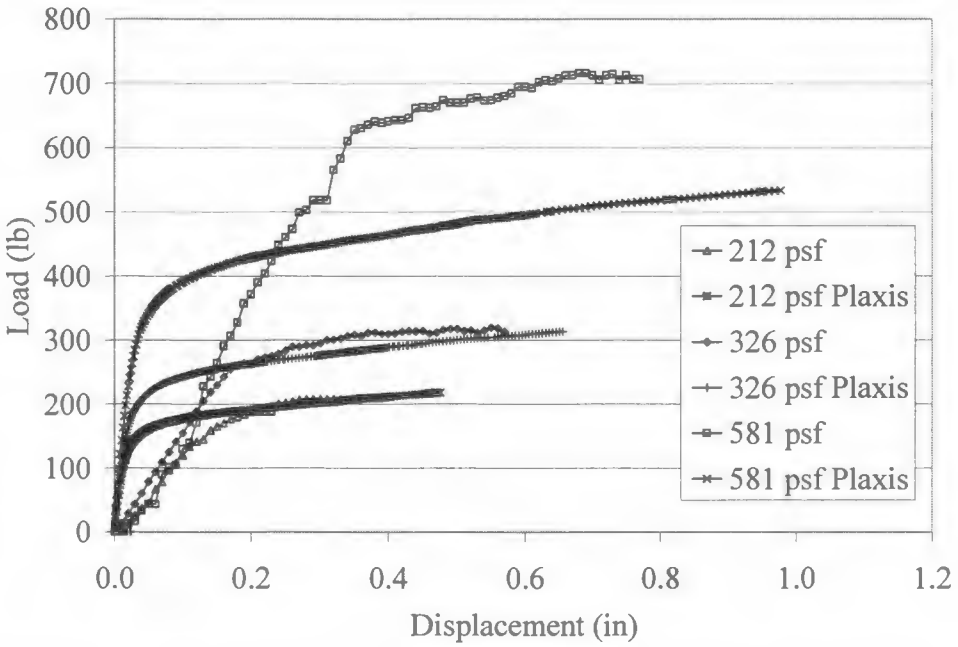

Figure 5.23. Load displacement curves comparing Plaxis results to pullout test data for a single level of mats with no lap zone (test configuration one).

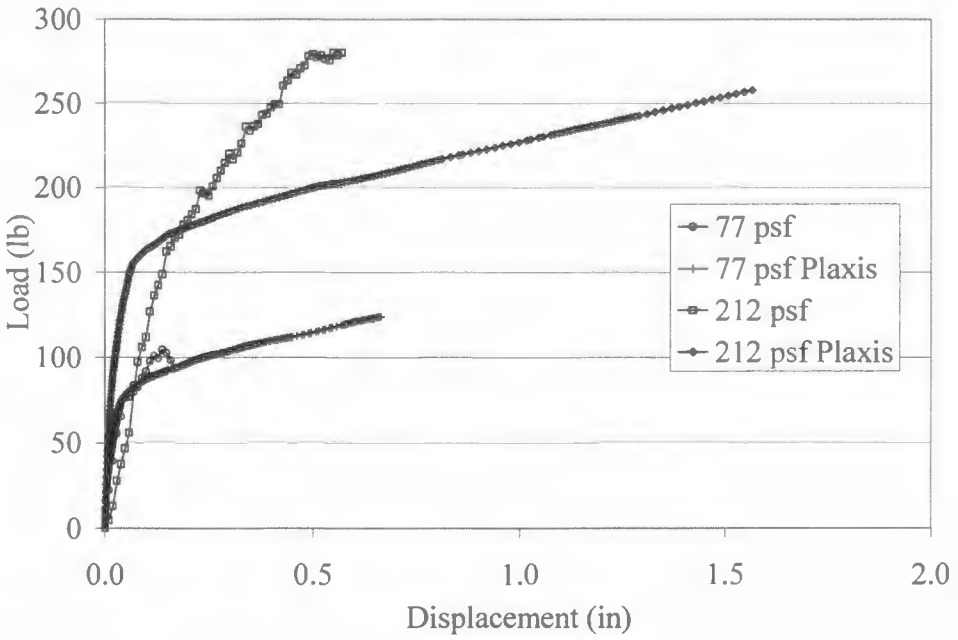

Figure 5.24. Load displacement curves comparing Plaxis results to pullout test data for three levels of mats with no lap zone (test configuration two).

for the model that closely resembles test configuration two (three levels of mats with no lap zone). The results from the computer models are plotted with the results from the equivalent scale pullout tests. At overburdens of 212 and 326 psf in Figure 5.23 and at overburdens of 77 and 212 psf in Figure 5.24, the ultimate measured pullout resistance for both the scale models and the Plaxis models closely resemble each other. At an overburden of 581 psf in Figure 5.23, however, the ultimate measured pullout resistance for the scale model and the Plaxis model differ significantly. It is also important to note that at low loading levels, looking at both Figure 5.23 and Figure 5.24, the load displacement curves for all of the Plaxis models are much steeper initially than those for the scale pullout models.

The different shape of the load displacement curves and the different ultimate measured pullout resistance at an overburden of 581 psf in Figure 5.23 show that more work needs to be done with the Plaxis soil model parameters so they more closely match the scale pullout test results. As useful as finite element computer modeling can be, it still needs to be checked against laboratory or field measurements for accuracy. However, the fact that the results from the Plaxis models match the data from the pullout tests with some degree of accuracy seems to validate the use of finite element modeling as a research tool.

CHAPTER 6

SUMMARY AND CONCLUSIONS

Summary

In November of 1999, Utah State University became involved with a research project at Kennecott Utah Copper. Two large Hilfiker retaining walls were built at the mouth of Bingham Canyon, just west of Copperton, Utah. These two identical 126-foot high walls were used as "reload" walls for the transportation of ore from the open pit mine to the processing facilities. As part of the wall design, two different lengths of reinforcement were utilized in the wall. In the lower 62 feet of the wall, the reinforcement consisted of single 50-foot welded-wire mats. In the upper 64 feet, the reinforcement length made a dramatic jump from 50 feet to 90 feet. In order to create the 90-foot lengths of reinforcement, two 50-foot mats were laid directly on top of one another, overlapping a distance of 10 feet. No mechanical connection was made between the two lapped mats. This 10-foot overlapped section was termed the "lap zone" for purposes of this research.

The focus of this research was to investigate the pullout performance of the lap zone in the 90-foot Hilfiker welded-wire mats, and to study whether complete or partial stress transfer occurs between the two lapped mats. There were two major areas of research that were used to investigate the lap zone. First, a parametric study of pullout testing was completed using the finite element computer program Plaxis. The parametric study investigated how overburden pressure, size of gap width, boundary effects, and transverse elements affect the pullout resistance of welded-wire mats.

The second part of the research dealt with scale pullout tests that were completed on campus at Utah State University. A scale pullout box and scale welded-wire mats were constructed to accommodate the pullout testing. Two sets of pullout tests were completed during the course of this research. With the first set of tests, four pullout test configurations were used: (one) a single layer of welded-wire mats without a lap zone; (two) three layers of mats without a lap zone; (three) a single layer of mats with one included lap zone; and (four) three layers of mats with three included lap zones. This initial set of pullout tests was performed at varying overburdens of 77, 212, 326, and 581 psf.

Once the first set of pullout tests was complete, the pullout box was modified and the second set of pullout tests was performed using five pullout test configurations (numbered in sequence from the previous four tests): (five) three levels of mats with three lap zones, free split box; (six) three levels of mats with three lap zones, fixed split box; (seven) three levels of mats with three lap zones, fixed box, pullout forces applied to left side only; (eight) three levels of mats with three lap zones, free box; (nine) three levels of mats with no lap zone, fixed box. All of the pullout tests for the final test configurations were performed at the overburden pressure of 326 psf.

Finally, in order to verify that the Plaxis computer program could accurately predict the pullout resistance obtained during the scale pullout testing, and to validate the parametric study completed using Plaxis, a final set of finite element models was completed. Two different computer models were completed whose results were similar to those obtained during the scale pullout testing.

Conclusions

The conclusions for the parametric study conducted using Plaxis are as follows:

1) Pullout resistance is a function of the overburden pressure. As the overburden pressures increase, so does the pullout resistance of the reinforcement.

2) The gap width, or the size of the opening in the face of the pullout box, has little effect on the pullout resistance of the reinforcement (for gap widths less than or equal to approximately 3 inches).

3) Boundary effects between the pullout box and the reinforcement can have a large effect on the measured pullout resistance. When the pullout box is less than 3 feet in height for full-scale pullout tests, the stress interaction between the pullout box and the reinforcement can increase the pullout resistance and give inaccurate results.

4) The first transverse bar of a welded-wire mat needs to be spaced horizontally a sufficient distance from the pullout box face so that the pullout resistance is not adversely increased. The ratio of the horizontal distance over the height of the transverse element (a ratio of d/t) of six should be sufficient, as shown in Figure 3.6, and should be followed for actual pullout tests.

The conclusions for the scale pullout tests on welded-wire mats can be summarized as:

1) The proving rings used to measure the pullout resistance of the welded-wire mats add flexibility to the system and make it so that all mats did not experience the same deflection. In future pullout tests, a more rigid pullout measurement system should be used.

2) Pullout resistance and lap resistance are controlled by vertical and horizontal stresses in soil.

a) Increasing σ_v increases the pullout and lap resistance.

b) Increasing σ_h by increasing the number of mats increases the pullout resistance.

c) Decreasing σ_h by splitting the pullout box decreases the lap resistance.

3) Conventional pullout testing does not account for effects of horizontal stress.

4) Lap performance is dependant upon the state of stress in the soil in the lap zone. Horizontal stresses could not be determined in these tests.

The conclusions that can be drawn from the final Plaxis models are:

1) The finite element model results matched the scale pullout test results with some degree of accuracy, thus validating both the parametric study and the scale pullout tests.

2) Finite element computer modeling is a viable research tool in helping to understand pullout testing, so long as it can be verified using field or laboratory tests.

3) More work needs to be done with the Plaxis soil model parameters so that the ultimate measured pullout resistance and the slope of the load displacement curve at low loading levels more closely match the scale pullout test results.

Recommendations

Though several conclusions were drawn from the results of the finite element models and the pullout tests, more work needs to be completed in order to fully

understand the stress transfer in the lap zone. Some recommendations for future studies would include:

1) Create a new system to measure the pullout forces and displacements of the scale welded-wire mats. A digital measurement system using strain gages and displacement transducers would eliminate the need for proving ring and dial gages. This, in turn, would eliminate both the proving ring flexibility issues and the human errors introduced while reading the dial gages.

2) Modify the pullout box frame. First, increase the strength of the loading plates so that the pullout tests can be performed at overburdens higher than 581 psf. Second, increase the length of the hand crank arm to make it easier to maintain a consistent rate of applied pullout force.

3) Perform more pullout tests for test configurations five through nine at numerous overburden pressures besides just 326 psf.

LITERATURE CITED

Anderson, L. R., J. Nelson, and C. L. Sampaco. 1995. Transportation research circular: Mechanically stabilized earth walls. Transportation Research Board 444 (ISSN 0097-8515). 17 p.

Barton, B. R. 2001. Instrumentation and analysis of a welded-wire mechanically stabilized earth wall at Kennecott Utah Copper. Unpublished MS thesis. Utah State University Library, Logan, Utah. 237 p.

Budhu, M. 1999. Soil mechanics and foundations. John Wiley & Sons, Inc., New York. 502 p.

Christopher, B. R., S. A. Gill, J. P. Giroud, I. Juran, J. K. Mitchell, F. Schlosser, and J. Dunnicliff. 1989. Reinforced soil structures: Design and construction guidelines. Federal Highway Administration, FHWA Report No. RD-89-043. 287 p.

Dunn, I. S., L. R. Anderson, and F. W. Kiefer. 1980. Fundamentals of geotechnical analysis. John Wiley and Sons, Inc., New York. 414 p.

Jewell, R. A., G. W. E. Milligan, R. W. Sarsby, and D. Dubois. 1984. Interaction between soil and geogrids. Symposium on Polymer Reinforcement in Civil Engineering, 1984, London, England. p. 19-29.

Juran, I. 1977. Dimensionnement interne des ouvrages en terre armee. Unpublished PhD dissertation. Laboratoire Central des Ponts et Chaussees, Juillet. 395 p.

Juran, I., and F. Schlosser. 1978. Theoretical analysis of failure in reinforced earth structures. Symposium on Earth Reinforcement, April 27, 1978, Pittsburgh, Pennsylvania. p. 528-555.

Lee, K. L., B. D. Adams, and J. J. Vagneron. 1973. Reinforced earth retaining walls. Journal of Soil Mechanics and Foundations Division 99(SM10):745-764.

Mitchell, J. K., and B. R. Christopher. 1990. North American practice in reinforced soil systems. Specialty Conference on Design and Performance of Earth Retaining Structures, June 18-21, 1990, Ithaca, New York. p. 322-346.

Mitchell, J. K., and W. C. B. Villet. 1987. Reinforcement of earth slopes and embankments. National Cooperative Highway Research Program Report No. 290. 323 p.

Nielsen, M. R. and L. R. Anderson. 1984. Pullout resistance of welded-wire mats embedded in soil. Report submitted to the Hilfiker Company, Hurst, Texas. Department of Civil and Environmental Engineering, Utah State University, Logan, Utah. 130 p.

Peterson, L. M., and L. R. Anderson. 1980. Pullout resistance of welded-wire mats embedded in soil. Report submitted to the Hilfiker Company, Hurst, Texas. Department of Civil and Environmental Engineering, Utah State University, Logan, Utah

Plaxis, B. V. 1998. Finite element code for soil and rock analyses. Version 7.11: Material models manual. A. A. Balkema, Rotterdam, Netherlands. 535 p.

Prandtl, L. 1921. Uber die eindringungsfestigkeit platisher baustoffe und die Fetsigkeit von Schneiden. Zeitschrift fur Angewandte Mathematik und Mechanik 1:15-20.

Reissner, H. 1924. Zum erddruckproblem. 1st International Conference on Applied Mechanics, 1924, Delft, The Netherlands. p. 295-311.

Schlosser, F. 1990. Mechanically stabilized earth retaining structures in Europe. Specialty Conference on Design and Performance of Earth Retaining Structures, June 18-21, 1990, Ithaca, New York. p. 347-378.

Schlosser, F. and V. Elias. 1978. Friction in reinforced earth. Symposium on Earth Reinforcement, April, 1978, Pittsburgh, Pennsylvania. p. 735-763.

Schlosser, F. and N. T. Long. 1974. Recent results in French research on reinforced earth. ASCE, Journal of Construction Division 100(CO3):223-237.

Vidal, H. 1969. The principle of reinforced earth. Highway Research Record 282:1-16.